



UNIVERSIDAD NACIONAL AUTÓNOMA DE MÉXICO
PROGRAMA DE MAESTRÍA Y DOCTORADO EN INGENIERÍA
INGENIERÍA ELÉCTRICA - CONTROL

CONTROL OF 2 CLASSES OF UNDERACTUATED MECHANICAL
SYSTEMS OF 2 DoF VIA CONTINUOUS HIGHER-ORDER
SLIDING-MODES

TESIS
QUE PARA OPTAR POR EL GRADO DE:
DOCTOR EN INGENIERÍA

PRESENTA:
DIEGO GUTIÉRREZ ORIBIO

TUTORES PRINCIPALES:
DR. LEONID FRIDMAN, UNAM
DR. JAIME ALBERTO MORENO PÉREZ, UNAM
PROGRAMA DE MAESTRÍA Y DOCTORADO EN INGENIERÍA

Ciudad Universitaria, Ciudad de México, Enero del 2021



Universidad Nacional
Autónoma de México



UNAM – Dirección General de Bibliotecas
Tesis Digitales
Restricciones de uso

DERECHOS RESERVADOS ©
PROHIBIDA SU REPRODUCCIÓN TOTAL O PARCIAL

Todo el material contenido en esta tesis esta protegido por la Ley Federal del Derecho de Autor (LFDA) de los Estados Unidos Mexicanos (México).

El uso de imágenes, fragmentos de videos, y demás material que sea objeto de protección de los derechos de autor, será exclusivamente para fines educativos e informativos y deberá citar la fuente donde la obtuvo mencionando el autor o autores. Cualquier uso distinto como el lucro, reproducción, edición o modificación, será perseguido y sancionado por el respectivo titular de los Derechos de Autor.

JURADO ASIGNADO

Presidente: Dr. Arteaga Pérez Marco Antonio

Secretario: Dr. Moreno Pérez Jaime Alberto

1er Vocal: Dr. Fridman Leonid

2do Vocal: Dr. Tang Xu Yu

3er Vocal: Dr. Dávila Montoya Jorge Ángel

Lugar donde se realizó la tesis:
POSGRADO DE INGENIERÍA, CIUDAD UNIVERSITARIA, CIUDAD DE MÉXICO

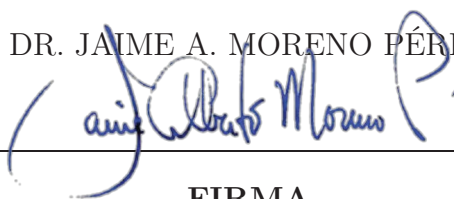
TUTORES DE TESIS:

DR. LEONID FRIDMAN



FIRMA

DR. JAIME A. MORENO PÉREZ



FIRMA

*Para Julieta,
mi mayor tesoro,
para que vea que los sueños si se cumplen
y luche siempre por su felicidad...*

Agradecimientos

Primero quiero agradecer a la Fundación Alberto y Dolores Andrade, por el apoyo y atención brindados a lo largo de 18 años.

Le doy gracias al CONACyT-SENER por el gran apoyo recibido en el CVU 624679, también al Programa UNAM-PAPIIT IN110719, IN115419 y proyecto 282013 de CONACyT.

Agradezco a todo el equipo del laboratorio de Modos Deslizantes de la UNAM, por su apoyo y amistad brindada en estos años.

También agradezco a mi comité tutorial, que cada semestre en la evaluación, me daban sus valiosos comentarios que fueron enriqueciendo mi trabajo.

Mas importante, es el agradecimiento a mis tutores, el Dr. Fridman y el Dr. Moreno, ya que sin su guía, enseñanza y apoyo, este logro no se hubiera realizado.

Por último, agradezco a todas las personas que me he encontrado en la vida que de alguna manera aportaron algo para que yo llegara hasta aquí, algunas siguen ahí y otras no, pero siempre seguirán en mi memoria.

México CDMX, Enero 2021.

Diego Gutiérrez Oribio



FIRMA

Abstract

In this PhD thesis, the design of robust controllers for two Classes of Underactuated Mechanical Systems of two DoF (Class-I and Class-III) is addressed. One of the controllers is able to drive the states of both Classes to the origin locally in finite-time, and the other controller stabilizes the origin globally asymptotically for the Class-I and locally asymptotically for the Class-III. The results were obtained despite the presence of matched Lipschitz perturbations and bounded uncertain control coefficient. Furthermore, the used sliding-modes algorithms have the discontinuity in an integral part, so the generated control signal is continuous and the chattering effect is attenuated. Simulations over the Reaction Wheel Pendulum, the TORA and the Cart-Pendulum systems and experimental validation over the Reaction Wheel Pendulum and the Cart-Pendulum systems are presented to validate the results.

Keywords. *Underactuated Systems, Continuous Higher-Order Sliding-Modes Control, Finite-Time convergence, Robust Control.*

Contents

List of Figures	xv
List of Tables	xvii
1 Introduction	1
1.1 State of the Art and Motivation	1
1.2 Problem Statement	3
1.3 General Objective	4
1.4 List of Contributions	5
1.5 Outline	5
2 Preliminaries	7
2.1 Sliding-Modes Control	7
2.1.1 First Generation	7
2.1.2 Second Generation	8
2.1.3 Third Generation	8
2.1.4 Fourth Generation	8
2.1.5 Fifth Generation	9
2.2 Homogeneity	9
2.2.1 Some properties of homogeneous functions	9
3 Control of Class-I of underactuated mechanical systems with two DoF	11
3.1 Class-I Model	11
3.1.1 Uncertain Model	13

3.1.2	Application Systems: RWP and TORA	14
3.2	Design of a Local Finite-Time Stabilizing (LFTS) Controller	17
3.2.1	Problem Statement	17
3.2.2	Controller Design	18
3.2.3	Gain design and scaling	20
3.2.4	Simulation Results	21
3.2.5	Experimental Validation: RWP System	23
3.3	Estimation of the Local Domain of Attraction: 3-RWP Case	24
3.3.1	Problem Statement	24
3.3.2	Controller Design	26
3.3.3	Simulation Results	28
3.3.4	Experimental Validation	29
3.4	Design of a Globally Asymptotically Stabilizing (GAS) Controller	31
3.4.1	Problem Statement	31
3.4.2	Controller Design	32
3.4.3	RWP Controller Design	34
3.4.4	TORA Controller Design	35
3.4.5	Simulation results	35
3.4.6	Experimental Validation: RWP System	37
3.5	Conclusions	40
4	Control of Class-III of underactuated mechanical systems with two DoF	43
4.1	Class-III Model	43
4.2	Design of a Local Finite-Time Stabilizing (LFTS) Controller	45
4.2.1	Problem Statement	45
4.2.2	Controller Design	47
4.2.3	Simulation Results	48
4.2.4	Experimental Validation	48
4.3	Design of a Local Asymptotic Stabilizing (LAS) Controller	50
4.3.1	Problem Statement	50
4.3.2	Controller Design	51

4.3.3	Simulation results	54
4.3.4	Experimental Validation	55
4.4	Conclusions	57
5	Conclusions	59
	Appendices	61
.1	Appendix A: Proof of Theorem 1 and 4	63
.2	Appendix B: LFTS Gain Selection	66
.3	Appendix C: Proof of Theorem 2	67
.4	Appendix D: Proof of Theorem 3 and 5	70
	Bibliography	73

List of Figures

3.1	Reaction wheel pendulum system.	14
3.2	TORA system.	16
3.3	Simulated states for the LFTS of the RWP.	22
3.4	Perturbation identification and uncertain control coefficient for the LFTS of the RWP simulations.	22
3.5	Continuous control signal for the LFTS of the RWP simulations.	22
3.6	Simulated states for the LFTS of the TORA.	23
3.7	Perturbation identification and uncertain control coefficient for the LFTS of the TORA simulations.	23
3.8	Continuous control signal for the LFTS of the TORA simulations.	24
3.9	Experimental values of the states for the LFTS of the RWP.	25
3.10	Continuous control signal for the LFTS of the RWP experiments.	25
3.11	Voltage control signal in the LFTS for the RWP experiments.	25
3.12	Equilibrium points of the RWP as function of 3-DIA's k_1	28
3.13	State trajectories in the 3-RWP simulations.	29
3.14	Perturbation identification in the 3-RWP simulations.	29
3.15	Control signal in the 3-RWP simulations.	30
3.16	State trajectories in the 3-RWP experiment.	30
3.17	Control signal in the 3-RWP experiment.	31
3.18	Voltage control signal in the 3-RWP experiment.	31
3.19	State trajectories in the GAS for the RWP simulations.	36
3.20	Finite-time state trajectories in the GAS for the RWP simulations.	36
3.21	Perturbation identification and uncertain control coefficient in the GAS for the RWP simulations.	37

3.22	Control signal in the GAS for the RWP simulations.	37
3.23	State trajectories in the GAS for the TORA simulations.	38
3.24	Finite-time state trajectories in the GAS for the TORA simulations.	38
3.25	Perturbation identification and uncertain control coefficient in the GAS for the TORA simulations.	38
3.26	Control signal in the GAS for the TORA simulations.	39
3.27	State trajectories in the GAS for the RWP experiments.	39
3.28	Finite-time state trajectories in the GAS for the RWP experiments.	40
3.29	Control signal in the GAS for the RWP experiments.	40
3.30	Voltage control signal in the GAS for the RWP experiments.	40
4.1	Cart-pendulum system.	44
4.2	Simulated states for the LFTS of the CP.	49
4.3	Perturbation identification and uncertain control coefficient for the LFTS of the CP simulations.	49
4.4	Continuous control signal for the LFTS of the CP simulations.	49
4.5	Experimental values of the states for the LFTS of the CP.	50
4.6	Voltage control signal in the LFTS for the CP experiments.	50
4.7	State trajectories in the LAS for the CP simulations.	55
4.8	Finite-time state trajectories in the LAS for the CP simulations.	55
4.9	Perturbation identification and uncertain control coefficient in the LAS for the CP simulations.	55
4.10	Control signal in the LAS for the CP simulations.	56
4.11	State trajectories in the LAS for the CP experiments.	56
4.12	Finite-time state trajectories in the LAS for the CP experiments.	57
4.13	Voltage control signal in the LAS for the CP experiments.	57
1	Level surfaces of the Lyapunov function.	69

List of Tables

3.1	Parameters of the Reaction Wheel Pendulum system	16
3.2	Parameters of the TORA system	17
3.3	Set of gains for the 4-DIA	20
4.1	Parameters of the Cart-Pendulum System	45

Chapter 1

Introduction

1.1 State of the Art and Motivation

Underactuated mechanical systems have less control inputs than degrees of freedom (DoF). Control design is a challenging task for this class of systems, which are numerous and very useful in practice. Some examples are given by aircraft and spacecraft vehicles, helicopters, flexible-link and mobile robots, locomotive systems, snake-type and swimming robots, acrobatic robots, satellites, surface vessels, and underwater vehicles. Many aspects are discussed in the Survey paper [31], that also contains a vast literature.

Underactuation may appear due to several reasons:

1. The natural dynamics of the system, as e.g. in aircraft, spacecraft and underwater vehicles, helicopters, and locomotive systems without wheels.
2. Due to the failure of an actuator in an otherwise full actuated system.
3. By design with the purpose of illustrating some features of this class of systems: the Acrobot, the Pendubot, the Cart-Pendulum system (CP), the Furuta Pendulum, the TORA system, the Reaction Wheel Pendulum (RWP).

The last underactuated mechanical systems from the previous lists, can be seen as pendulum-like systems. The study of the pendulum has been one of the most studied topics of the control theory, due to its nonlinear dynamics and unstable equilibrium points, for example. The application of these systems can be found in the missile control, cranes and transport vehicles (like the Segway) stability and in biomechanics (gait, balance and human posture).

Since underactuated systems are not globally feedback linearizable (see e.g. [42]), the control design for these pendulum-like systems, is usually separated in two tasks: First swinging-up from the downward position to (a neighborhood of) the upright position of the pendulum, and then switching to a (local) stabilizing controller. This includes swing up control using energy-based methods for the RWP [57] and [3], the Acrobot [54],

the Pendubot [56], the cart-pendulum system [8] and the Furuta pendulum [4]. With respect to the stabilizing controller, some examples are partial linearization methods [52, 53], passivity-based methods [21] and Energy-Shaping Method [1, 69], using small nested saturations [61], stabilization by output feedback [62], discontinuous stabilizing feedback [46], adaptive control [17], PD control [44] and LQR [66] control, and sliding-mode control techniques [68, 3, 60, 20, 18].

The local stabilizing controller in the previous approaches can be designed using a *local feedback linearization* design. However, these controllers can be applied only locally, since they possess singularities. A way to overcome this difficulty and to arrive at a *Global controller* for a class of underactuated mechanical systems of two DoF is to find a partially linearizing output that renders the zero dynamics asymptotically stable (see [16, 30] and the references therein). In this case stabilizing the linearized subsystem results in a global asymptotic stabilization. However, this approach is not useful when the zero dynamics is not asymptotically stable. Olfati-Saber [40, 42, 43] has gone one step further and has classified the underactuated mechanical systems (having some symmetries) in eight classes, according to the properties of the normal form to which they can be globally transformed. In particular, systems with two DoF belonging to the *Class-I* in Olfati-Saber's classification, can be globally transformed to a partially linearized system in strict feedback form. In this case the zero dynamics can be globally stabilized using a virtual control variable and a back-stepping design leads to global stabilization of the equilibrium point [42, 43]. Moreover, in [42] the non-linearities are supposed to be fully compensated so that the stabilization can be performed through a linear controller. For other classes in Olfati-Saber's taxonomy a *global* control design method has been also proposed [42].

A major drawback of these global results [40, 42, 43] is that they do not consider the action of external disturbances and/or the effect of model or parameter uncertainties. They also rely on full compensation of the system's non linearities, which is clearly hardly achieved in a real set-up. Dealing with non constant uncertainties and/or disturbances requires a Robust Control strategy, such as e.g. Sliding-Mode Control. Paper [70] proposes a First-Order Sliding-Mode strategy for underactuated systems, that aim at dealing with the uncertainties/perturbations. This approach has two main disadvantages: (i) Since the control law is discontinuous, the *chattering effect* can be prohibitive for a real application. (ii) The whole design is based on a form which is valid only *locally*, and so no global results are obtained. The effect of chattering can be eventually attenuated by using Higher-Order Sliding-Mode controllers. This has been studied in several works as e.g. [47, 10, 11, 23, 32]. However, these works only achieve *local* stabilization, and they are based on the modification of a First-Order Sliding-Mode control strategy.

Continuous Higher-Order Sliding-Mode Algorithms (CHOSMA, see [7, 12, 24, 63, 38, 39]) are a class of homogeneous sliding mode controllers capable of compensating Lipschitz uncertainties and/or perturbations theoretically exactly, but using a continuous control signal. When the actuator is fast (see [45]), the chattering effect caused by the discontinuity and discretization is strongly attenuated.

These algorithms consist in a static homogeneous finite-time controller for the nominal model of the system and a discontinuous integral action, aimed at estimating and compensating the uncertainties and perturbations. They are an extension of the (classical) Super-Twisting ([25, 26, 48, 49]), and are related to the Continuous Twisting Algorithm (CTA) ([36, 35, 65]) and Discontinuous Integral Algorithm (DIA) ([38], [39]).

1.2 Problem Statement

Consider a mechanical system having as configuration vector $q = [q_1, q_2]^T$, an inertia matrix depending only on q_2 , *i.e.*, $M = M(q_2)$. Its Lagrangian is

$$L(q, \dot{q}) = \frac{1}{2} \dot{q}^T \begin{bmatrix} m_{11}(q_2) & m_{12}(q_2) \\ m_{21}(q_2) & m_{22}(q_2) \end{bmatrix} \dot{q} - V(q), \quad (1.1)$$

where $V(q)$ is the potential energy of the system, and the Euler-Lagrange equations of motion are

$$\begin{aligned} m_{11}(q_2)\ddot{q}_1 + m_{12}(q_2)\ddot{q}_2 + d_{11}(q_2)\dot{q}_1\dot{q}_2 + d_{12}(q_2)\dot{q}_2^2 - g_1(q_1, q_2) &= \tau_1, \\ m_{21}(q_2)\ddot{q}_1 + m_{22}(q_2)\ddot{q}_2 - \frac{1}{2}d_{21}(q_2)\dot{q}_1^2 + \frac{1}{2}d_{22}(q_2)\dot{q}_2^2 - g_2(q_1, q_2) &= \tau_2, \end{aligned} \quad (1.2)$$

where $g_i(q_1, q_2) = -\frac{\partial V(q)}{\partial q_i}$, $i = 1, 2$ and $d_i(q_2) = \frac{d}{dq_2}m_i(q_2)$.

Olfati-Saber [42, 43] has classified the underactuated mechanical systems in eight classes, according to the properties of the normal form to which they can be transformed. In the system (1.2), if $\tau_1 = 0$, *i.e.*, the actuated variable is q_2 , the system is named as Class-I. On the contrary, if $\tau_2 = 0$, *i.e.*, the actuated variable is q_1 , $m_{11}(q_2)$ is constant, and $V(q_2)$, the system is named as Class-III. Due to the fact that these two classes have only one input and two DoF, they are underactuated systems.

Although underactuated (mechanical) systems are not globally state feedback linearizable, it is possible to obtain a partial feedback linearization [34, 40, 43, 16, 30] and transform the system (1.2) (at least locally) in

$$\begin{aligned} \dot{z}_1 &= \rho_1(z), \\ \dot{z}_2 &= \rho_2(z), \\ \dot{z}_3 &= z_4, \\ \dot{z}_4 &= u. \end{aligned} \quad (1.3)$$

For the Class-I, in [42, 43] it is proposed a back-stepping approach to globally stabilize the equilibrium point $z = 0$ using a continuous control u . The problem with this, is that in presence of parameter or dynamics uncertainties as well as external perturbations, the

nominal model (1.3) is no longer valid. A more appropriate model can be given by the equations

$$\begin{aligned}\dot{z}_1 &= \rho_1(z), \\ \dot{z}_2 &= \rho_2(z), \\ \dot{z}_3 &= z_4, \\ \dot{z}_4 &= \beta(t, z) [u + \varphi(t)] ,\end{aligned}\tag{1.4}$$

where $\beta(t, z)$ is an uncertain control coefficient and $\varphi(t)$ is a perturbation term. Now, the task to design a robust controller able to reject these new terms, is crucial to stabilize the origin of the system.

For the Class-III, in [68] it is designed a robust controller to locally stabilize the origin of the system when $\beta(t, z) = 1$ and $|\varphi(t)| \leq M$. Now, the problem with this approach is the use of a First Order Sliding-Mode control, meaning, a discontinuous control signal u . The use of such controllers may cause damage on the actuators of a real plant with the *chattering* effect.

1.3 General Objective

The objective of this work is to design *robust* controllers for the Class-I and Class-III of underactuated mechanical systems of two DoF, presented in [42], using a continuous HOSM strategy. Two kinds of controller designs are presented:

1. One based on a model of the systems valid only locally. The controller generates a fifth-order sliding-mode and achieves Local Finite-Time Stability (LFTS).
2. The other uses the globally valid cascade normal form proposed in [40, 42, 43] for the Class-I and the locally valid cascade normal form proposed in [68], to design a robust controller that provides Global Asymptotic Stability (GAS) for the Class-I and Local Asymptotic Stability (LAS) for the Class-III. A third-order sliding manifold is generated, that is reached in finite-time, but the convergence to the equilibrium is asymptotic.

All these controllers are able to compensate matched Lipschitz disturbances and/or uncertainties, coping with an uncertain control coefficient and generating a *continuous* control signal, possibly reducing the chattering effect. The proposed strategy is valid for the whole Class-I systems, but the cases of study presented in this thesis are the RWP and the TORA systems for the Class-I, both as full fourth order systems. The Class-III only contains the CP system and is contained as case of study. Finally, evidence of the performance of the controllers is provided, in simulations for the RWP, the TORA and CP systems, and through experiments carried on in laboratory setup of the real RWP and CP systems.

1.4 List of Contributions

- Robust local finite-time stabilization of the Class-I origin.
- Design of the Fourth Order Discontinuous Integral Algorithm gains.
- Numerical estimation of the attraction domain of the Third Order Discontinuous Integral Algorithm and the Reaction Wheel Pendulum.
- Robust global asymptotic stabilization of the Class-I origin.
- Robust local finite-time stabilization of the Class-III origin.
- Robust local asymptotic stabilization of the Class-III origin, valid when the pendulum position lies in the interval $(-\pi/2, \pi/2)$.
- Simulations and experimental validation of the presented control strategies.

1.5 Outline

Some useful Preliminaries for the reader are presented in Section 2. The presentation of the Class-I, the systems belonging to such class considered in this work as the cases of study (the RWP and the TORA systems), and the design of the robust controllers for this Class, are given in Section 3. The presentation of the Class-III, the system belonging to such class as the case of study (the CP system), and the design of the robust controllers for this Class, are given in Section 4. Each Section presents simulations of the controller and experimental validation on the RWP system and the CP system. Conclusions of this thesis are presented in Section 5. The proofs of the Theorems presented throughout the work are presented in the Appendices.

Notation: Define the function $[\cdot]^\gamma := |\cdot|^\gamma \text{sign}(\cdot)$, for any $\gamma \in \mathbb{R}_{\geq 0}$.

Chapter 2

Preliminaries

2.1 Sliding-Modes Control

Control in the presence of uncertainties and perturbations is one of the main topics of modern control theory. These dynamics mostly come from external disturbances, unknown plant parameters, and parasitic dynamics. Designing control laws that provide the desired closed-loop system performance in the presence of these disturbances/uncertainties is a very challenging task for a control engineer. This has led to intense interest in the development of the so-called robust control methods, which are supposed to solve this problem [51]. One of these robust control is the so-called Sliding-Modes Control (SMC).

In the next sections, a brief history of the algorithms developed in the SMC theory is presented (see [15] for more details).

2.1.1 First Generation

The classical theory of first order SMC (FOSM) was established by 1980 and later reported in Prof. Utkin's monograph in Russian, in 1981 (english version [67]). Consider a first order uncertain system

$$\dot{\sigma} = \beta(t, \sigma) [u + \varphi(t, \sigma)]. \quad (2.1)$$

Here, and always below, the solution of all the systems will be understood in the sense of A. Filippov [14].

In the FOSM control design, $\sigma = 0$ (sliding surface) is designed and the control $u(\sigma)$ takes the form of a discontinuous (relay or unit) controller ensuring the sliding-modes (σ stays in zero despite the presence of bounded and positive β and bounded φ). Nevertheless, the main disadvantage of the FOSM is discontinuous control and the chattering effect.

2.1.2 Second Generation

In order to compensate the chattering effect, in the early 80's, the second order sliding modes (SOSM) concept was introduced in the Ph.D. dissertation of A. Levant. Consider a second order uncertain system

$$\ddot{\sigma} = \beta(t, \sigma, \dot{\sigma}) [u + \varphi(t, \sigma, \dot{\sigma})].$$

The objective of the SOSM is to design the control $u(\sigma, \dot{\sigma})$ able to drive $\sigma = \dot{\sigma} = 0$ in finite-time, despite the presence of bounded and positive β and bounded φ . Examples of SOSM controls are the Twisting Algorithm [13] and the Terminal Algorithm [33]. However, the main disadvantage of the SOSM is that the discontinuous control and the chattering effect still persist in systems with relative degree two.

2.1.3 Third Generation

The Super-Twisting Algorithm (STA) [25]

$$\begin{aligned} u &= -k_1 [\sigma]^{\frac{1}{2}} + \zeta, \\ \dot{\zeta} &= -k_2 [\sigma]^0, \end{aligned}$$

can drive $\sigma = \dot{\sigma} = 0$ in finite-time, despite the presence of bounded and positive β and Lipschitz φ for the system (2.1).

The main advantages of the STA are the use of a continuous control signal u and that it can be used to differentiate a signal [29]. Nevertheless, the main disadvantage of the STA is that the design of a sliding surface is still needed in systems with relative degree $r \geq 2$.

2.1.4 Fourth Generation

Consider an uncertain system of order n

$$\sigma^{(n)} = \beta(t, \sigma, \dot{\sigma}, \dots, \sigma^{(n-1)}) [u + \varphi(t, \sigma, \dot{\sigma}, \dots, \sigma^{(n-1)})]. \quad (2.2)$$

The objective of the algorithms in this generation, is to design the control $u(\sigma, \dot{\sigma}, \dots, \sigma^{(n-1)})$ able to drive $\sigma = \dot{\sigma} = \dots = \sigma^{(n-1)} = 0$ in finite-time, despite the presence of bounded and positive β and bounded φ . An example of these controls are the Nested Arbitrary Order Sliding-Mode Controllers [27].

The main advantage of these algorithms is that they don't put a restriction over the relative degree of the system. Nevertheless, they still use a discontinuous control signal.

2.1.5 Fifth Generation

Based on the STA, consider the Continuous Higher-Order Sliding-Mode (CHOSM) control as

$$\begin{aligned} u &= \rho_1(\sigma, \dot{\sigma}, \dots, \sigma^{(n-1)}) + \zeta, \\ \dot{\zeta} &= \rho_2(\sigma, \dot{\sigma}, \dots, \sigma^{(n-1)}), \end{aligned}$$

where $\rho_2(\sigma, \dot{\sigma}, \dots, \sigma^{(n-1)})$ is a discontinuous signal. CHOSM are able to stabilize $\sigma = \dot{\sigma} = \dots = \sigma^{(n-1)} = 0$ in finite-time, despite the presence of bounded and positive β and Lipschitz φ for the system (2.2). Note that CHOSM have a continuous control signal and this can attenuate the chattering effect.

Examples of CHOSM are the Continuous Twisting Algorithm (CTA) ([36, 35, 65]) and the Discontinuous Integral Algorithm (DIA) ([38], [39]).

2.2 Homogeneity

For a vector $x = (x_1, \dots, x_n) \in \mathbb{R}^n$ the *dilation operator* is the family of linear transformations defined by $\Delta_\epsilon^{\mathbf{r}}x = (\epsilon^{r_1}x_1, \dots, \epsilon^{r_n}x_n)$, $\forall \epsilon > 0$. For $i = 1, \dots, n$, $r_i > 0$ is the *weight* of the component x_i and $\mathbf{r} = (r_1, \dots, r_n)$ is the vector of weights. A function $V : \mathbb{R}^n \rightarrow \mathbb{R}$ (respectively, a vector field $f : \mathbb{R}^n \rightarrow \mathbb{R}^n$, or vector-set $F(x) \subset \mathbb{R}^n$) is called \mathbf{r} -homogeneous of *degree* $m \in \mathbb{R}$ if for all $x \in \mathbb{R}^n$ and all $\epsilon > 0$ $V(\Delta_\epsilon^{\mathbf{r}}x) = \epsilon^m V(x)$ holds (respectively, $f(\Delta_\epsilon^{\mathbf{r}}x) = \epsilon^m \Delta_\epsilon^{\mathbf{r}}f(x)$, $F(\Delta_\epsilon^{\mathbf{r}}x) = \epsilon^m \Delta_\epsilon^{\mathbf{r}}F(x)$) [5, 38].

For a given vector \mathbf{r} , the homogeneous norm is defined by $\|x\|_{\mathbf{r},p} := \left(\sum_{i=1}^n |x_i|^{\frac{p}{r_i}} \right)^{\frac{1}{p}}$, $\forall x \in \mathbb{R}^n$, for any $p \geq 1$. The set $S = \{x \in \mathbb{R}^n : \|x\|_{\mathbf{r},p} = 1\}$ is the homogeneous unit sphere [5].

2.2.1 Some properties of homogeneous functions

Let V_1 and V_2 two continuously differentiable \mathbf{r} -homogeneous functions (respectively, a vector field f_1) of degree m_1, m_2 (respectively, l_1), then [5]:

- (i) $V_1 V_2$ is homogeneous of degree $m_1 + m_2$,
- (ii) There exist a constant $c_1 > 0$, such that $V_1 \leq c_1 \|x\|_{\mathbf{r},p}^{m_1}$, moreover if V_1 is positive definite, there exists c_2 such that $V_1 \geq c_2 \|x\|_{\mathbf{r},p}^{m_1}$,
- (iii) $\partial V_1(x)/\partial x_i$ is homogeneous of degree $m_1 - r_i$,
- (iv) $L_f V_1(x)$, the Lie derivative of V_1 along f , is homogeneous of degree $m_1 + l_1$.

The following property of *continuous* homogeneous functions is well-known.

Lemma 1 [2, 38] *Let $\eta : \mathbb{R}^n \rightarrow \mathbb{R}$ and $\gamma : \mathbb{R}^n \rightarrow \mathbb{R}$ two homogeneous and continuous functions, with the same weights $\mathbf{r} = (r_1, \dots, r_n)$ and degree m . Let $\gamma(x) \geq 0$ for all $x \in \mathbb{R}^n$ and suppose that*

$$\{x \in \mathbb{R}^n \setminus \{0\} \mid \gamma(x) = 0\} \subseteq \{x \in \mathbb{R}^n \setminus \{0\} \mid \eta(x) > 0\}.$$

Then, there exists a real number λ^ so that, for all $\lambda > \lambda^*$, for all $x \in \mathbb{R}^n \setminus \{0\}$ and for some $c > 0$, it is true that*

$$\eta(x) + \lambda\gamma(x) \geq c\|x\|_{\mathbf{r},p}^m.$$

The previous Lemma 1 requires the functions to be *continuous*. The following lemma, proven in [9], extends this result to *semi-continuous* functions. This permits to handle multivalued functions.

Lemma 2 [9] *Let $\eta : \mathbb{R}^n \rightarrow \mathbb{R}$ and $\gamma : \mathbb{R}^n \rightarrow \mathbb{R}$ two homogeneous and lower semi-continuous single-valued functions, with the same weights $\mathbf{r} = (r_1, \dots, r_n)$ and degree m . Let $\gamma(x) \geq 0$ for all $x \in \mathbb{R}^n$ and suppose that*

$$\{x \in \mathbb{R}^n \setminus \{0\} \mid \gamma(x) = 0\} \subseteq \{x \in \mathbb{R}^n \setminus \{0\} \mid \eta(x) > 0\}.$$

Then there exists a real number λ^ so that, for all $\lambda > \lambda^*$, for all $x \in \mathbb{R}^n \setminus \{0\}$ and for some $c > 0$, it is true that*

$$\eta(x) + \lambda\gamma(x) \geq c\|x\|_{\mathbf{r},p}^m.$$

We will make use of the following property of the "power-signed" function $\lceil x \rceil^\beta$, $\beta > 0$, which is a consequence of its monotonicity: For any real numbers $x \neq y \in \mathbb{R}$, $(\lceil x + y \rceil^\beta - \lceil x \rceil^\beta) x > 0$. As a consequence

$$\text{sign}\left(\lceil x + y \rceil^\beta - \lceil y \rceil^\beta\right) = \text{sign}(x), \quad \beta > 0. \quad (2.3)$$

Chapter 3

Control of Class-I of underactuated mechanical systems with two DoF

3.1 Class-I Model

Class-I of underactuated mechanical system of two Degrees-of-Freedom (DoF), having as configuration vector $q = [q_1, q_2]^T$, have an inertia matrix depending only on q_2 , *i.e.*, $M = M(q_2)$, and the variable q_2 is actuated. The Lagrangian is

$$L(q, \dot{q}) = \frac{1}{2} \dot{q}^T \begin{bmatrix} m_{11}(q_2) & m_{12}(q_2) \\ m_{21}(q_2) & m_{22}(q_2) \end{bmatrix} \dot{q} - V(q), \quad (3.1)$$

where $V(q)$ is the potential energy of the system, and the Euler-Lagrange equations of motion are

$$\begin{aligned} m_{11}(q_2)\ddot{q}_1 + m_{12}(q_2)\ddot{q}_2 + d_{11}(q_2)\dot{q}_1\dot{q}_2 + d_{12}(q_2)\dot{q}_2^2 - g_1(q_1, q_2) &= 0, \\ m_{21}(q_2)\ddot{q}_1 + m_{22}(q_2)\ddot{q}_2 - \frac{1}{2}d_{21}(q_2)\dot{q}_1^2 + \frac{1}{2}d_{22}(q_2)\dot{q}_2^2 - g_2(q_1, q_2) &= \tau, \end{aligned} \quad (3.2)$$

where $g_i(q_1, q_2) = -\frac{\partial V(q)}{\partial q_i}$, $i = 1, 2$ and $d_i(q_2) = \frac{d}{dq_2}m_i(q_2)$.

Using the global change of variables

$$\begin{aligned} x_1 &:= q_1, \\ x_2 &:= \dot{q}_1, \\ x_3 &:= q_2, \\ x_4 &:= \dot{q}_2, \end{aligned} \quad (3.3)$$

the system achieves the state space representation

$$\begin{aligned}
 \dot{x}_1 &= x_2, \\
 \dot{x}_2 &= -\frac{m_{22}(x_3) [d_{11}(x_3)x_2x_4 + d_{12}(x_3)x_4^2 - g_1(x_1, x_3)]}{\eta(x_3)} \\
 &\quad - \frac{m_{12}(x_3) \left[\frac{1}{2}d_{21}(x_3)x_2^2 - \frac{1}{2}d_{22}(x_3)x_4^2 + g_2(x_1, x_3) + \tau \right]}{\eta(x_3)}, \\
 \dot{x}_3 &= x_4, \\
 \dot{x}_4 &= \frac{m_{21}(x_3) [d_{11}(x_3)x_2x_4 + d_{12}(x_3)x_4^2 - g_1(x_1, x_3)]}{\eta(x_3)} + \\
 &\quad \frac{m_{11}(x_3) \left[\frac{1}{2}d_{21}(x_3)x_2^2 - \frac{1}{2}d_{22}(x_3)x_4^2 + g_2(x_1, x_3) + \tau \right]}{\eta(x_3)}
 \end{aligned} \tag{3.4}$$

where $\eta(x_3) = m_{11}(x_3)m_{22}(x_3) - m_{12}(x_3)m_{21}(x_3) > 0$.

System (3.4) can be transformed *globally* to a cascade normal form.

Proposition 3 [42, Proposition 3.9.1],[43, Theorem 1] *Consider the Class-I underactuated system with two DoF (3.4). Then the following global change of coordinates, obtained from the Lagrangian of the system,*

$$\begin{aligned}
 z_1 &= x_1 + \gamma(x_3), \\
 z_2 &= m_{11}(x_3)x_2 + m_{12}(x_3)x_4, \\
 z_3 &= x_3, \\
 z_4 &= x_4,
 \end{aligned} \tag{3.5}$$

transforms the dynamics of the system into a cascade nonlinear system in strict feedback form

$$\begin{aligned}
 \dot{z}_1 &= \frac{z_2}{m_{11}(z_3)}, \\
 \dot{z}_2 &= g_1(z_1 - \gamma(z_3), z_3), \\
 \dot{z}_3 &= z_4, \\
 \dot{z}_4 &= u,
 \end{aligned} \tag{3.6}$$

where

$$\gamma(x_3) = \int_0^{x_3} \frac{m_{12}(\theta)}{m_{11}(\theta)} d\theta, \quad g_1(q_1, q_2) = -\frac{\partial V(q)}{\partial q_1}, \tag{3.7}$$

and u is the new control variable obtained from a collocated partial feedback linearization (see [52, 55])

$$\begin{aligned}
 \tau &= \frac{\eta(z_3)u - m_{21}(z_3) \left[d_{11}(z_3) \left[\frac{z_2 - m_{12}(z_3)z_4}{m_{11}(z_3)} \right] z_4 + d_{12}(z_3)z_4^2 - g_1(z_1 - \gamma(z_3), z_3) \right]}{m_{11}(z_3)} \\
 &\quad - \frac{1}{2}d_{21}(z_3) \left[\frac{z_2 - m_{12}(z_3)z_4}{m_{11}(z_3)} \right]^2 + \frac{1}{2}d_{22}(z_3)z_4^2 - g_2(z_1 - \gamma(z_3), z_3).
 \end{aligned} \tag{3.8}$$

System (3.6) is in the Byrnes-Isidori Normal Form, with the zero dynamics subsystem (z_1, z_2) . Although it is not assumed that the system is strictly minimum phase, since it is in strict feedback form, the (global) stabilization of the whole system reduces to the (global) stabilization of the zero dynamics. This characterizes this Class-I systems.

3.1.1 Uncertain Model

In presence of parameter or dynamics uncertainties as well as external perturbations, the nominal model (3.6) is no longer valid. A more appropriate model can be given by the equations

$$\begin{aligned}\dot{z}_1 &= \frac{z_2}{m_{11}(z_3)} + \delta_1(z), \\ \dot{z}_2 &= g_1(z_1 - \gamma(z_3), z_3) + \delta_2(z), \\ \dot{z}_3 &= z_4 + \delta_3(z), \\ \dot{z}_4 &= \beta(t, z) [u + \varphi(t)] + \delta_4(z),\end{aligned}$$

where the terms $\delta_i(z)$ represent vanishing perturbations, i.e. $\delta_i(0) = 0$, while the uncertain control coefficient $\beta(t, z)$ and the matching perturbation term $\varphi(t)$ are assumed to be bounded (without changing sign) and Lipschitz continuous as a function of time, respectively, i.e.

$$0 < b_m \leq |\beta(t, z)| \leq b_M, \quad \left| \frac{d\varphi(t)}{dt} \right| \leq L. \quad (3.9)$$

In what follows it will be only considered the non-vanishing perturbation $\varphi(t)$ and the uncertain control coefficient $\beta(t, z)$, that is, we use the uncertain model

$$\begin{aligned}\dot{z}_1 &= \frac{z_2}{m_{11}(z_3)}, \\ \dot{z}_2 &= g_1(z_1 - \gamma(z_3), z_3), \\ \dot{z}_3 &= z_4, \\ \dot{z}_4 &= \beta(t, z) [u + \varphi(t)],\end{aligned} \quad (3.10)$$

to design the controllers. It is well-known (see e.g. [22, Chapter 9] for smooth nonlinear systems, or [6, Corollary 5.5] for homogeneous systems) that for sufficiently small and vanishing perturbations with a triangular structure, i.e. $|\delta_i(z)| \leq \epsilon \|(z_1, \dots, z_i)\|$, if the origin of the system (3.10) is Asymptotically Stable (GAS) so is also the origin of the perturbed system. Further details of these results are not provided here.

The presence of the non-vanishing perturbation $\varphi(t)$ in (3.10) prevents a continuous static state-feedback controller to achieve convergence to the origin $z = 0$. The objective in this chapter is to design *dynamic and homogeneous* state-feedback controllers that are able to stabilize the origin $z = 0$ despite of the presence of the Lipschitz perturbation term $\varphi(t)$,

and the uncertain control coefficient $\beta(t, z)$, and using a *continuous* control signal $u(t)$. It is used a *local* homogeneous approximation of system (3.10) to design a *locally finite-time* stabilizing dynamic controller in Section 3.2. In Section 3.3, a numerical estimation of the Local Domain of Attraction for the third order Reaction Wheel Pendulum (3-RWP) with the locally finite-time stabilizing dynamic controller is performed. This is neglecting the wheel position, for practical purposes, and achieving the swing-up and stabilization of the system in one step. For *global* (asymptotic) stabilization of the origin $z = 0$, it is used the globally valid model (3.10) to design a *dynamic and homogeneous* feedback controller in Section 3.4. This extends the results presented in [40, 42, 43]. In the next paragraphs it is presented two examples of Class-I systems, that will be used to illustrate the results in simulations and experiments.

3.1.2 Application Systems: RWP and TORA

The Acrobot, the Reaction Wheel Pendulum (RWP), and the Translational Oscillator with Rotational Actuator (TORA) systems are all Class-I underactuated systems and can be globally transformed into the form (3.6) using an explicit global change of coordinates (3.5) [42, Corollary 3.9.1]. In this work the RWP and the TORA will be studied and controlled, so their dynamics will be presented in the following sections.

Reaction Wheel Pendulum (RWP)

Consider the RWP shown in Fig. 3.1. This figure describes a pendulum rotating in a vertical plane and its pivot pin is mounted in a stationary base. The pivot pin of the wheel is attached to the pendulum. The axes of rotation of the pendulum and the wheel are parallel to each other. The wheel is actuated by the torque τ [Nm]. The states vector is $x = [x_1, x_2, x_3, x_4]^T$, where x_1 [rad] is the angle between the upward direction and the pendulum, which is measured counter-clockwise ($x_1 = 0$ for the upright position of the pendulum), x_2 [rad/s] is the pendulum angular velocity, x_3 [rad] is the wheel angular position, and x_4 [rad/s] is the wheel angular velocity.

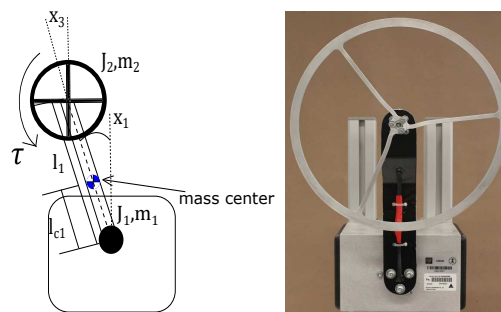


Figure 3.1: Reaction wheel pendulum system.

The system dynamics was originally presented in [58] and can be described by the

following equations:

$$\begin{aligned}
\dot{x}_1 &= x_2, \\
\dot{x}_2 &= \frac{d_{22}W \sin(x_1) + d_{12}b_2x_4 - d_{12}\tau}{D}, \\
\dot{x}_3 &= x_4, \\
\dot{x}_4 &= \frac{-d_{21}W \sin(x_1) - d_{11}b_2x_4 + d_{11}\tau}{D},
\end{aligned} \tag{3.11}$$

where

$$\begin{aligned}
d_{21} = d_{12} = d_{22} = J_2, & & d_{11} = m_1l_{c1}^2 + m_2l_1^2 + J_1 + J_2 \\
D = d_{11}d_{22} - d_{12}d_{21} > 0, & & \bar{m} = m_1l_{c1} + m_2l_1, & & W = \bar{m}g.
\end{aligned}$$

According to Proposition 3 the following global change of coordinates (similar to the one used in [41])

$$\begin{aligned}
z_1 &= d_{11}x_1 + d_{12}x_3, \\
z_2 &= d_{11}x_2 + d_{12}x_4, \\
z_3 &= x_1, \\
z_4 &= x_2,
\end{aligned} \tag{3.12}$$

brings the RWP system to the cascade form

$$\begin{aligned}
\dot{z}_1 &= z_2, \\
\dot{z}_2 &= W \sin(z_3), \\
\dot{z}_3 &= z_4, \\
\dot{z}_4 &= \frac{d_{22}W \sin(z_3) + b_2(z_2 - d_{11}z_4) - d_{12}\tau}{D}.
\end{aligned} \tag{3.13}$$

The feedback control transformation

$$\tau = \frac{d_{22}W \sin(z_3) + b_2(z_2 - d_{11}z_4) - Du}{d_{12}}, \tag{3.14}$$

partially linearizes the system, and we obtain the normal form (3.6)

$$\begin{aligned}
\dot{z}_1 &= z_2, \\
\dot{z}_2 &= W \sin(z_3), \\
\dot{z}_3 &= z_4, \\
\dot{z}_4 &= \beta(t, z) [u + \varphi(t)].
\end{aligned} \tag{3.15}$$

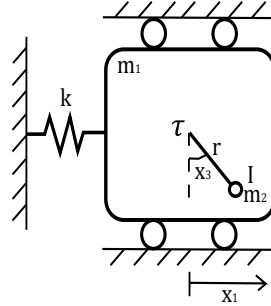
The used system parameters were obtained with an off-line identification algorithm and they are given in Table 3.1.

Table 3.1: Parameters of the Reaction Wheel Pendulum system

Name	Description	Value
\bar{m}	Equivalent mass of the system	0.191[kgm]
d_{11}	Equivalent moment of inertia of the system	0.0543[kgm ²]
J_2	Moment of inertia of the wheel	0.0027[kgm ²]
b_2	Friction coefficient of the wheel	0.01[Ns/m ²]
g	Acceleration of the gravity	9.81[m/s ²]

Translational Oscillator with Rotational Actuator (TORA)

Consider the TORA system shown in Fig. 3.2. This figure describes a pendulum rotating in a vertical plane and its pivot pin is mounted in a mass m_1 . The actuation on the pendulum by the torque τ [Nm] makes the mass to move in a translational manner. The states vector is $x = [x_1, x_2, x_3, x_4]^T$, where x_1 [m] is the position of the mass m_1 , x_2 [m/s] is the velocity, x_3 [rad] is the angle between the downward direction and the pendulum, which is measured counter-clockwise ($x_3 = 0$ for the downright position of the pendulum), and x_4 [rad/s] is the pendulum angular velocity.

**Figure 3.2:** TORA system.

The system's dynamics can be described by the following equations:

$$\begin{aligned}
 \dot{x}_1 &= x_2, \\
 \dot{x}_2 &= -\frac{\eta_1(kx_1 - \eta_3x_4^2) + \eta_2(\tau - g\eta_3)}{\eta_4}, \\
 \dot{x}_3 &= x_4, \\
 \dot{x}_4 &= \frac{\eta_2(kx_1 - \eta_3x_4^2) + (m_1 + m_2)(\tau - g\eta_3)}{\eta_4},
 \end{aligned} \tag{3.16}$$

where

$$\eta_1 = m_2r^2 + I, \quad \eta_2 = m_2r \cos(x_3), \quad \eta_3 = m_2r \sin(x_3), \quad \eta_4 = (m_1 + m_2)\eta_1 - \eta_2^2 > 0.$$

The global change of coordinates

$$\begin{aligned}
 z_1 &= x_1 + \frac{\eta_3}{m_1 + m_2}, \\
 z_2 &= (m_1 + m_2)x_2 + \eta_2 x_4, \\
 z_3 &= x_3, \\
 z_4 &= x_4,
 \end{aligned} \tag{3.17}$$

together with the feedback transformation

$$\tau = \frac{\eta_3 u - \eta_2 (kx_1 - m_2 r z_4^2 \sin(z_3))}{m_1 + m_2} + m_2 g r \sin(z_3), \tag{3.18}$$

bring the system to the normal form (3.6)

$$\begin{aligned}
 \dot{z}_1 &= \frac{z_2}{m_1 + m_2}, \\
 \dot{z}_2 &= -kz_1 + \frac{km_2 r \sin(z_3)}{m_1 + m_2}, \\
 \dot{z}_3 &= z_4, \\
 \dot{z}_4 &= \beta(t, z) [u + \varphi(t)].
 \end{aligned} \tag{3.19}$$

The used system parameters are the same as in [42], and are given in Table 3.2.

Table 3.2: Parameters of the TORA system

Name	Description	Value
m_1	Mass of the platform	10 [kg]
m_2	Mass of the pendulum	1 [kg]
k	Coefficient of the spring	5 [kg/s ²]
r	Length of the pendulum	1 [Ns/m ²]
I	Moment of inertia of the pendulum	1 [kgm ²]
g	Acceleration of the gravity	9.81 [m/s ²]

3.2 Design of a Local Finite-Time Stabilizing (LFTS) Controller

3.2.1 Problem Statement

In this section, it is performed the design of a controller to attain *local finite-time* stability of the origin $z = 0$ of the uncertain system (3.10). Since it will be used for u homogeneous

controllers, it is considered the following *local homogeneous* approximation of system (3.10) for this purpose

$$\begin{aligned}
 \dot{z}_1 &= \alpha_1 z_2, \\
 \dot{z}_2 &= \alpha_2 z_3, \\
 \dot{z}_3 &= z_4, \\
 \dot{z}_4 &= \beta(t, z) [u + \varphi(t)] ,
 \end{aligned} \tag{3.20}$$

where $\alpha_1, \alpha_2 \in \mathbb{R}$ are given by

$$\alpha_1 = \frac{1}{m_{11}(0)}, \quad \alpha_2 = \left. \frac{\partial g_1(z_1 - \gamma(z_3), z_3)}{\partial z_3} \right|_{z=0} .$$

Local controllability of the system (3.10) assures that $\alpha_1 \neq 0, \alpha_2 \neq 0$.

Since the nominal system (3.20), *i.e.*, with $\beta(t, z)$ constant and $\varphi(t) \equiv 0$, is homogeneous of negative degree, system (3.10) can be seen as a "perturbation" of (3.20)

$$\begin{aligned}
 \dot{z}_1 &= \alpha_1 z_2 + \delta_1(z), \\
 \dot{z}_2 &= \alpha_2 z_3 + \delta_2(z), \\
 \dot{z}_3 &= z_4, \\
 \dot{z}_4 &= \beta(t, z) [u + \varphi(t)] ,
 \end{aligned}$$

where the perturbation terms $\delta_1(z)$ and $\delta_2(z)$ are assumed to be of higher homogeneity degree.

Approximation models similar to (3.20) have been used in the literature to attain a *local exact feedback linearization* for local stabilization of several underactuated systems, as e.g. [57, 3, 54, 56, 8, 4, 21, 46, 17, 3, 60, 20, 18].

In this section, the design of a local finite-time stabilizing dynamic controller for the equilibrium point $z = 0$ of system (3.20) is done, despite the presence of $\beta(t, z)$ and $\varphi(t)$, using a continuous control signal. Due to Hermes' Theorem for homogeneous systems [6, Corollary 5.5], this controller will also locally stabilize in finite-time the origin of system (3.10).

3.2.2 Controller Design

Since the approximation system (3.20) is an uncertain chain of integrators of order 4, a Discontinuous Integral Algorithm (DIA) [38, 39, 18, 37] can be used to stabilize the origin. These algorithms consist in a static homogeneous finite-time controller for the nominal model of the system and a discontinuous integral action, aimed at estimating and compensating the uncertainties and perturbations.

For system (3.20), it is proposed here the Fourth Order Discontinuous Integral Algorithm (4-DIA), given by

$$\begin{aligned} u &= -k_4 \left[[z_4]^{\frac{5}{2}} + k_{\frac{5}{3}} [z_3]^{\frac{5}{3}} + k_{\frac{5}{2}} k_{\frac{5}{3}} [z_2]^{\frac{5}{4}} + k_{\frac{5}{2}} k_{\frac{5}{3}} k_1^{\frac{5}{4}} z_1 \right]^{\frac{1}{5}} + \zeta, \\ \dot{\zeta} &= -k_{I1} \left[z_1 + k_{I2} [z_2]^{\frac{5}{4}} + k_{I3} [z_3]^{\frac{5}{3}} + k_{I4} [z_4]^{\frac{5}{2}} \right]^0. \end{aligned} \quad (3.21)$$

The first term in (3.21) is a continuous and homogeneous static feedback controller, providing finite-time convergence for the nominal system (without perturbations), and is obtained using a back-stepping-like approach as in [9]. The second term in (3.21) is a *discontinuous integral term*, that ensures theoretically exact compensation of Lipschitz disturbances $\varphi(t)$. This is in contrast to the classical integral controllers (see e.g. [22, Chapter 14]), which are only able to fully compensate *constant* perturbations $\varphi(t)$.

Note that due to the fact that the discontinuous function *sign* is integrated, the control signal generated by (3.21) is *continuous*, so that the chattering effect can be strongly attenuated (see [45]).

Introducing a new state variable, $z_5 = \zeta + \varphi(t)$, which corresponds to the sum of the integral variable ζ and the non-vanishing perturbation term $\varphi(t)$, the dynamics of the closed-loop system, formed by system (3.20) with the controller (3.21), is

$$\begin{aligned} \dot{z}_1 &= \alpha_1 z_2, \\ \dot{z}_2 &= \alpha_2 z_3, \\ \dot{z}_3 &= z_4, \\ \dot{z}_4 &= \beta(t, z) \left\{ -k_4 \left[[z_4]^{\frac{5}{2}} + k_{\frac{5}{3}} [z_3]^{\frac{5}{3}} + k_{\frac{5}{2}} k_{\frac{5}{3}} [z_2]^{\frac{5}{4}} + k_{\frac{5}{2}} k_{\frac{5}{3}} k_1^{\frac{5}{4}} z_1 \right]^{\frac{1}{5}} + z_5 \right\}, \\ \dot{z}_5 &\in -k_{I1} \left[[z_1 + k_{I2} [z_2]^{\frac{5}{4}} + k_{I3} [z_3]^{\frac{5}{3}} + k_{I4} [z_4]^{\frac{5}{2}} \right]^0 + [-\bar{L}, \bar{L}], \end{aligned} \quad (3.22)$$

where $\bar{L} = \frac{L}{k_{I1}}$. The following Theorem presents the stability analysis of the 4-DIA applied to the uncertain Class-I system (3.10).

Theorem 1 *The origin of the uncertain system (3.10) is finite-time locally stable, even in presence of uncertainties fulfilling conditions (3.9), when the control τ is given by (3.8), (3.5) and (3.21), and the set of gains k_i and k_{Ii} , for $i = 1, 2, 3, 4$, are properly chosen.*

Proof. The proof is presented in the Appendix .1. ■

It is shown in the proof, using a homogeneous Lyapunov function, that the origin of system (3.22) is Globally Finite-Time stable for all uncertainties satisfying (3.9). Since (3.20) is a local approximation of the plant (3.10), local finite-time stability follows for the latter system, using the same Lyapunov function.

Remark 1 *Since the closed loop system with the controller of Theorem 1 is homogeneous with homogeneity degree $d = -1$ and weights $(r_1, r_2, r_3, r_4, r_5) = (5, 4, 3, 2, 1)$, the point $z = 0$ is a fifth-order sliding-mode. Due to homogeneity properties [28], the theoretical precision of the states after the transient are $|z_1| < \Delta_1 \bar{\tau}^5$, $|z_2| < \Delta_2 \bar{\tau}^4$, $|z_3| < \Delta_3 \bar{\tau}^3$, $|z_4| < \Delta_4 \bar{\tau}^2$ and $|z_5| < \Delta_5 \bar{\tau}$, where $\Delta_i > 0$ with $i = 1, \dots, 5$ and $\bar{\tau}$ as the sample time.*

Homogeneous approximation of RWP and TORA Systems

The uncertain local approximation of the RWP system is

$$\begin{aligned}\dot{z}_1 &= z_2, \\ \dot{z}_2 &= W z_3, \\ \dot{z}_3 &= z_4, \\ \dot{z}_4 &= \beta(t, z) [u + \varphi(t)],\end{aligned}$$

and for the TORA system is:

$$\begin{aligned}\dot{z}_1 &= \frac{1}{m_1 + m_2} z_2, \\ \dot{z}_2 &= \frac{km_2 r}{m_1 + m_2} z_3, \\ \dot{z}_3 &= z_4, \\ \dot{z}_4 &= \beta(t, z) [u + \varphi(t)].\end{aligned}$$

3.2.3 Gain design and scaling

The calculation of appropriate values for the gains of the 4-DIA are provided in Appendix .2, and they are given by the expressions (A.2)–(B.5). The gains k_{I2} , k_{I3} and k_{I4} can take any value. For the maximization of the functions in the design of k_2 , k_3 , k_4 and k_{I1} , it is necessary to choose the value of k_1 , $\gamma_1, \gamma_2, \gamma_3 > 0$ and $m \geq 9$.

Some set of gains obtained with this procedure are shown in Table 3.3, using $b_m = k_{I1} = 1$, $k_{I2} = k_{I3} = k_{I4} = 0$ and $L = 0.9$.

Table 3.3: Set of gains for the 4-DIA

Set	k_1	k_2	k_3	k_4
1	2	2	5	45
2	2	2	20	55
3	2	3	7	45

Gain Scaling

As a consequence of homogeneity, it is possible to perform a useful gain scaling:

$$\mathbf{k} = (k_1, k_2, k_3, k_4, k_{I1}, k_{I2}, k_{I3}, k_{I4}) \rightarrow \mathbf{k}_\lambda = \left(\lambda^{\frac{1}{5}}k_1, \lambda^{\frac{1}{4}}k_2, \lambda^{\frac{1}{3}}k_3, \lambda^{\frac{1}{2}}k_4, \lambda k_{I1}, \lambda^{-\frac{1}{4}}k_{I2}, \lambda^{-\frac{2}{3}}k_{I3}, \lambda^{-\frac{3}{2}}k_{I4} \right). \quad (3.23)$$

If the set of gains \mathbf{k} stabilizes the origin for a perturbation of size L , then for every $\lambda > 0$ the set of gains \mathbf{k}_λ also stabilizes the origin for a perturbation of size λL . This can be easily proved: Applying the linear transformation

$$\hat{z}_i = \lambda z_i, \quad i = 1, \dots, 5, \quad 0 < \lambda \in \mathbb{R},$$

to system (3.22) with gains \mathbf{k} leads to an equivalent system with gains \mathbf{k}_λ .

3.2.4 Simulation Results

RWP System

The Local Finite-Time Stabilizing (LFTS) controller given by the law (3.14), the transformation (3.12) and the 4-DIA described by (3.21) with gains $k_1 = k_2 = 2$, $k_3 = 5$, $k_4 = 45$, $k_{I1} = 8$, $k_{I2} = k_{I3} = k_{I4} = 0$ and scaling $\lambda = 0.2$, was implemented in Matlab Simulink with the Runge-Kutta's integration method with fixed step and a sampling time equal to 1×10^{-4} [s]. As perturbation, the unbounded signal $\varphi(t) = 0.1 \sin(t) + 0.1t + 0.5$ was used and $\beta(t, z) = 2.5 + \sin(z_1) + \cos(z_2)$ was taken as uncertain control coefficient.

Two initial conditions are presented: one "near" the upward equilibrium $x_0 = [-0.55, 0, 0, 0]^T$, and one "far" from it $x_0 = [\pi, 0, 0, 0]^T$, which corresponds to the downward position. Fig. 3.3 shows that for both initial conditions the controller is able to stabilize the origin, although theoretically only local stability is guaranteed. This simulation illustrates that the controller solves both, the swing-up and the stabilization problems despite the presence of the unbounded disturbance and the uncertain control coefficient (shown in Fig 3.4), but this does not follow from the stability analysis.

Fig. 3.4 presents the behaviour of the output signal ζ of the integrator. It identifies exactly and in finite time the (unbounded) perturbation. Fig. 3.5 shows that the control signal is continuous.

TORA system

For the TORA system, the control (3.18), the transformation (3.17) and the 4-DIA described by (3.21) with $k_1 = k_2 = 2$, $k_3 = 5$, $k_4 = 45$, $k_{I1} = 8$, $k_{I2} = k_{I3} = k_{I4} = 0$ and scaling $\lambda = 0.2$, were implemented in Matlab Simulink with the Runge-Kutta's integration method with fixed step and a sampling time equal to 1×10^{-4} [s]. The simulations were made with an unbounded perturbation $\varphi(t) = 0.1 \sin(t) + 0.1t + 0.5$ and $\beta(t, z) = 2.5 + \sin(z_1) + \cos(z_2)$ was taken as uncertain control coefficient.

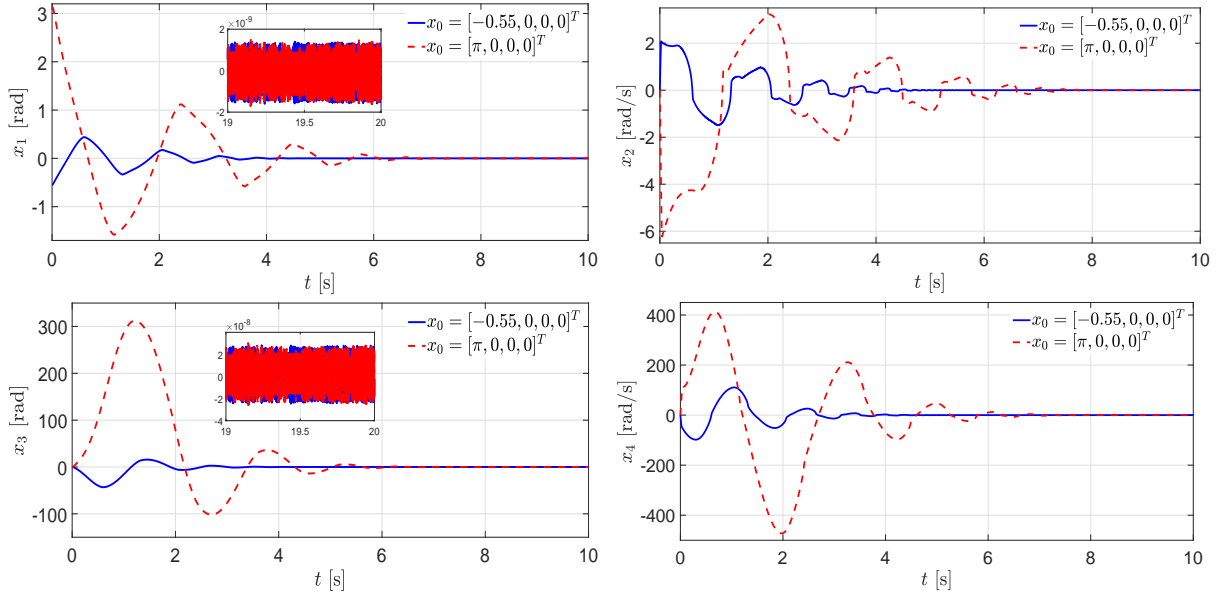


Figure 3.3: Simulated states for the LFTS of the RWP.

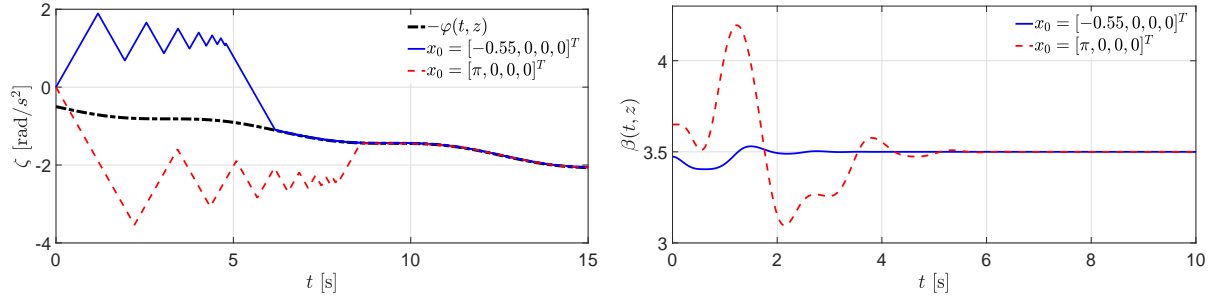


Figure 3.4: Perturbation identification and uncertain control coefficient for the LFTS of the RWP simulations.

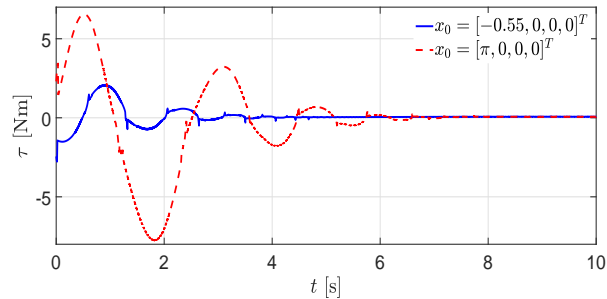


Figure 3.5: Continuous control signal for the LFTS of the RWP simulations.

In Figs. 3.6-3.8, the simulations results are shown. As in the LFTS simulations of the RWP system, two initial conditions were tested to check the performance of the algorithm: close to the origin $x_0 = [0, 0, -1, 0]^T$ and far from the origin $x_0 = [0.5, 0, \pi, 0]^T$. The plots show that for both initial conditions the four states reach the origin in finite-time with

a continuous control signal shown in Fig. 3.8, despite the presence of the unbounded disturbance and the uncertain control coefficient (shown in Fig 3.7). In Fig. 3.7 the integrator ζ is shown and it is observed how it identifies the negative value of the unbounded perturbation.

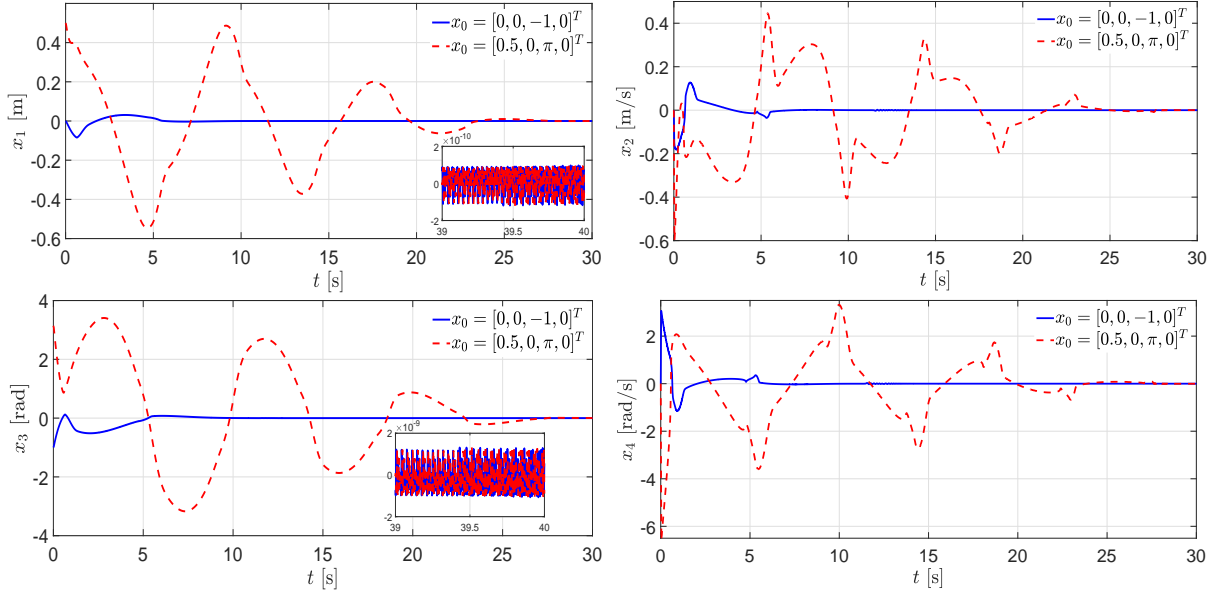


Figure 3.6: Simulated states for the LFTS of the TORA.

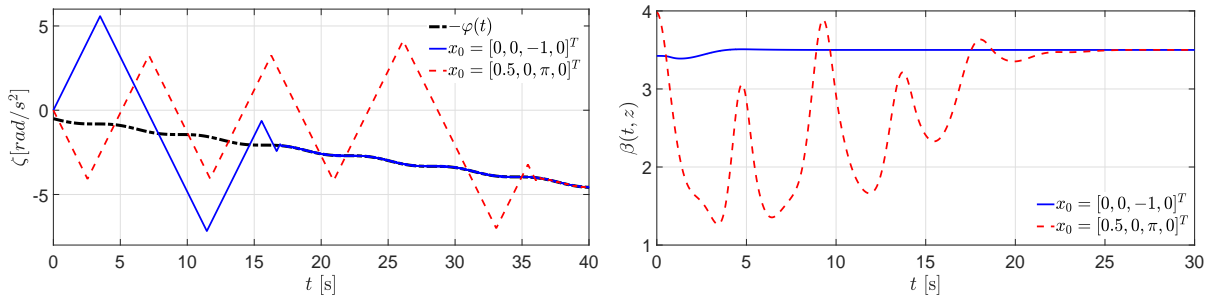


Figure 3.7: Perturbation identification and uncertain control coefficient for the LFTS of the TORA simulations.

3.2.5 Experimental Validation: RWP System

The experimental setup for the RWP, illustrated in Fig. 3.1, was developed at the Institut für Regelungs- und Automatisierungstechnik of TU Graz, Austria. The experiments are performed in Matlab Simulink over a data-acquisition board connected to the RWP system.

Since the actual RWP system only measures positions, a second order robust exact differentiator [29] was implemented in order to estimate the velocities x_2, x_4 required by

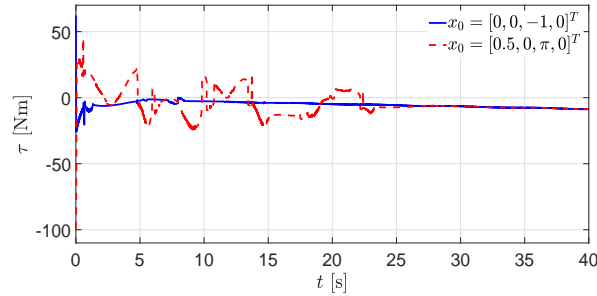


Figure 3.8: Continuous control signal for the LFTS of the TORA simulations.

the controller. The control signal τ from the algorithm is converted to a voltage signal by the expression $V = -0.2778\tau + 3.6 \times 10^{-5}x_4$. This signal is saturated between $[-0.9, 0.9]$ [V] and, after an amplification stage, is connected to a 12[V] DC motor.

The control (3.14) and the 4-DIA described by (3.21) with $k_1 = k_2 = 2$, $k_3 = 20$, $k_4 = 55$, $k_{I1} = 0.3$, $k_{I2} = k_{I3} = k_{I4} = 0$ and scaling gain $\lambda = 0.09$, were implemented in the real RWP system. This was done using the Runge-Kutta's integration method with fixed-step and a sampling time equal to 1×10^{-4} [s].

The experiments were made with two initial conditions, $x_0 = [-0.55, 0, 0, 0]^T$ and $x_0 = [\pi, 0, 0, 0]^T$, to see if the same behaviour as in simulations is obtained. In the experiment starting in the downward position the wheel position encoder was reset once the pendulum reached a position near to the origin. This was made to avoid that the wheel has to perform several rotations.

Fig. 3.9 shows how the four states reach the origin, even in presence of uncertainties in the system parameters and non-modelled dynamics. Fig. 3.10 shows the continuous control signal τ generated by the 4-DIA, while Fig 3.11 presents the voltage signal controlling the DC motor. Note that during the swinging-up phase the control reaches the saturation, and this explains why the 4-DIA controller produces some oscillations of the pendulum until the upward position is reached. This phenomenon does not appear in the simulations, where there is no saturation, and the pendulum goes to the upward position in just one movement. These results show that the 4-DIA is capable of stabilizing the four states even with saturation in the real control.

3.3 Estimation of the Local Domain of Attraction: 3-RWP Case

3.3.1 Problem Statement

In the previous section, both in simulations and experiments over the RWP system, the LFTS was able to drive the states from the downward position of the pendulum to its

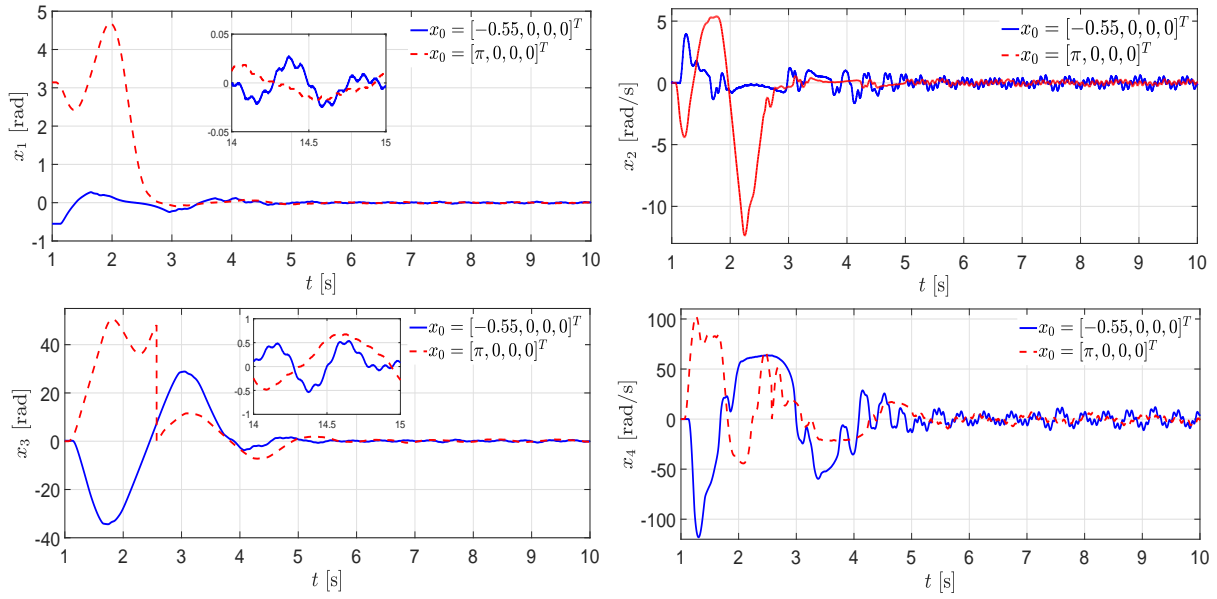


Figure 3.9: Experimental values of the states for the LFTS of the RWP.

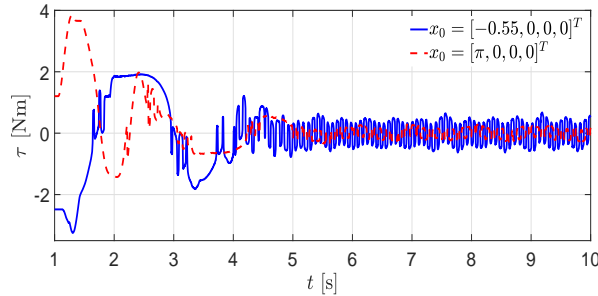


Figure 3.10: Continuous control signal for the LFTS of the RWP experiments.

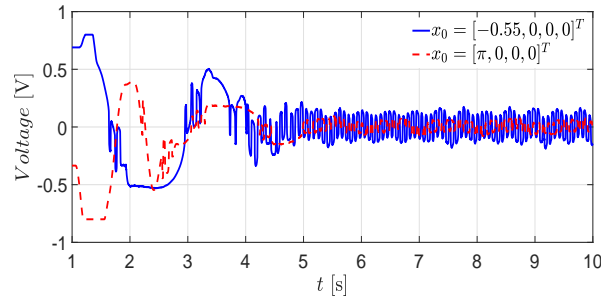


Figure 3.11: Voltage control signal in the LFTS for the RWP experiments.

upright position, in one step. These simulations and experiments pushed the further research on the properties of the DIA and the possibilities to enlarge the DIA's attraction domain allowing to cover both the upright and downward position.

For this purpose, to simplify the numerical calculations but without losing generality,

in this section will be considered the Third Order of the RWP system (3-RWP), *i.e.*, without taking into account the wheel position for the control. Then, it will be used a global transformation of the 3-RWP model like the one used in 3.12, and then apply a Third Order Discontinuous Integral Algorithm (3-DIA) to solve the problem. Selecting appropriately the 3-DIA's gains, it is possible to include the RWP's downward position in the attraction domain.

3.3.2 Controller Design

Neglecting the state x_3 (wheel position) of the system (3.11) as a control objective and defining the next global change of coordinates (similar to the one used in [41])

$$\begin{aligned} z_1 &:= d_{11}x_2 + d_{12}x_4, \\ z_2 &:= x_1, \\ z_3 &:= x_2, \end{aligned} \tag{3.24}$$

the system can be rewritten as

$$\begin{aligned} \dot{z}_1 &= W \sin(z_2), \\ \dot{z}_2 &= z_3, \\ \dot{z}_3 &= \frac{d_{22}W \sin(z_2) + b_2(z_1 - d_{11}z_3) - d_{12}\tau}{D}. \end{aligned} \tag{3.25}$$

Now, if the control τ becomes

$$\tau = \frac{d_{22}W \sin(z_2) + b_2(z_1 - d_{11}z_3) - D\nu}{d_{12}}, \tag{3.26}$$

partially linearizes the system, and we obtain a similar system as the normal form (3.6)

$$\begin{aligned} \dot{z}_1 &= W \sin(z_2), \\ \dot{z}_2 &= z_3, \\ \dot{z}_3 &= \beta(t, z) [u + \varphi(t)], \end{aligned} \tag{3.27}$$

where $\varphi(t)$ and $\beta(t, z)$ are assumed as (3.9).

Now, it is presented the Third Order Discontinuous Integral Algorithm (3-DIA), which is a controller derived from (3.21)

$$\begin{aligned} \nu &= -k_3 \left[[z_3]^{\frac{4}{2}} + k_2^{\frac{4}{2}} [z_2]^{\frac{4}{3}} + k_2^{\frac{4}{2}} k_1^{\frac{4}{3}} z_1 \right]^{\frac{1}{4}} + \zeta \\ \dot{\zeta} &= -k_{I1} \left[z_1 + k_{I2} [z_2]^{\frac{4}{3}} + k_{I3} [z_3]^{\frac{4}{2}} \right]^0. \end{aligned} \tag{3.28}$$

Introducing a new state variable, $z_4 = \zeta + \varphi(t)$, which corresponds to the sum of the integral variable ζ and the non-vanishing perturbation term $\varphi(t)$, the dynamics of the closed-loop system, formed by system (3.27) with the controller (3.28)

$$\begin{aligned}\dot{z}_1 &= W \sin(z_2), \\ \dot{z}_2 &= z_3, \\ \dot{z}_3 &= \beta(t, z) \left\{ -k_3 \left[|z_3|^{\frac{4}{2}} + k_2^{\frac{4}{2}} |z_2|^{\frac{4}{3}} + k_2^{\frac{4}{2}} k_1^{\frac{4}{3}} z_1 \right]^{\frac{1}{4}} + z_4 \right\}, \\ \dot{z}_4 &\in -k_{I1} \left[|z_1 + k_{I2} |z_2|^{\frac{4}{3}} + k_{I3} |z_3|^{\frac{4}{2}} \right]^0 + [-\bar{L}, \bar{L}],\end{aligned}\tag{3.29}$$

where $\bar{L} = \frac{L}{k_{I1}}$.

Remark 2 *Close to the origin, the system (3.29) is homogeneous of degree $d = -1$ and weights $(r_1, r_2, r_3, r_4) = (4, 3, 2, 1)$. Due to homogeneity properties [28], the theoretical precision of the states after the transient are $|z_1| < \Delta_1 \bar{\tau}^4$, $|z_2| < \Delta_2 \bar{\tau}^3$, $|z_3| < \Delta_3 \bar{\tau}^2$ and $|z_4| < \Delta_4 \bar{\tau}$, where $\Delta_i > 0$ with $i = 1, \dots, 5$ and $\bar{\tau}$ as the sample time.*

One of the reasons that started the study of how the DIA is able to perform the swing-up and the stabilization in one step, is to clarify how this controller acts from an equilibrium point x^* of the original system (3.11) (the downward position of the pendulum). This can be seen obtaining such equilibrium points

$$x^* = [n\pi, 0, p, 0]^T, \quad p \in \mathfrak{R}, \quad n \in \mathcal{Z}.\tag{3.30}$$

and comparing them with the equilibrium points z^* of the closed loop system (3.29) without taking into account the integral part z_4

$$z^* = [-k_1^{-\frac{4}{3}} |n\pi|^{\frac{4}{3}}, n\pi, 0]^T, \quad n \in \mathcal{Z},\tag{3.31}$$

and the equilibrium points in the original coordinates x^*

$$x^* = [n\pi, 0, p, -d_{12}^{-1} k_1^{-\frac{4}{3}} |n\pi|^{\frac{4}{3}}]^T, \quad p \in \mathfrak{R}, \quad n \in \mathcal{Z}.\tag{3.32}$$

One can notice that the equilibrium points (3.32) of the RWP can be affected by the value of the 3-DIA's gain k_1 , this is showed in Fig. 3.12. In the RWP without control, the downward position of the pendulum is an equilibrium point, but for the closed loop system (3.29), this position is no longer an equilibrium point. Therefore, the presented controller could start to act from the downward position of the pendulum.

The following Theorem presents the stability analysis of the 3-DIA applied to the 3-RWP.

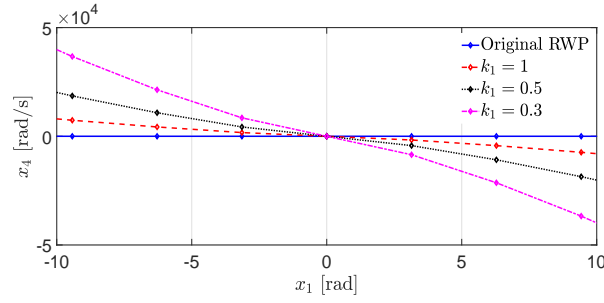


Figure 3.12: Equilibrium points of the RWP as function of 3-DIA's k_1 .

Theorem 2 *The origin of system (3.27) is finite-time locally stable, without taking into account the wheel position, when the control τ takes the form of (3.26), (3.24) and (3.28), and the set of gains k_i , with $i = 1, 2, 3$, are chosen properly. The points $x = [\pi, 0, 0, 0]^T$ and $x = [-\pi, 0, 0, 0]^T$, belong to an estimated domain of attraction.*

Proof. The proof is given in Appendix .3. ■

Remark 3 *In the proof, it is possible to see that the origin of system (3.29) is locally stable in finite-time. Therefore, the point $(x_1, x_2, x_4) = 0$ in system (3.11) is locally stable in finite-time as well and the integral action ζ converges to the negative of perturbation $\varphi(t)$. The not controlled state x_3 tends to a constant value, due to the fact that x_4 converges to zero.*

Now, to test the proposed algorithm and the estimated domain of attraction, some simulations and experiments over the RWP system were made.

3.3.3 Simulation Results

The control (3.26), the transformation (3.24) and the 3-DIA described by (3.28) with $k_1 = 0.55$, $k_2 = 2.3$, $k_3 = 13$, $k_{I1} = 0.15$, $k_{I2} = k_{I3} = 0$, were implemented in Matlab Simulink with the Runge-Kutta's integration method of fixed step and a sampling time equal to 1×10^{-4} [s]. The simulations were made with an unbounded perturbation $\varphi(t) = 0.1 \sin(0.4t) + 0.1t + 0.5$, $\beta(t, z) = 1$, and the initial conditions $x_0 = [\pi, 0, 0, 0]^T$ and $x_0 = [-\pi, 30, 0, 2000]^T$ (this last one also belongs to the region of attraction, but is far from the origin, in order to test the proposed algorithm).

Also, to compare the 3-DIA with another algorithm, it was designed a linear controller $\nu = -Kz$ from the linearized approximation of the system (3.27) around the origin, with $K = [3.1623, 9.0792, 5.3064]$, the control (3.26) and the transformation (3.24). The simulations were made with the same unbounded perturbation $\varphi(t)$ and the initial condition $x_0 = [0.5, 0, 0, 0]^T$, as this algorithm only can guarantee the stability close the origin.

The results are shown in Figs. 3.13-3.15. It can be clearly seen that the 3-DIA can compensate the unbounded perturbation and drive the states to the origin, starting far from it, using a continuous control signal. The linear algorithm was not able fight the perturbation and after a time, the states start to move off the origin.

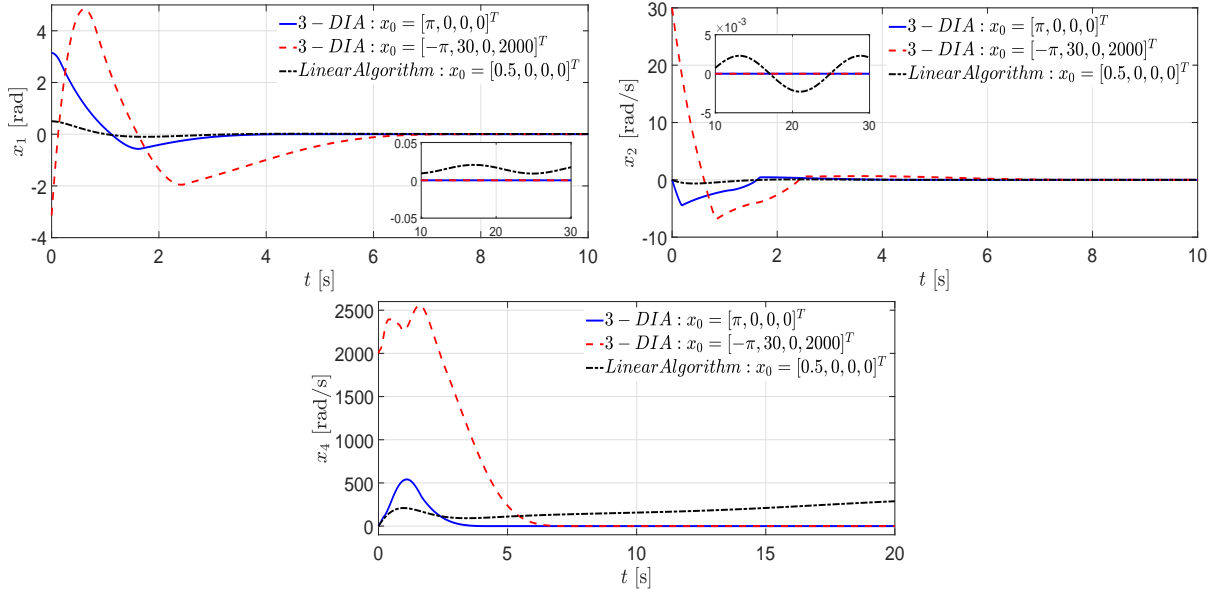


Figure 3.13: State trajectories in the 3-RWP simulations.

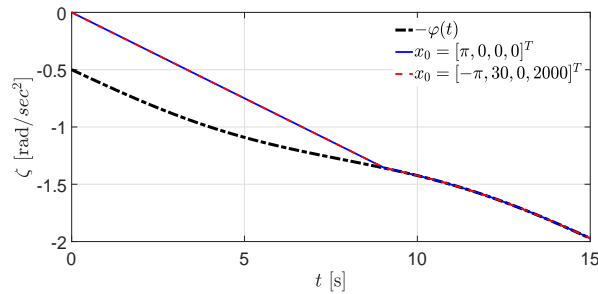


Figure 3.14: Perturbation identification in the 3-RWP simulations.

3.3.4 Experimental Validation

The control (3.26), the transformation (3.24) and the 3-DIA described by (3.28) with $k_1 = 0.55$, $k_2 = 2.3$, $k_3 = 13$, $k_{I1} = 0.15$ and $k_{I2} = k_{I3} = 0$, were implemented in the real RWP system. This, using the Runge-Kutta's integration method of fixed-step and a sampling time equal to 1×10^{-4} [s] and the initial condition $x_0 = [\pi, 0, 0, 0]^T$.

Also, it was tested the same linear algorithm $\nu = -Kz$ with a gain $K = [3.1623, 9.0792, 5.3064]$, the control (3.26) and the transformation (3.24). The experiments were made with the initial condition $x_0 = [0.5, 0, 0, 0]^T$.

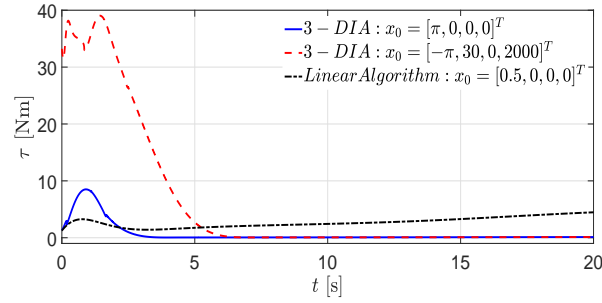


Figure 3.15: Control signal in the 3-RWP simulations.

The results are shown in Figs. 3.16-3.18. The 3-DIA can compensate some Lipschitz uncertainties of non-modelled dynamics, and drive the states to the origin starting from the downward position, using a continuous and saturated control signal (because of the real control that is a Voltage, as seen in Fig. 3.11). The linear algorithm can only drive the states to the origin starting really near from it but not hold them there, as it can be seen in the wheel velocity.

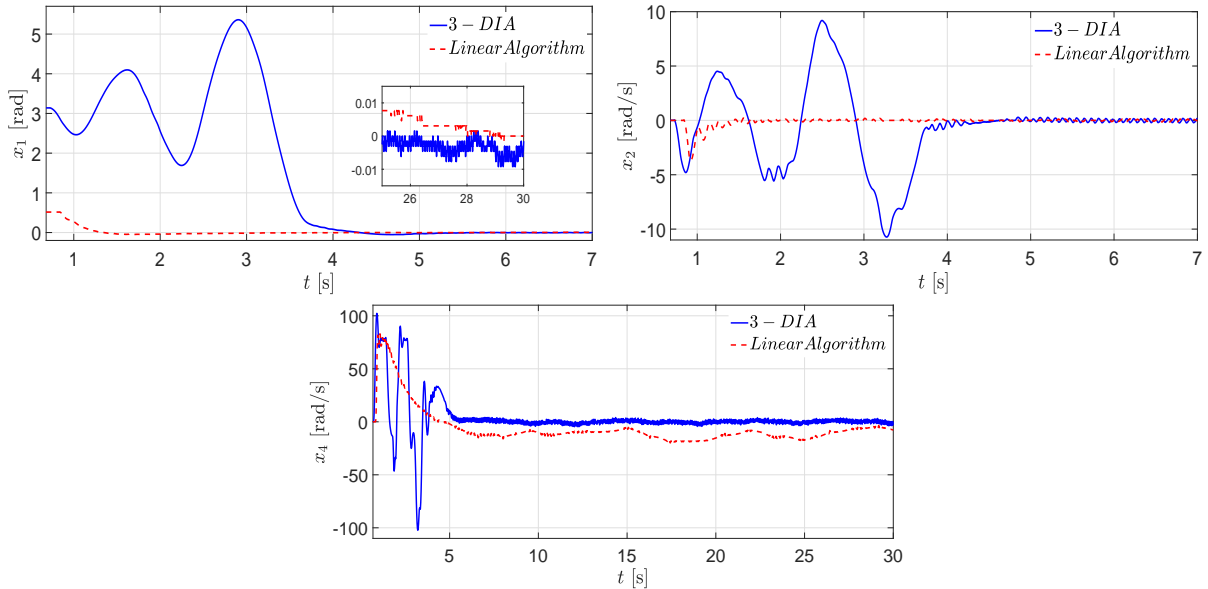


Figure 3.16: State trajectories in the 3-RWP experiment.

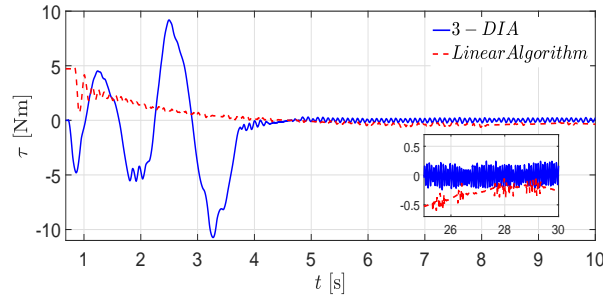


Figure 3.17: Control signal in the 3-RWP experiment.

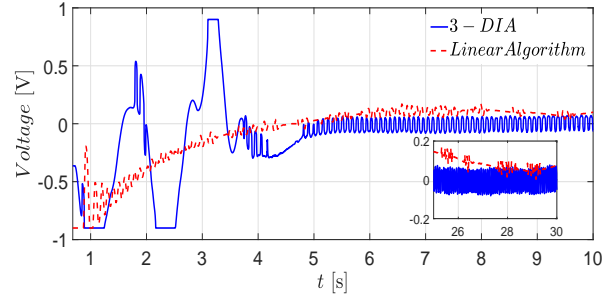


Figure 3.18: Voltage control signal in the 3-RWP experiment.

3.4 Design of a Globally Asymptotically Stabilizing (GAS) Controller

3.4.1 Problem Statement

In this section, the objective is to design a controller to (robustly) attain *global asymptotic* stability of the origin $z = 0$ of the uncertain system (3.10), in spite of the uncertainties and/or perturbations satisfying (3.9).

To reach the objective it can be followed the main strategy used in [42, 40, 43] for the Class-I of underactuated systems *without uncertainties/perturbations*. Since system (3.10) is a cascade system in strict feedback form, the controller design can be divided in two steps:

Step 1: For the virtual control variable z_3 of the Slave subsystem (z_1, z_2) in (3.10) find a smooth control law $z_3 = \sigma(z_1, z_2)$ that renders the origin $(z_1, z_2) = 0$ Globally Asymptotically Stable (GAS).

Step 2: For the (nominal linear) Master subsystem (z_3, z_4) a Back-Stepping design leads to the global stability of the state $z = 0$.

In this design, Step 1 is not modified but for Step 2 it is designed a *discontinuous and homogeneous* integral term, which is able to cope with the uncertainties and/or perturbations

satisfying (3.9).

3.4.2 Controller Design

Virtual controller for the Slave subsystem

An interesting feature of the Slave subsystem for the Class-I systems is that the function $g_1(z_1 - \gamma(z_3), z_3)$ is usually periodic in z_3 . For example, for the RWP it is given by $g_1(z_1 - \gamma(z_3), z_3) = W \sin(z_3)$, while for the TORA system it is $g_1(z_1 - \gamma(z_3), z_3) = -k_1 z_1 + \frac{km_2 r}{m_1 + m_2} \sin(z_3)$. This issue leads to a challenging global stabilization problem for the Slave subsystem. A nice solution proposed in [42, 40, 43] is to use a *saturated* virtual control law, $z_3 = \sigma(\kappa(z_1, z_2))$, where $\sigma(w)$ is a sigmoidal function, i.e. a smooth, saturated and monotonic increasing function, as e.g. $\tanh(w)$ or $\arctan(w)$, and $\kappa(z_1, z_2)$ is a smooth scalar function of the states. Below it will be shown for the two application examples, the RWP and the TORA systems, how GAS of the Slave subsystem can be attained. Moreover, Input-to-State Stability (ISS) of the system with respect to z_3 is also achieved. This is important for the stability of the cascade system.

Robust Controller for the Master subsystem

Once the virtual GAS controller for the slave is obtained, the global stabilization of the origin of the whole system is reduced to the global asymptotic stabilization of the transformed system, which in the nominal case is given by

$$\begin{aligned}\dot{z}_1 &= \frac{z_2}{m_{11}(\mu_1 + \sigma(\kappa(z_1, z_2)))}, \\ \dot{z}_2 &= g_1(z_1 - \gamma(\mu_1 + \sigma(\kappa(z_1, z_2))), \mu_1 + \sigma(\kappa(z_1, z_2))), \\ \dot{\mu}_1 &= \mu_2, \\ \dot{\mu}_2 &= \nu,\end{aligned}\tag{3.33}$$

where the variables are defined as

$$\begin{aligned}\mu_1 &:= z_3 - \sigma(\kappa(z_1, z_2)), \\ \mu_2 &:= \dot{\mu}_1, \\ \nu &:= \dot{\mu}_2.\end{aligned}\tag{3.34}$$

where

$$u = \nu + \ddot{\sigma}(\kappa(z_1, z_2)).\tag{3.35}$$

The origin of system (3.33) is globally asymptotically stable if the new control variable ν is designed properly to globally stabilize the origin of the μ_1, μ_2 subsystem. This task,

in principle, is rather simple, since it is a second order linear system. However, in presence of uncertainties and perturbations, a more realistic model is

$$\begin{aligned}\dot{z}_1 &= \frac{z_2}{m_{11}(\mu_1 + \sigma(\kappa(z_1, z_2)))}, \\ \dot{z}_2 &= g_1(z_1 - \gamma(\mu_1 + \sigma(\kappa(z_1, z_2))), \mu_1 + \sigma(\kappa(z_1, z_2))), \\ \dot{\mu}_1 &= \mu_2, \\ \dot{\mu}_2 &= \beta(t, z)[\nu + \varphi(t)],\end{aligned}\tag{3.36}$$

where $\beta(t, z)$ and $\varphi(t)$ are assumed to satisfy the conditions (3.9). In this case, the design of a robust control ν is vital to achieve the task of driving the states to the origin globally. The objective in this section is the design of a robust and global stabilizing controller for system (3.36), despite the presence of Lipschitz uncertainties/disturbances, *i.e.*, $|\dot{\varphi}(t)| \leq L$, and uncertain control coefficient $\beta(t, z)$. In order to attenuate the *chattering* effect the control signal will be continuous.

To solve this task, two Continuous Higher Order Sliding Modes Algorithms (CHOSMA) will be proposed: the second order Continuous Twisting Algorithm (2-CTA) (introduced in [64, 65]):

$$\begin{aligned}\nu &= -k_1 \lceil \mu_1 \rceil^{\frac{1}{3}} - k_2 \lceil \mu_2 \rceil^{\frac{1}{2}} + \zeta, \\ \dot{\zeta} &= -k_3 \lceil \mu_1 \rceil^0 - k_4 \lceil \mu_2 \rceil^0,\end{aligned}\tag{3.37}$$

and the second order Discontinuous Integral Algorithm (2-DIA):

$$\begin{aligned}\nu &= -k_2 \left[\lceil \mu_2 \rceil^{\frac{3}{2}} + k_1^{\frac{3}{2}} \mu_1 \right]^{\frac{1}{3}} + \zeta \\ \dot{\zeta} &= -k_{I1} \left[\mu_1 + k_{I2} \lceil \mu_2 \rceil^{\frac{3}{2}} \right]^0.\end{aligned}\tag{3.38}$$

which is an integral extension of the static controller presented in [9]. In both algorithms, the static part ν drives the states μ_1, μ_2 to the origin in finite-time, while the integral part ζ rejects the disturbance $\varphi(t)$. Note that since the discontinuous function *sign* is in the integrator, the generated control signal in both algorithms is continuous. The following theorem is the main result of this section:

Theorem 3 *The origin of μ_1, μ_2 -system in (3.36) is globally finite-time stable, despite the presence of the Lipschitz disturbances/uncertainties $\varphi(t)$ and the uncertain coefficient β satisfying (3.9). Moreover, z_1, z_2 will be driven to the origin globally and asymptotically, when the control τ takes the form of (3.8) and (3.35), with the state transformations (3.5) and (3.34), and ν takes the form of (3.37) or (3.38).*

Proof. The proof is shown in Appendix 4. ■

Remark 4 *As a consequence of the Theorem 3, the states of the original system (3.2), are globally and asymptotically driven to the origin.*

Remark 5 *The closed loop systems (D.2) and (D.3) (the μ subsystem with the 2-CTA and the 2-DIA, respectively) are homogeneous of degree $d = -1$ and weights $(r_1, r_2, r_3) = (3, 2, 1)$. Due to homogeneity properties [28], the theoretical precision of the states after the transient are $|\mu_1| < \Delta_1 \bar{\tau}^3$, $|\mu_2| < \Delta_2 \bar{\tau}^2$ and $|\mu_3| < \Delta_3 \bar{\tau}$, where $\Delta_i > 0$ with $i = 1, \dots, 3$ and $\bar{\tau}$ as the sample time.*

In the following Sections, the control design able to globally stabilize the origin of the RWP and the TORA systems will be presented.

3.4.3 RWP Controller Design

Defining the needed sigmoidal function $\sigma(\kappa(z_1, z_2))$ (for simplicity we just write $\sigma(z_1, z_2)$) as

$$\sigma(z_1, z_2) := -c_0 \tanh(c_1 z_1 + c_2 z_2), \quad (3.39)$$

where $0 > c_0 > \pi/2$ and $c_1, c_2 > 0$. Using the variables (3.34) the dynamics of system (3.15) becomes

$$\begin{aligned} \dot{z}_1 &= z_2, \\ \dot{z}_2 &= W \sin(\sigma(z_1, z_2) + \mu_1), \\ \dot{\mu}_1 &= \mu_2, \\ \dot{\mu}_2 &= \beta(t, z)[\nu + \varphi(t)], \end{aligned}$$

where

$$\begin{aligned} u &= \nu + \ddot{\sigma}, \\ \ddot{\sigma} &= -c_0(1 - \tanh^2(c_1 z_1 + c_2 z_2)) [c_1 W \sin(z_3) + c_2 W \cos(z_3) z_4 \\ &\quad - 2 \tanh(c_1 z_1 + c_2 z_2) (c_1 z_2 + c_2 W \sin(z_3))^2], \end{aligned} \quad (3.40)$$

and the ν control can take the form of (3.37) or (3.38) to achieve the global stabilization of the RWP origin.

Remark 6 *The sigmoidal function (3.39) is similar to the one used in the control of the RWP in [42], with the difference that in this work we are controlling the RWP of fourth order and in the other work the RWP of third order (neglecting the position of the wheel).*

3.4.4 TORA Controller Design

Defining the same sigmoidal function $\sigma(z_1, z_2)$ as (3.39) and the same change of coordinates as (3.34), transform the system (3.19) to

$$\begin{aligned}\dot{z}_1 &= \frac{z_2}{m_1 + m_2}, \\ \dot{z}_2 &= -kz_1 + \frac{km_2r \sin(\sigma(z_1, z_2) + \mu_1)}{m_1 + m_2}, \\ \dot{\mu}_1 &= \mu_2, \\ \dot{\mu}_2 &= \beta(t, z)[\nu + \varphi(t)],\end{aligned}$$

where

$$\begin{aligned}u &= \nu + \ddot{\sigma}, \\ \ddot{\sigma} &= -c_0(1 - \tanh^2(c_1z_1 + c_2z_2)) \left[\frac{c_1k}{m_1 + m_2} \left(-z_1 + \frac{m_2r \sin(z_3)}{m_1 + m_2} \right) + \right. \\ &\quad \left. \frac{c_2k}{m_1 + m_2} (-z_2 + m_2r \cos(z_3)z_4) - \right. \\ &\quad \left. 2 \tanh(c_1z_1 + c_2z_2) \left(c_1 \frac{z_2}{m_1 + m_2} - c_2kz_1 + c_2 \frac{km_2r \sin(z_3)}{m_1 + m_2} \right)^2 \right],\end{aligned}\tag{3.41}$$

and the ν control can take the form of (3.37) or (3.38) to achieve the global stabilization of the origin of the TORA.

3.4.5 Simulation results

RWP System

For the GAS, the control (3.14) and (3.40), the transformations (3.12) and (3.34), the 2-DIA described by (3.38) with $k_1 = 4.16$, $k_2 = 28.5$, $k_{I1} = 6.3$, $k_{I2} = 0$, the 2-CTA described by (3.37) with $k_1 = 47.57$, $k_2 = 19.84$, $k_3 = 16.1$, $k_4 = 7.7$ were implemented in Matlab Simulink with the Runge-Kutta's integration method of fixed step and a sampling time equal to 1×10^{-4} [s]. Also, to perform a comparison with another kind of algorithm, a linear algorithm (2-LA) was tested:

$$\nu = -k_1\mu_1 - k_2\mu_2,\tag{3.42}$$

with $k_1 = k_2 = 10$. The simulations were made with the same unbounded perturbation $\varphi(t) = 2 \sin(2t) + 2t + 2$, uncertain control coefficient $\beta(t, z) = 2.5 + \sin(z_1) + \cos(z_2)$, the same initial condition $x_0 = [100\pi, -50, -100\pi, 50]^T$ and the same gains $c_0 = 1.5$ and $c_1 = 3, c_2 = 5$.

The results are shown in Figs. 3.19-3.22. The sliding-modes algorithms drive the μ_1, μ_2 states to the origin in finite-time, making the original states of the RWP system to be attracted to the origin asymptotically and maintained there despite the presence of the unbounded disturbance (due to the fact that they are able to identify the disturbance exactly as shown in Fig. 3.21). The 2-LA can drive the states near to the origin, but as the disturbance grows, it is not able to compensate it and the states start to grow. With respect to the control signal, the three algorithms present a continuous one, as shown in Fig. 3.22.

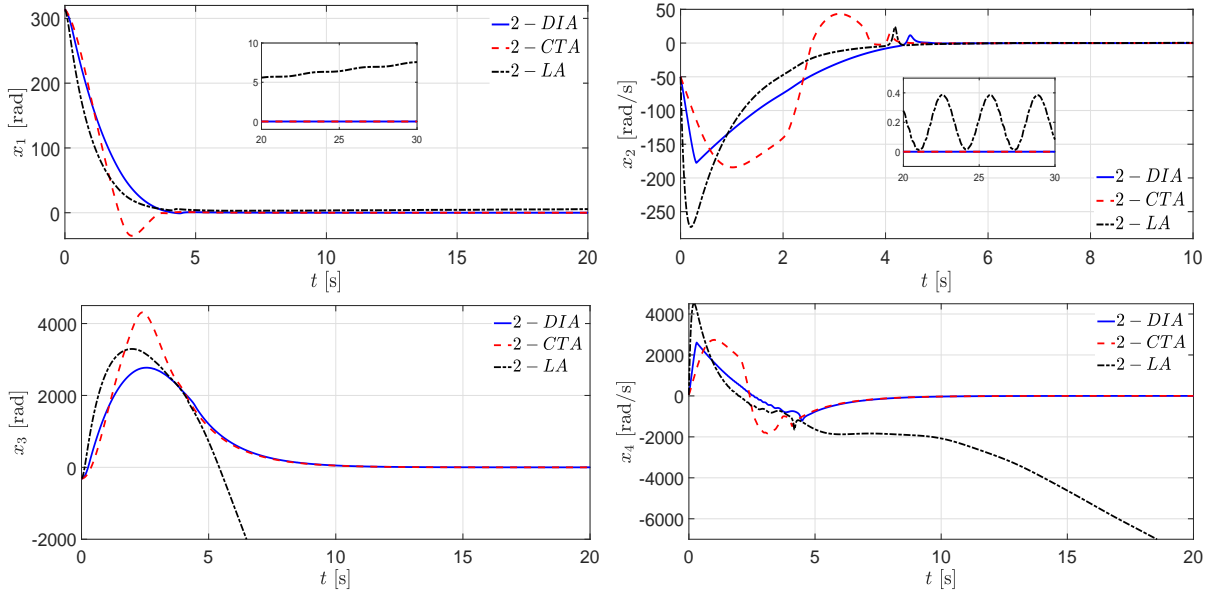


Figure 3.19: State trajectories in the GAS for the RWP simulations.

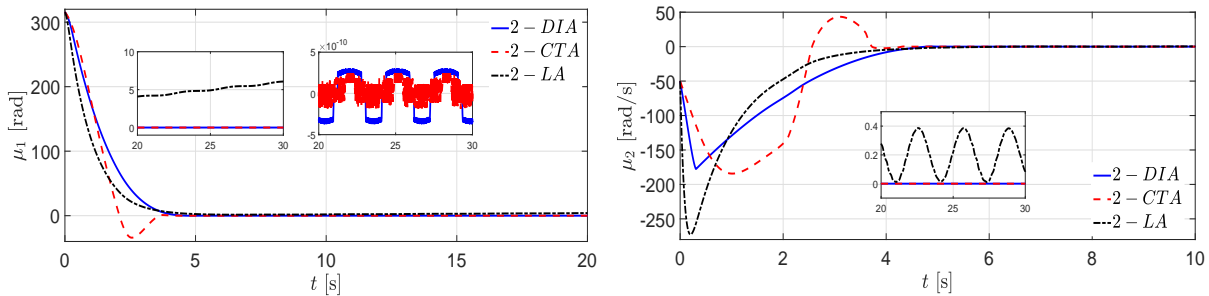


Figure 3.20: Finite-time state trajectories in the GAS for the RWP simulations.

TORA System

For the GAS, the control (3.18) and (3.41), the transformations (3.17) and (3.34), the 2-DIA described by (3.38) with $k_1 = 4.16$, $k_2 = 28.5$, $k_{I1} = 6.3$, $k_{I2} = 0$, the 2-CTA described by (3.37) with $k_1 = 47.57$, $k_2 = 19.84$, $k_3 = 16.1$, $k_4 = 7.7$, and the 2-LA

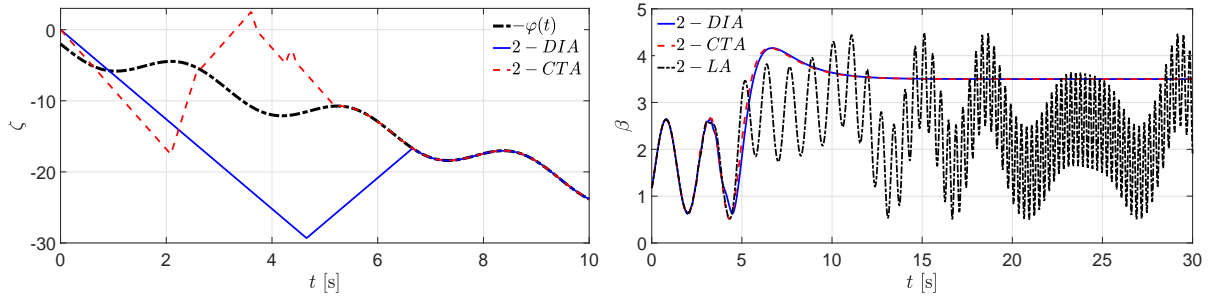


Figure 3.21: Perturbation identification and uncertain control coefficient in the GAS for the RWP simulations.

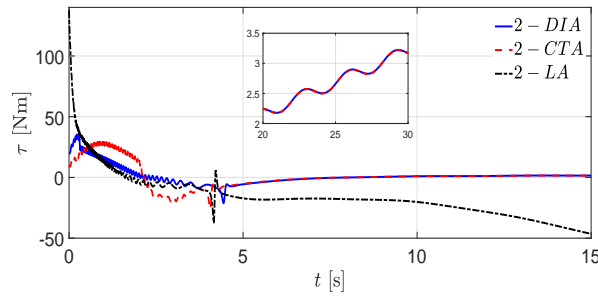


Figure 3.22: Control signal in the GAS for the RWP simulations.

described by (3.42) with $k_1 = k_2 = 10$, were implemented in Matlab Simulink with the Runge-Kutta's integration method of fixed step and a sampling time equal to 1×10^{-4} [s]. The simulations were made with the same unbounded perturbation $\varphi(t) = 2 \sin(2t) + 2t + 2$, uncertain control coefficient $\beta(t, z) = 2.5 + \sin(z_1) + \cos(z_2)$, the same initial condition $x_0 = [0, -1, 100\pi, -1]^T$ and the same gains $c_0 = 1.5$ and $c_1 = 3, c_2 = 5$.

The results are shown in Figs. 3.23-3.26. Again, the sliding modes can compensate the matched unbounded disturbance and drive the μ_1, μ_2 states to the origin in finite-time. Then the original states of the TORA are attracted to the origin asymptotically. The 2-LA behaves in the same way as the RWP system and drives the states near to the origin until it can not compensate the disturbance. Also, the control signal is continuous in the three algorithms.

3.4.6 Experimental Validation: RWP System

The experiments were made again in the real RWP system. The control (3.14) and (3.40), the transformations (3.12) and (3.34), the 2-DIA described by (3.38) with $k_1 = 2.43$, $k_2 = 14.62$, $k_{I1} = 1.26$, $k_{I2} = 0$, $c_0 = 1.5$, $c_1 = 0.17$ and $c_2 = 7.5$, the 2-CTA described by (3.37) with $k_1 = 36.3$, $k_2 = 19.84$, $k_3 = 4.02$, $k_4 = 1.92$, $c_0 = 1.5$, $c_1 = 0.5$ and $c_2 = 7$, and the 2-LA described by (3.42) with $k_1 = 16$, $k_2 = 24$, $c_0 = 1.5$, $c_1 = 1.6$ and $c_2 = 3.6$ were implemented in the real RWP system with the Runge-Kutta's integration method of

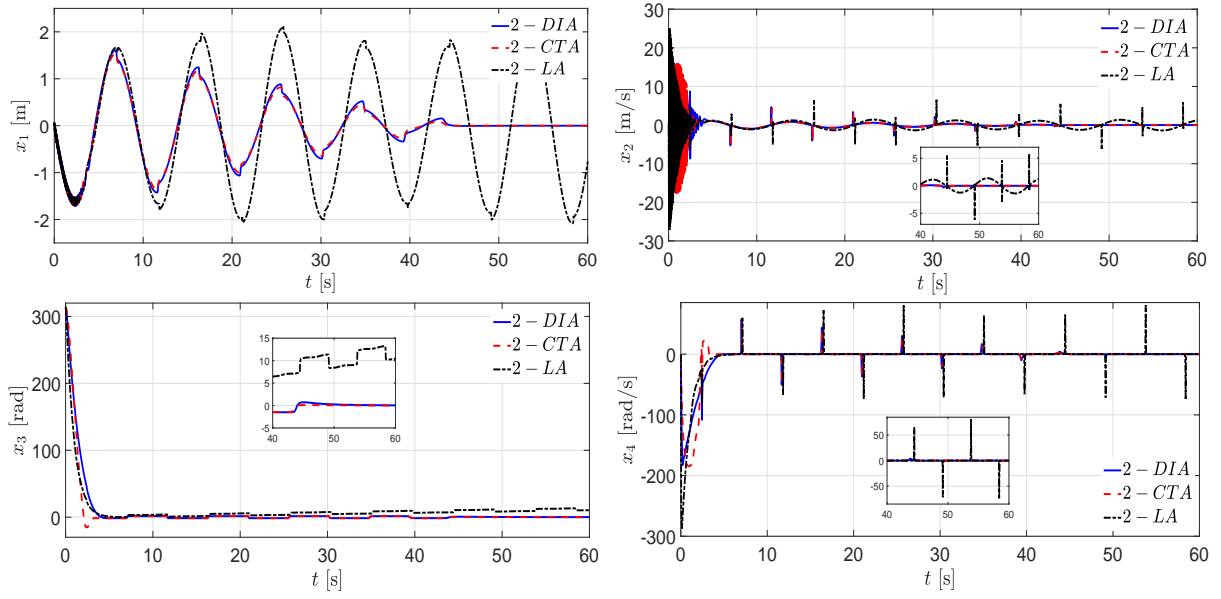


Figure 3.23: State trajectories in the GAS for the TORA simulations.

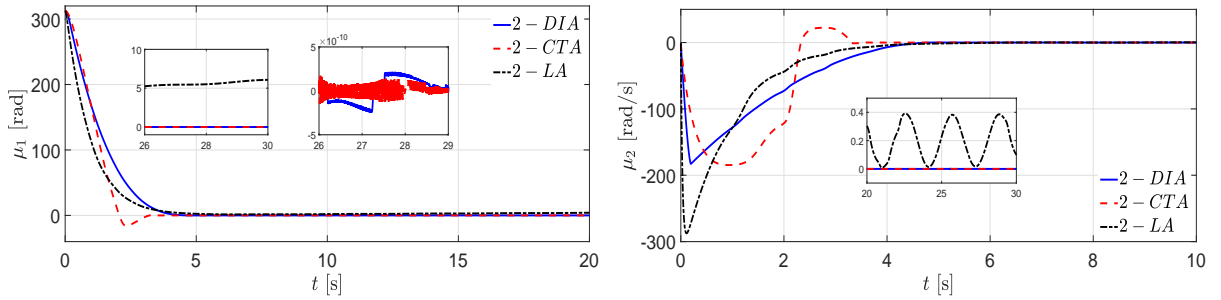


Figure 3.24: Finite-time state trajectories in the GAS for the TORA simulations.

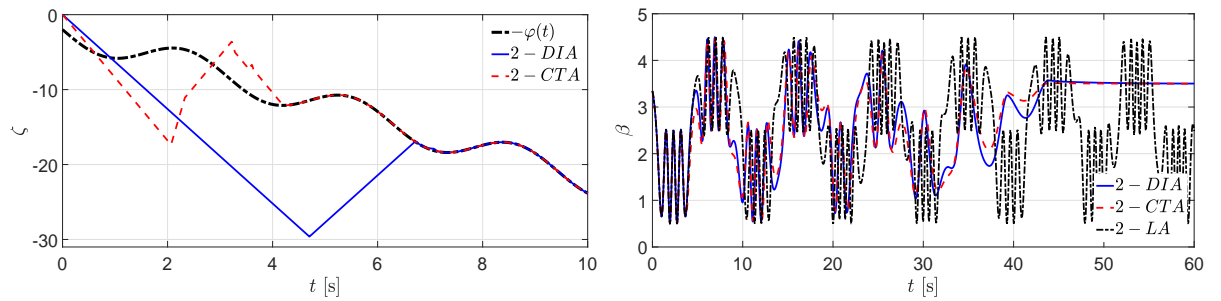


Figure 3.25: Perturbation identification and uncertain control coefficient in the GAS for the TORA simulations.

fixed step and a sampling time equal to 1×10^{-4} [s]. The experiments were made with the same initial condition $x_0 = [\pi, 0, 0, 0]^T$.

The results are shown in Figs. 3.27-3.30. The continuous sliding modes algorithms

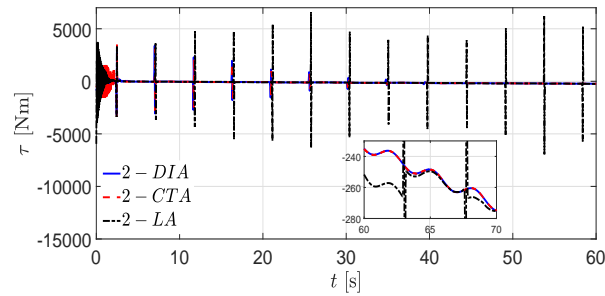


Figure 3.26: Control signal in the GAS for the TORA simulations.

drive the states of the pendulum from the downward position close to the origin and stay around it, although the 2-CTA make it slower and with a larger control signal. The 2-LA can take the pendulum to the upright position, but due to the presence of uncertainties that it can not compensate, the wheel position can only be maintained around the origin and the pendulum falls in many times. Seeing the μ_1 and μ_2 plots, one can notice how the 2-DIA and the 2-CTA can maintain them in the origin and the 2-LA does not. Again, the chattering effect is diminished as seen in the continuous control signal of the sliding modes algorithms.

In theory, the three algorithms can achieve global stabilization, but in practice, with the saturation of the real control signal (voltage) is no longer possible. Despite this, the sliding modes algorithms achieve the swing-up and stabilization in one step.

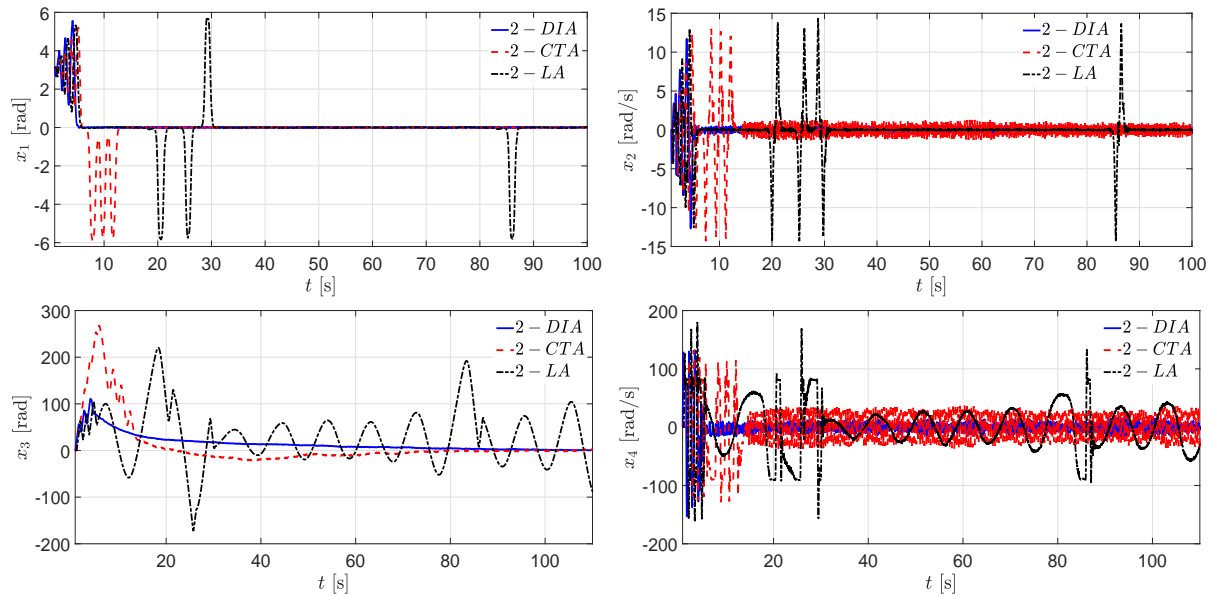


Figure 3.27: State trajectories in the GAS for the RWP experiments.

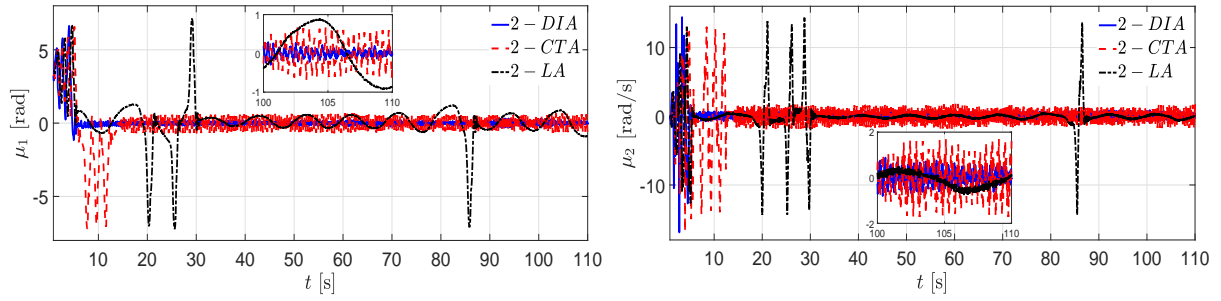


Figure 3.28: Finite-time state trajectories in the GAS for the RWP experiments.

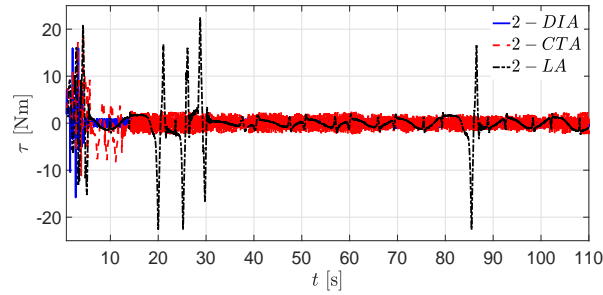


Figure 3.29: Control signal in the GAS for the RWP experiments.

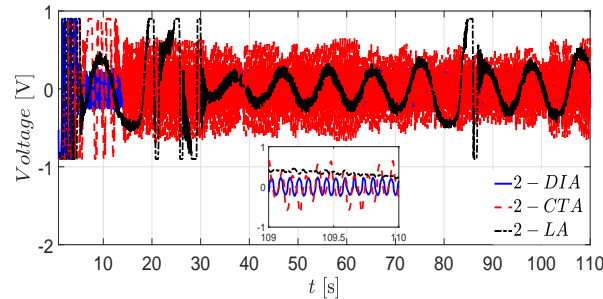


Figure 3.30: Voltage control signal in the GAS for the RWP experiments.

3.5 Conclusions

In this chapter, *robust* controllers were designed for the Class-I of underactuated mechanical systems of two DoF, using a continuous Higher-Order Sliding-Modes strategy. Two kinds of controller designs were presented: One generates a fifth-order sliding-mode and achieves Local Finite-Time Stability (LFTS). For this controller, an estimation of the domain of attraction was made in the 3-RWP, showing that it can be inflated the attraction domain of the upright position of the 3-RWP, enclosing the RWP's downward position. With this, it can be explained why the controller is able to perform the swing-up and stabilization in one step, despite it is a local stabilizer.

The other is a robust controller that provides Global Asymptotic Stability (GAS).

These controllers compensate matched Lipschitz disturbances and/or uncertainties, cope with an uncertain control coefficient and generate a *continuous* control signal, possibly reducing the chattering effect.

Evidence of the performance of the controllers is provided using simulations for the RWP and the TORA systems, and by means of experiments on the RWP system.

Chapter 4

Control of Class-III of underactuated mechanical systems with two DoF

4.1 Class-III Model

Class-III of underactuated mechanical system of two DoF contains only the Cart-Pendulum System (CP). Having as configuration vector $q = [q_1, q_2]^T$, the inertia matrix depends only on q_2 , *i.e.*, $M = M(q_2)$, but the variable q_1 is actuated, contrary to the Class-I. The Lagrangian is

$$L(q, \dot{q}) = \frac{1}{2} \dot{q}^T \begin{bmatrix} m_{11}(q_2) & m_{12}(q_2) \\ m_{21}(q_2) & m_{22}(q_2) \end{bmatrix} \dot{q} - V(q_2), \quad (4.1)$$

where $V(q_2)$ is the potential energy of the system, and the Euler-Lagrange equations of motion are

$$\begin{aligned} m_{11}(q_2)\ddot{q}_1 + m_{12}(q_2)\ddot{q}_2 + d_{11}(q_2)\dot{q}_1\dot{q}_2 + d_{12}(q_2)\dot{q}_2^2 - g_1(q_1, q_2) &= F, \\ m_{21}(q_2)\ddot{q}_1 + m_{22}(q_2)\ddot{q}_2 - \frac{1}{2}d_{21}(q_2)\dot{q}_1^2 + \frac{1}{2}d_{22}(q_2)\dot{q}_2^2 - g_2(q_1, q_2) &= 0, \end{aligned} \quad (4.2)$$

where $g_i(q_1, q_2) = -\frac{\partial V(q)}{\partial q_i}$, $i = 1, 2$ and $d_i(q_2) = \frac{d}{dq_2}m_i(q_2)$.

Using the global change of variables

$$\begin{aligned} x_1 &:= q_1, \\ x_2 &:= \dot{q}_1, \\ x_3 &:= q_2, \\ x_4 &:= \dot{q}_2, \end{aligned} \quad (4.3)$$

the system achieves the state space representation

$$\begin{aligned}\dot{x}_1 &= x_2, \\ \dot{x}_2 &= \frac{a_1 \omega_1(x, V) + g \sin(x_3) \cos(x_3)}{d(x)}, \\ \dot{x}_3 &= x_4, \\ \dot{x}_4 &= \frac{\cos(x_3) \omega_1(x, V) + a_2 g \sin(x_3)}{d(x)},\end{aligned}\tag{4.4}$$

where

$$\begin{aligned}\omega_1(x, V) &= k_1 V - x_2^2 \sin(x_3) - k_2 x_2, & d(x) &= b - \cos^2(x_3), \\ a_1 &= J_p / (ml), & a_2 &= 1/l, & b &= a_1 a_2, \\ k_1 &= p_1 / (ml), & k_2 &= (f_c - p_2) / (ml).\end{aligned}$$

and u [V] is the signal of a DC motor.

The previous model system results from the CP shown in Fig. 4.1. This figure describes a pendulum rotating in a vertical plane and its pivot pin is mounted in a cart. The cart can move along a horizontal rail, lying in the plane of rotation. The states vector is $x = [x_1, x_2, x_3, x_4]^T$, where x_1 [m] is cart position, x_2 [m/s] is the cart velocity, x_3 [rad] is the pendulum position measured counter clockwise ($x_3 = 0$ for the upright position of the pendulum) and x_4 [rad/s] is the pendulum angular velocity.

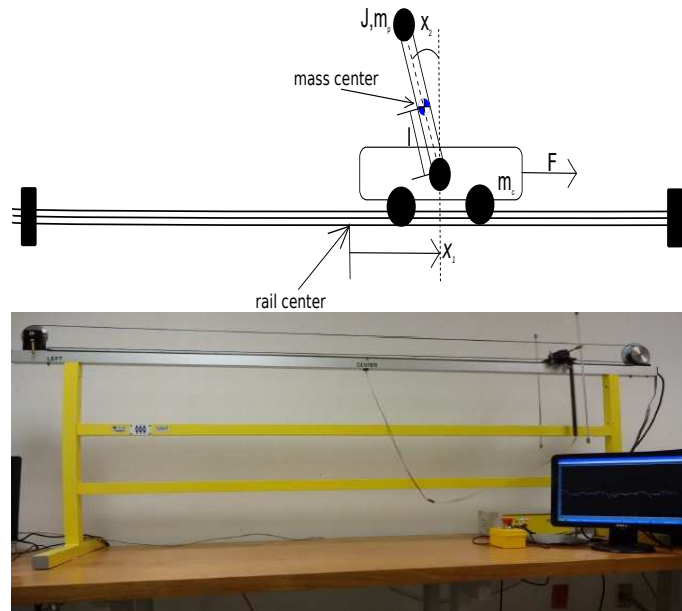


Figure 4.1: Cart-pendulum system.

The used system parameters were provided by Inteco [19] and they are given in Table 4.1.

Table 4.1: Parameters of the Cart-Pendulum System

Name	Description	Units
m	Cart and Pendulum mass	0.872[kg]
l	Distance of the rotation axis to the mass center	0.011[m]
f_c	Dynamic friction coefficient	0.5[Ns/m]
p_1	Force and PWM signal ratio	9.4[N]
p_2	Force and cart velocity ratio	-0.548[Ns/m]
J_p	Pendulum moment of inertia	0.0034[kgm ²]

The presence of the term $\cos(x_3)$ in the x_4 dynamics, results in a controllability problem. When the pendulum position is in the horizontal plane ($\cos(x_3) = 0$), the cart is not able to affect the pendulum dynamics. As a result of this, the task to find a control that globally stabilizes the system is in principle a difficult challenge. That is why most of the papers that deal with this kind of systems, separate the problem in two: the swing-up and stabilization ([4], [50], [59], [42], [68]).

The objective in this chapter is to design *dynamic and homogeneous* state-feedback controllers that are able to locally stabilize the origin $x = 0$ despite the presence of Lipschitz perturbation term $\varphi(t)$, and the uncertain control coefficient $\beta(t, z)$, and using a *continuous* control signal $u(t)$. It is used a *local* homogeneous approximation of system (3.10) to design a *locally finite-time* stabilizing dynamic controller in Section 4.2. For a bigger domain of attraction than the one presented in Section 4.2, local asymptotic stabilization of the origin $x = 0$ is achieved, using a globally valid model to design a *dynamic and homogeneous* feedback controller in Section 4.3. In every section presented, the terms $\varphi(t)$ and $\beta(t, z)$ will be presented separately.

4.2 Design of a Local Finite-Time Stabilizing (LFTS) Controller

4.2.1 Problem Statement

In this section it is performed the design of a controller to attain *local finite-time* stability of the origin $x = 0$ of the CP system (4.4). For this purpose, a *local homogeneous* approximation of system (4.4) will be considered, like the Class-I system.

It is well known that a controllable system can be transformed (at least locally) to its controllability canonical form. This is the case of the CP system, which can be represented in the form

$$\dot{x} = f(x) + g(x)u, \quad (4.5)$$

and can be obtained a local approximation around the origin

$$\dot{x} = Ax + Bu \quad (4.6)$$

where $A = \left. \frac{\partial f(x)}{\partial x} \right|_{x=0}$ and $B = \left. \frac{\partial g(x)}{\partial x} \right|_{x=0}$. This system can be transformed to

$$\begin{aligned} \dot{z}_1 &= z_2, \\ \dot{z}_2 &= z_3, \\ \dot{z}_3 &= z_4, \\ \dot{z}_4 &= u, \end{aligned} \quad (4.7)$$

with a transformation

$$z = Tx \quad (4.8)$$

and u is the new control variable obtained from a feedback linearization.

In presence of parameter or dynamics uncertainties as well as external perturbations, the nominal model (4.7) is no longer valid. A more appropriate model can be given by the equations

$$\begin{aligned} \dot{z}_1 &= z_2 + \delta_1(z), \\ \dot{z}_2 &= z_3 + \delta_2(z), \\ \dot{z}_3 &= z_4 + \delta_3(z), \\ \dot{z}_4 &= \beta(t, z) [u + \varphi(t)] + \delta_4(z), \end{aligned}$$

where the terms $\delta_i(z)$ represent vanishing perturbations, i.e. $\delta_i(0) = 0$, while the uncertain control coefficient $\beta(t, z)$ and the matching perturbation term $\varphi(t)$ are assumed to be bounded (without changing sign) and Lipschitz continuous as a function of time, respectively, i.e.

$$0 < b_m \leq |\beta(t, z)| \leq b_M, \quad \left| \frac{d\varphi(t)}{dt} \right| \leq L. \quad (4.9)$$

In what follows it will be only considered the non-vanishing perturbation $\varphi(t)$ and the uncertain control coefficient $\beta(t, z)$, that is, we use the uncertain model

$$\begin{aligned} \dot{z}_1 &= z_2, \\ \dot{z}_2 &= z_3, \\ \dot{z}_3 &= z_4, \\ \dot{z}_4 &= \beta(t, z) [u + \varphi(t)], \end{aligned} \quad (4.10)$$

to design the controller. As the Class-I, for sufficiently small and vanishing perturbations with a triangular structure, i.e. $\delta_i(z) \leq \epsilon \|(z_1, \dots, z_i)\|$, if the origin of the system (4.10) is Asymptotically Stable (GAS) so is also the origin of the perturbed system.

In this section the design of a local finite-time stabilizing dynamic controller for the equilibrium point $z = 0$ of system (4.10) is done, despite of the presence of $\beta(t, z)$ and $\varphi(t)$, using a continuous control signal. Due to Hermes' Theorem for homogeneous systems [6, Corollary 5.5], this controller will also locally stabilize in finite-time the origin of system (4.4).

4.2.2 Controller Design

Since the approximation system (4.10) is an uncertain chain of integrators of order 4, the 4-DIA can be used again to stabilize the origin:

$$\begin{aligned} u &= -k_4 \left[[z_4]^{\frac{5}{2}} + k_3^{\frac{5}{2}} [z_3]^{\frac{5}{3}} + k_3^{\frac{5}{2}} k_2^{\frac{5}{3}} [z_2]^{\frac{5}{4}} + k_3^{\frac{5}{2}} k_2^{\frac{5}{3}} k_1^{\frac{5}{4}} z_1 \right]^{\frac{1}{5}} + \zeta, \\ \dot{\zeta} &= -k_{I1} \left[z_1 + k_{I2} [z_2]^{\frac{5}{4}} + k_{I3} [z_3]^{\frac{5}{3}} + k_{I4} [z_4]^{\frac{5}{2}} \right]^0. \end{aligned} \quad (4.11)$$

Introducing a new state variable, $z_5 = \zeta + \varphi(t)$, which corresponds to the sum of the integral variable ζ and the non-vanishing perturbation term $\varphi(t)$, the dynamics of the closed-loop system, formed by system (4.10) with the controller (4.11), is

$$\begin{aligned} \dot{z}_1 &= z_2, \\ \dot{z}_2 &= z_3, \\ \dot{z}_3 &= z_4, \\ \dot{z}_4 &= \beta(t, z) \left\{ -k_4 \left[[z_4]^{\frac{5}{2}} + k_3^{\frac{5}{2}} [z_3]^{\frac{5}{3}} + k_3^{\frac{5}{2}} k_2^{\frac{5}{3}} [z_2]^{\frac{5}{4}} + k_3^{\frac{5}{2}} k_2^{\frac{5}{3}} k_1^{\frac{5}{4}} z_1 \right]^{\frac{1}{5}} + z_5 \right\}, \\ \dot{z}_5 &\in -k_{I1} \left[[z_1 + k_{I2} [z_2]^{\frac{5}{4}} + k_{I3} [z_3]^{\frac{5}{3}} + k_{I4} [z_4]^{\frac{5}{2}} \right]^0 + [-\bar{L}, \bar{L}], \end{aligned} \quad (4.12)$$

where $\bar{L} = \frac{L}{k_{I1}}$. The following Theorem presents the stability analysis of the 4-DIA applied to the uncertain Class-III system (4.10).

Theorem 4 *The origin of the system (4.4) is finite-time locally stable, even in presence of uncertainties fulfilling conditions (4.9), when the control u is given by (4.11), the canonical transformation is given by (4.8), and the set of gains k_i and k_{Ii} , for $i = 1, 2, 3, 4$, are properly chosen.*

Proof. The proof is similar to the one presented in the Appendix .1, only with $\alpha_1 = \alpha_2 = 1$. ■

It is shown in the proof, using a homogeneous Lyapunov function, that the origin of system (4.12) is Globally Finite-Time stable for all uncertainties satisfying (4.9). Since (4.10) is a local approximation of the plant (4.4), local finite-time stability follows for the latter system, using the same Lyapunov function.

Remark 7 As the Class-I LFTS closed loop system, the closed loop system 4.12 is homogeneous and the theoretical precision of the states after the transient are $|z_1| < \Delta_1 \bar{\tau}^5$, $|z_2| < \Delta_2 \bar{\tau}^4$, $|z_3| < \Delta_3 \bar{\tau}^3$, $|z_4| < \Delta_4 \bar{\tau}^2$ and $|z_5| < \Delta_5 \bar{\tau}$, where $\Delta_i > 0$ with $i = 1, \dots, 5$ and $\bar{\tau}$ as the sample time.

4.2.3 Simulation Results

The Local Finite-Time Stabilizing (LFTS) controller given by the transformation

$$z = Tx = \begin{bmatrix} -307.8943 & 0 & 11.1251 & 0 \\ 0 & -307.8943 & 0 & 11.1251 \\ 0 & 0 & 31.3858 & 0 \\ 0 & 0 & 0 & 31.3858 \end{bmatrix}^{-1} x$$

and the 4-DIA described by (4.11) with gains $k_1 = k_2 = 2$, $k_3 = 5$, $k_4 = 45$, $k_{I1} = 8$, $k_{I2} = k_{I3} = k_{I4} = 0$ and scaling $\lambda = 0.2$, was implemented in Matlab Simulink with the Runge-Kutta's integration method with fixed step and a sampling time equal to 1×10^{-4} [s]. As perturbation, the unbounded signal $\varphi(t) = 0.1 \sin(t) + 0.1t + 0.5$ was used and $\beta(t, z) = 2.5 + \sin(z_1) + \cos(z_2)$ was taken as uncertain control coefficient.

Two initial conditions are presented: one "near" the upward equilibrium $x_0 = [0, 0, -0.2, 0]^T$, and one "far" from it $x_0 = [0.5, -1, 0.7, -1]^T$, where the homogeneous approximation is still valid. Fig. 4.2 shows that for both initial conditions the controller is able to stabilize the origin despite of the presence of the unbounded disturbance and the uncertain control coefficient (shown in Fig 4.3).

Fig. 4.3 presents the behaviour of the output signal ζ of the integrator. It identifies exactly and in finite time the (unbounded) perturbation. Fig. 4.4 shows that the control signal is continuous.

4.2.4 Experimental Validation

The experimental setup for the CP, illustrated in Fig. 4.1, was developed by INTECO. The experiments are performed in Matlab Simulink over a data-acquisition board RT-DAC4/PC1c connected to the CP system.

Since the actual CP system only measures positions, a second order robust exact differentiator [29] was implemented in order to estimate the velocities x_2 , x_4 required by the controller. The control signal u is saturated between $[-0.5, 0.5]$ [V] and, after an amplification stage, is connected to a 12[V] DC motor.

The Local Finite-Time Stabilizing (LFTS) controller given by the transformation (4.2.3) and the 4-DIA described by (4.11) with $k_1 = k_2 = 2$, $k_3 = 20$, $k_4 = 55$, $k_{I1} = 0.3$, $k_{I2} = k_{I3} = k_{I4} = 0$ and scaling gain $\lambda = 0.00035$, were implemented in the real CP

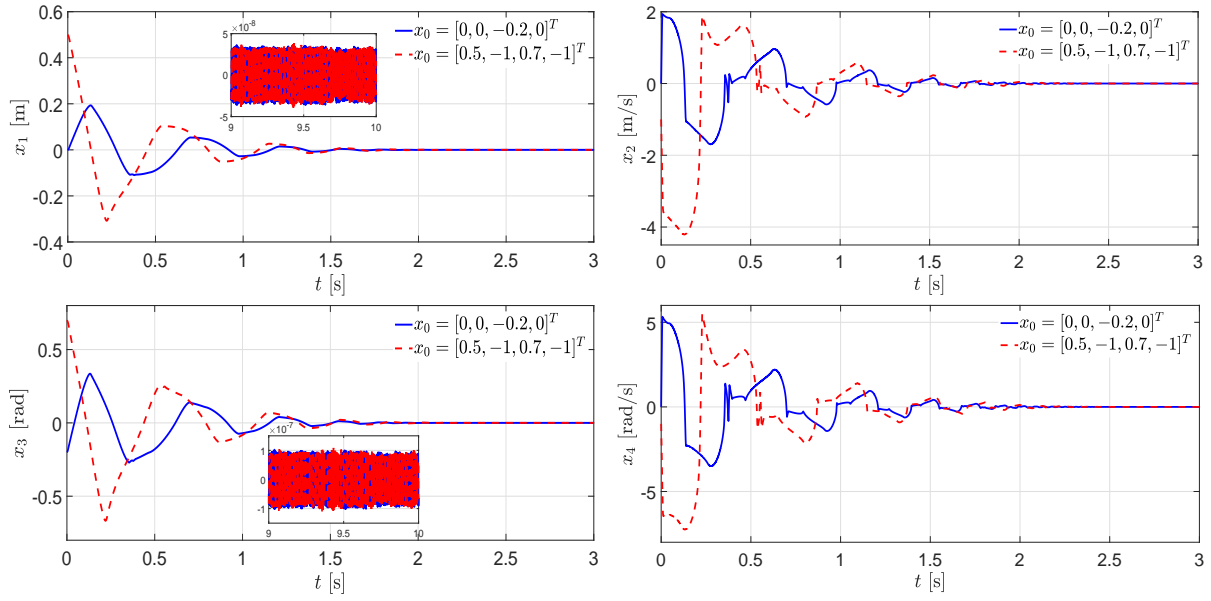


Figure 4.2: Simulated states for the LFTS of the CP.

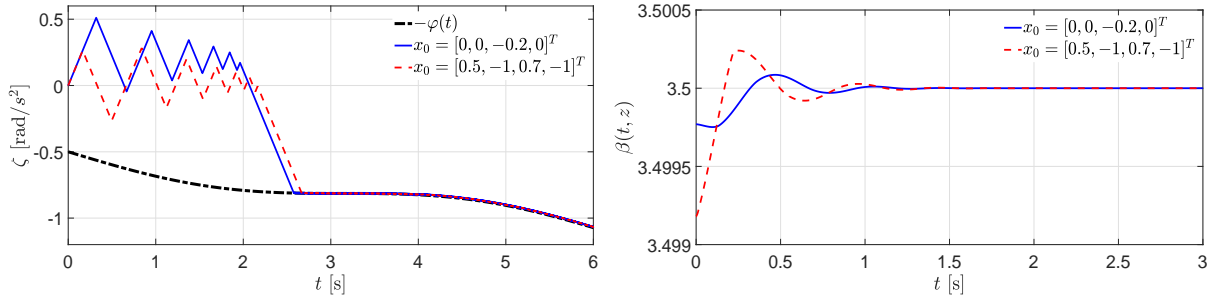


Figure 4.3: Perturbation identification and uncertain control coefficient for the LFTS of the CP simulations.

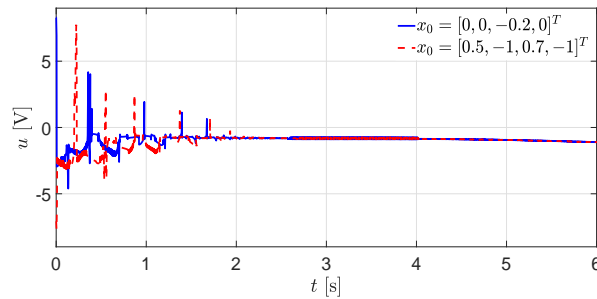


Figure 4.4: Continuous control signal for the LFTS of the CP simulations.

system. This was done using the Runge-Kutta's integration method with fixed-step and a sampling time equal to 1×10^{-3} [s].

The experiments were made with two initial conditions, $x_0 = [0, 0, 0.2, 0]^T$ and $x_0 =$

$[-0.3, 0, -0.4, 0]^T$. Fig. 4.5 shows how the four states reach the origin, even in presence of uncertainties in the system parameters and non-modelled dynamics. Fig. 4.6 shows the continuous control signal V generated by the 4-DIA. The initial condition most far from the origin reaches the saturation of the control, nevertheless, the local stabilization of the origin is ensured.

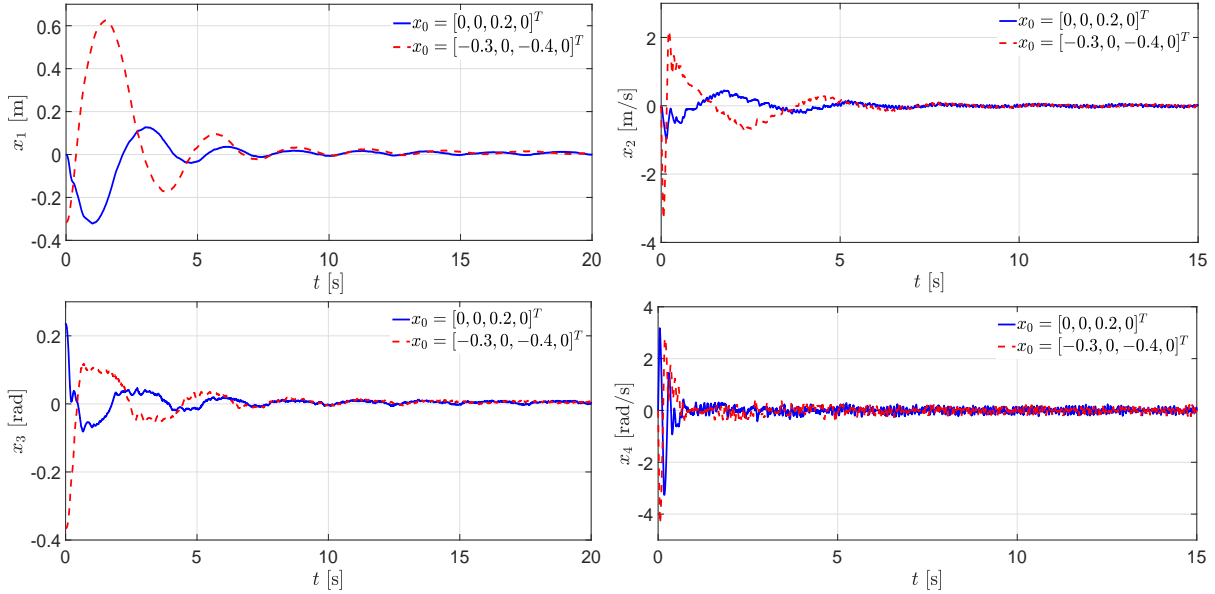


Figure 4.5: Experimental values of the states for the LFTS of the CP.

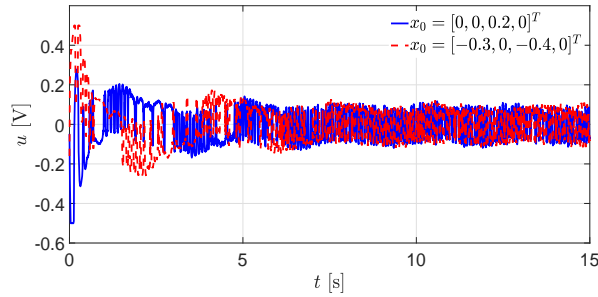


Figure 4.6: Voltage control signal in the LFTS for the CP experiments.

4.3 Design of a Local Asymptotic Stabilizing (LAS) Controller

4.3.1 Problem Statement

In the previous section, a finite-time controller was able to stabilize the origin of the CP despite the presence of perturbations and uncertain control coefficient. Nevertheless, this

result is conditioned to the local homogeneous approximation (really close to the origin) as seen in the simulations.

In this section the objective is to design a controller to (robustly) attain *local asymptotic* stability of the origin $x = 0$ of the CP system, but with a greater domain of attraction than the obtained in the previous section.

To reach the objective it can be followed the same strategy used for the GAS controller of Class-I 3.4 and the sliding surface design presented in [68] for the CP system *using a discontinuous controller*. The controller design can be divided in three steps:

Step 1: Obtain a cascade system in strict feedback form z (similar to (3.10)) for the CP system (so-called *regular form* in [68]).

Step 2: Design the virtual control variable z_3 of the Slave subsystem (z_1, z_2) and find a smooth control law $z_3 = k(z_1, z_2)$ that renders the origin $(z_1, z_2) = 0$ Locally Asymptotically Stable (LAS).

Step 2: For the (nominal linear) Master subsystem (z_3, z_4) a Back-Stepping design leads to the global stability of the state $z = 0$.

In this design, Step 1 and 2 are not modified but for Step 3 it is designed a *discontinuous and homogeneous* integral term, which is able to cope with the uncertainties and/or perturbations satisfying (4.9).

4.3.2 Controller Design

Normal Form

Consider the Class-III underactuated system with two DoF (4.4). Then the following local change of coordinates (see [68]),

$$\begin{aligned} z_1 &= x_1 - a_1 \ln(\tan(x_3) + \sec(x_3)), \\ z_2 &= x_2 - a_1 \frac{x_4}{\cos(x_3)}, \\ z_3 &= x_3, \\ z_4 &= x_4, \end{aligned} \tag{4.13}$$

transforms the dynamics of the system into the local normal form

$$\begin{aligned} \dot{z}_1 &= z_2, \\ \dot{z}_2 &= \frac{-a_1 \tan(z_3) z_4^2 - g \sin(z_3)}{\cos(z_3)}, \\ \dot{z}_3 &= z_4, \\ \dot{z}_4 &= \frac{\cos(z_3) \hat{\omega}_1(z, V) + a_2 g \sin(z_3)}{\hat{d}(z)}, \end{aligned} \tag{4.14}$$

where

$$\hat{\omega}_1(z, V) = k_1 V - z_4^2 \sin(z_3) - k_2 \left[z_2 + a_1 \frac{z_4}{\cos(z_3)} \right], \quad \hat{d}(z) = b - \cos^2(z_3).$$

Remark 8 *Note that system (4.14) is a local representation of the CP system, due to the term $\cos(z_3)$ in the z_2 dynamics. This results in the system to be valid only in when the pendulum is in its upward position or is in its downward position (avoiding the horizontal plane). Due to the fact that this section deals with the stabilization of the CP origin, in the next lines, the local normal form (4.14) will be used for the pendulum on its upward position.*

Virtual controller for the Slave subsystem

The dynamics of z_2 can be seen as $\dot{z}_2 = G(z_3, z_4) \tan(z_3)$, where $G(z_3, z_4) = -a_1 \frac{z_4^2}{\cos(z_3)} - g < 0 \forall z_3 \in (-\pi/2, \pi/2), z_4 \in \mathfrak{R}$. The procedure presented in [68] was to design a sliding surface of relative degree one, to apply a discontinuous control and achieve local asymptotic stabilization of the CP origin. For this purpose, using a Lyapunov approach, the zero dynamics of the system with respect to z_3 is proven to be LAS, in the domain $D = \{z \in \mathfrak{R}^4 \mid z_3 \in (-\pi/2, \pi/2)\}$. This is important for the stability of the cascade system.

Robust Controller for the Master subsystem

Once the virtual LAS controller for the slave is obtained, the local stabilization of the origin of the whole system is reduced to the local asymptotic stabilization of the transformed system, which in the nominal case is given by

$$\begin{aligned} \dot{z}_1 &= z_2, \\ \dot{z}_2 &= G(z_3, z_4)(\mu_1 + \sigma(z_1, z_2)), \\ \dot{\mu}_1 &= \mu_2, \\ \dot{\mu}_2 &= \nu, \end{aligned} \tag{4.15}$$

where the variables are defined as

$$\begin{aligned} \mu_1 &:= \tan(z_3) - \sigma(z_1, z_2), \\ \mu_2 &:= \dot{\mu}_1, \\ \nu &:= \dot{\mu}_2. \end{aligned} \tag{4.16}$$

where

$$\begin{aligned}
 \sigma(z_1, z_2) &= c_0 (c_1 z_1 + c_2 z_2), \\
 V &= \frac{1}{k_1} \left[\frac{\hat{d}\frac{\alpha}{\beta} - a_2 g \sin(z_3)}{\cos(z_3)} + z_4^2 \sin(z_3) + k_2 \left[z_2 + a_1 \frac{z_4}{\cos(z_3)} \right] \right], \\
 \alpha &= \nu - 2z_4^2 \sec(z_3)^2 \tan(z_3) \\
 &\quad + c_0 \left[c_1 G(z_3, z_4) \tan(z_3) - \frac{c_2 a_1 z_4^3 \sin(z_3) \tan(z_3)}{\cos(z_3)^2} + c_2 G(z_3, z_4) z_4 \sec(z_3)^2 \right], \\
 \beta &= \sec(z_3)^2 + \frac{2c_0 c_2 a_1 z_4}{\cos(z_3)}.
 \end{aligned} \tag{4.17}$$

The origin of system (4.15) is locally asymptotically stable if the new control variable ν is designed properly to globally stabilize the origin of the μ_1, μ_2 subsystem. This task, in principle, is rather simple, since it is a second order linear system. However, in presence of uncertainties and perturbations, a more realistic model is

$$\begin{aligned}
 \dot{z}_1 &= z_2, \\
 \dot{z}_2 &= G(z_3, z_4)(\mu_1 + \sigma(z_1, z_2)), \\
 \dot{\mu}_1 &= \mu_2, \\
 \dot{\mu}_2 &= \beta(t, z)[\nu + \varphi(t)],
 \end{aligned} \tag{4.18}$$

where $\beta(t, z)$ and $\varphi(t)$ are assumed to satisfy the conditions (4.9). In this case, the design of a robust control ν is vital to achieve the task of driving the states to the origin globally. The objective in this section is the design of a robust and local stabilizing controller for system (4.18), despite the presence of Lipschitz uncertainties/disturbances, *i.e.*, $|\dot{\varphi}(t)| \leq L$, and uncertain control coefficient $\beta(t, z)$. In order to attenuate the *chattering* effect the control signal will be continuous.

To solve this task, the 2-CTA:

$$\begin{aligned}
 \nu &= -k_1 [\mu_1]^{\frac{1}{3}} - k_2 [\mu_2]^{\frac{1}{2}} + \zeta, \\
 \dot{\zeta} &= -k_3 [\mu_1]^0 - k_4 [\mu_2]^0,
 \end{aligned} \tag{4.19}$$

and the 2-DIA:

$$\begin{aligned}
 \nu &= -k_2 \left[[\mu_2]^{\frac{3}{2}} + k_1^{\frac{3}{2}} \mu_1 \right]^{\frac{1}{3}} + \zeta \\
 \dot{\zeta} &= -k_{I1} [\mu_1 + k_{I2} [\mu_2]^{\frac{3}{2}}]^0.
 \end{aligned} \tag{4.20}$$

will be used as in Class-I. The following theorem is the main result of this section:

Theorem 5 *The origin of μ_1, μ_2 -system in (4.18) is globally finite-time stable, despite the presence of the Lipschitz disturbances/uncertainties $\varphi(t)$ and the uncertain coefficient*

β satisfying (4.9). Moreover, z_1, z_2 will be driven to the origin locally and asymptotically (with domain of attraction $D = \{z \in \mathfrak{R}^4 \mid z_3 \in (-\pi/2, \pi/2)\}$), when the control V takes the form of (4.17), with the state transformations (4.13) and (4.16), and ν takes the form of (4.19) or (4.20).

Proof. Due to the fact that the μ_1, μ_2 subsystem is globally stable in finite-time (proof shown in Appendix .4) and the zero-dynamics z_1, z_2 is LAS with domain of attraction $D = \{z \in \mathfrak{R}^4 \mid z_3 \in (-\pi/2, \pi/2)\}$ (proof shown in [68]), the origin of (4.18) is LAS with same domain of attraction. ■

Remark 9 As a consequence of the Theorem 5, the states of the original system (4.4), are locally and asymptotically driven to the origin.

Remark 10 As in the Class-I GAS, the closed loop systems of the μ subsystem with the 2-CTA and the 2-DIA are homogeneous of degree $d = -1$ and weights $(r_1, r_2, r_3) = (3, 2, 1)$, and the theoretical precision of the states after the transient are $|\mu_1| < \Delta_1 \bar{\tau}^3$, $|\mu_2| < \Delta_2 \bar{\tau}^2$ and $|\mu_3| < \Delta_3 \bar{\tau}$, where $\Delta_i > 0$ with $i = 1, \dots, 3$ and $\bar{\tau}$ as the sample time.

4.3.3 Simulation results

For the LAS, the control (4.17), the transformations (4.13) and (4.16), the 2-DIA described by (4.20) with $k_1 = 4.16$, $k_2 = 28.5$, $k_{I1} = 6.3$, $k_{I2} = 0$, the 2-CTA described by (4.19) with $k_1 = 42.92$, $k_2 = 18.37$, $k_3 = 13.8$, $k_4 = 6.6$ were implemented in Matlab Simulink with the Runge-Kutta's integration method of fixed step and a sampling time equal to 1×10^{-4} [s]. Also, to perform a comparison with another kind of algorithm, a linear algorithm (2-LA) was tested:

$$\nu = -k_1 \mu_1 - k_2 \mu_2, \quad (4.21)$$

with $k_1 = k_2 = 10$. The simulations were made with the same unbounded perturbation $\varphi(t) = 2 \sin(2t) + 2t + 2$, uncertain control coefficient $\beta(t, z) = 2.5 + \sin(z_1) + \cos(z_2)$, the same initial condition $x_0 = [-1, -0.2, 1.5, -0.2]^T$ (inside the domain of attraction of the LAS control) and the same gains $c_0 = 0.03$ and $c_1 = c_2 = 1$.

The results are shown in Figs. 4.7-4.10. The sliding modes algorithm drive the μ_1, μ_2 states to the origin in finite-time, making the original states of the CP system to be attracted to the origin asymptotically and maintained there despite the presence of the unbounded disturbance (due to the fact that they are able to identify the disturbance exactly as shown in Fig. 4.9). The 2-LA can drive the states near to the origin, but as the disturbance grows, is not able to compensate it and the states start to grow. With respect to the control signal, the three algorithms present a continuous one, as shown in Fig. 4.4.

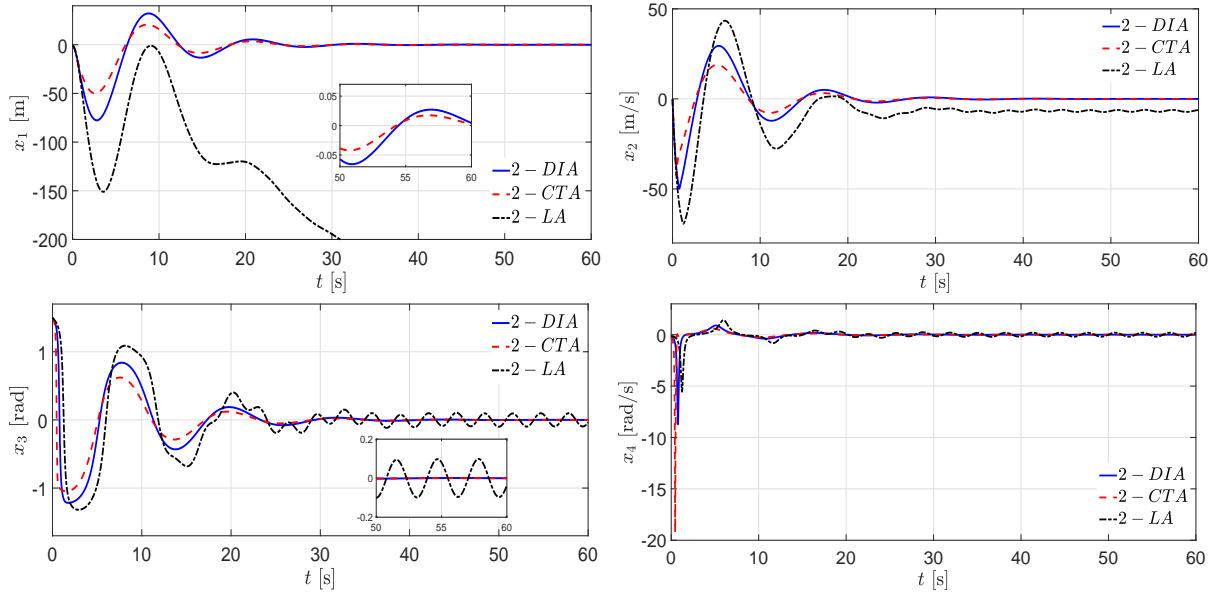


Figure 4.7: State trajectories in the LAS for the CP simulations.

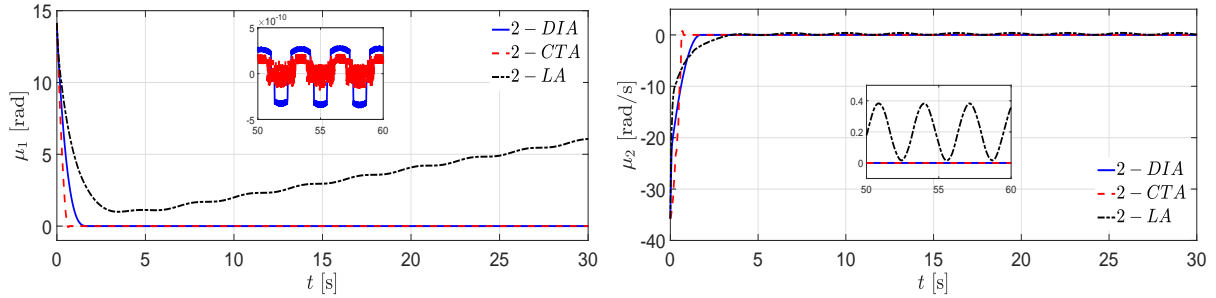


Figure 4.8: Finite-time state trajectories in the LAS for the CP simulations.

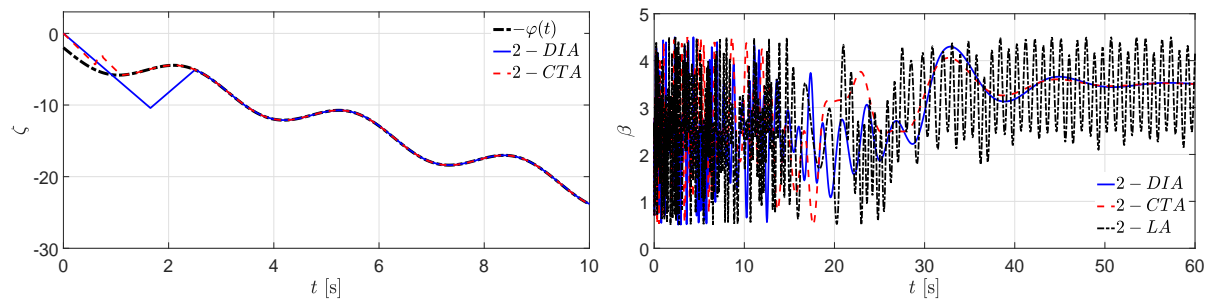


Figure 4.9: Perturbation identification and uncertain control coefficient in the LAS for the CP simulations.

4.3.4 Experimental Validation

The control (4.17), the transformations (4.13) and (4.16), the 2-CTA described by (4.19) with $k_1 = 36.3$, $k_2 = 19.84$, $k_3 = 4.02$, $k_4 = 1.92$, $c_0 = 1.5$, $c_1 = c_2 = 1$, was implemented

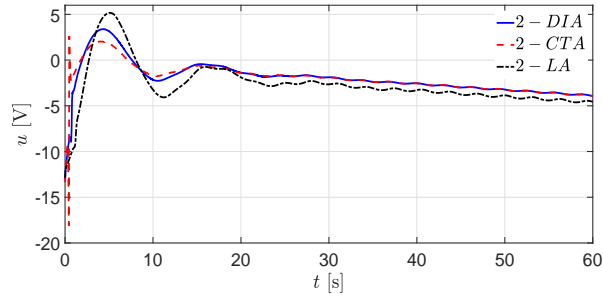


Figure 4.10: Control signal in the LAS for the CP simulations.

in the real CP system with the Runge-Kutta's integration method of fixed step and a sampling time equal to 1×10^{-3} [s].

Due to the fact that the LAS works when $x_3 \in (-\pi/2, \pi/2)$, for the experiment, a swing-up controller developed for INTECO was used. When the pendulum position was $x_3 = 1$ [rad], this swing-up controller changed to the LAS algorithm. This can be seen around 1.73 [s] from the beginning of the experiment (a vertical line was drawn in the Figs. in order to see were the LAS started to work).

The results are shown in Figs. 4.11-4.13. The continuous sliding-mode algorithm drives the states of the pendulum from the initial condition to the origin and stay around it. Seeing the μ_1 and μ_2 plots, one can notice how the 2-CTA can maintain them in the origin despite the uncertainties and non-modelled dynamics. The chattering effect is diminished as seen in the continuous control signal of the sliding-modes algorithm.

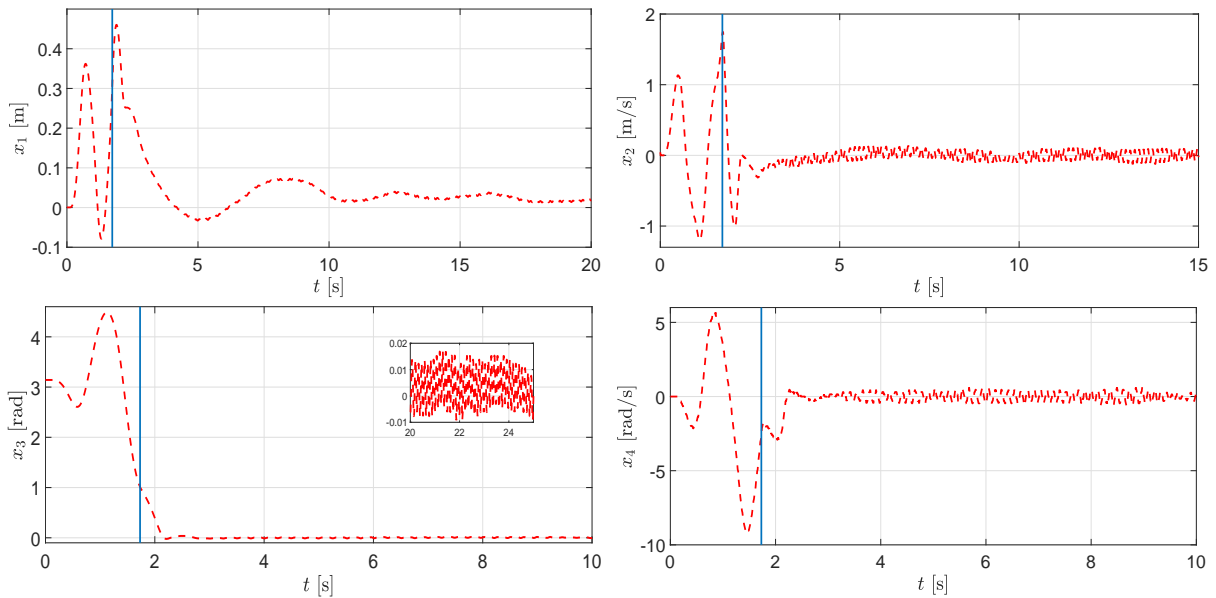


Figure 4.11: State trajectories in the LAS for the CP experiments.

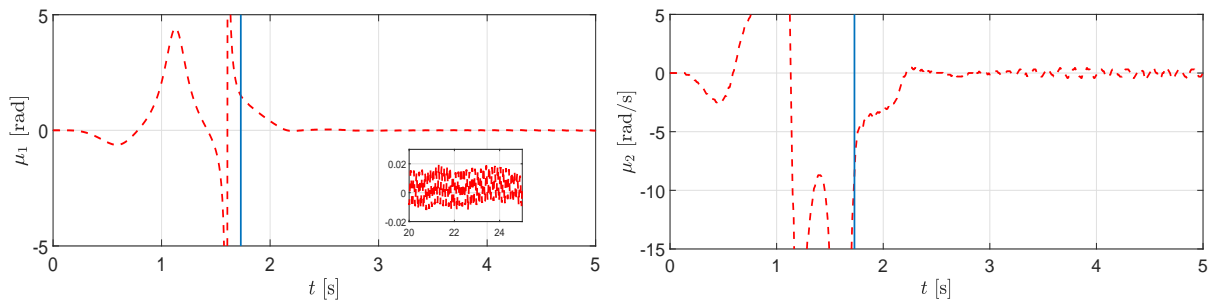


Figure 4.12: Finite-time state trajectories in the LAS for the CP experiments.

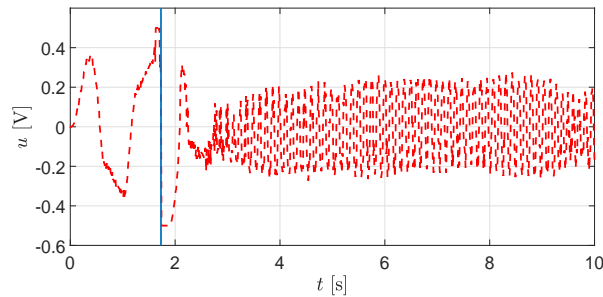


Figure 4.13: Voltage control signal in the LAS for the CP experiments.

4.4 Conclusions

In this chapter, *robust* controllers were designed for the Class-III of underactuated mechanical systems of two DoF, using a continuous Higher-Order Sliding-Modes strategy. Two kinds of controller designs were presented: One generates a fifth-order sliding-mode and achieves Local Finite-Time Stability (LFTS). The other is a robust controller that provides Local Asymptotic Stability (LAS), but with a greater domain of attraction than the LFTS. These controllers compensate matched Lipschitz disturbances and/or uncertainties, cope with an uncertain control coefficient and generate a *continuous* control signal, possibly reducing the chattering effect.

Evidence of the performance of the controllers is provided using simulations and experiments over the real CP system.

Chapter 5

Conclusions

- Robust control strategies were designed for two Classes of Underactuated Mechanical Systems of two DoF: Class-I and Class-III from the classification presented in [42].
- For the Class-I:
 - Local Finite-Time Stabilization (LFTS) of the origin was obtained using a homogeneous approximation of the system and a Fourth Order Discontinuous Integral Sliding-Mode Algorithm.
 - The numerical estimation of the attraction domain of the LFTS was obtained for the Reaction Wheel Pendulum of third order (a system belonging to the Class-I). This explains why the used algorithm is able to perform the swing-up and the stabilization in one step.
 - Global Asymptotic Stabilization of the origin was obtained using a backstepping-like procedure and two Second Order Discontinuous Integral Sliding-Mode Algorithms.
- For the Class-III:
 - Local Finite-Time Stabilization of the origin was obtained using a homogeneous approximation of the system and a Fourth Order Discontinuous Integral Sliding-Mode Algorithm.
 - Local Asymptotic Stabilization of the origin was obtained using a backstepping-like procedure and two Second Order Discontinuous Integral Sliding-Mode Algorithms, but with a greater domain of attraction than the LFTS.
- The results were obtained despite the presence of matched Lipschitz perturbations and bounded uncertain control coefficient.
- Due to the fact that the used sliding-modes algorithms have the discontinuity in an integral part, the generated control signal is continuous and the chattering effect is attenuated.

- The presented strategies were tested in simulations over the Reaction Wheel Pendulum, the TORA and the Cart-Pendulum systems, and experiments over the real Reaction Wheel Pendulum and the Cart-Pendulum systems.
- Disadvantages of the proposed controller strategies:
 - The integral term adds a new state variable to be analysed in the stability analysis of the systems.
 - The integral term also induces more gains to be tuned as in comparison to the linear algorithms presented.
 - These CHOSM algorithms need a small sampling-time in the simulations/experiments to present good results. If the sampling-time grows, the precision of the states gets worse.
- Future work:
 - System stability analysis adding a state dependant perturbation.
 - Analysis of the controllers' saturation.
 - Comparison with other similar algorithms that are able to compensate perturbations.

Appendices

.1 Appendix A: Proof of Theorem 1 and 4

Using the back-stepping-like procedure to obtain the state-feedback controller and its Lyapunov Function used in [9], and introducing an additional term and a modification, it is obtained the following homogeneous candidate Lyapunov function of degree m

$$V_4(z) = \gamma_3 V_3 + \frac{2}{m} |z_4|^{\frac{m}{2}} + k_3^{\frac{m-2}{2}} \left[|z_3|^{\frac{5}{3}} + k_2^{\frac{5}{3}} |z_2|^{\frac{5}{4}} + k_2^{\frac{5}{3}} k_1^{\frac{5}{4}} \xi_1 \right]^{\frac{m-2}{5}} z_4 + \left(1 - \frac{2}{m} \right) k_3^{\frac{m}{2}} \left| |z_3|^{\frac{5}{3}} + k_2^{\frac{5}{3}} |z_2|^{\frac{5}{4}} + k_2^{\frac{5}{3}} k_1^{\frac{5}{4}} \xi_1 \right|^{\frac{m}{5}} + \frac{1}{m} |z_5|^m,$$

where

$$\xi_1 = z_1 - k_\xi |z_5|^5, \quad \dot{\xi}_1 = \alpha_1 z_2 - 5k_\xi |z_5|^4 \dot{z}_5, \quad k_\xi = k_4^{-5} k_3^{-\frac{5}{2}} k_2^{-\frac{5}{3}} k_1^{-\frac{5}{4}},$$

$$V_3(\xi_1, z_2, z_3) = \gamma_2 V_2 + \frac{3}{m} |z_3|^{\frac{m}{3}} + k_2^{\frac{m-3}{3}} \left[|z_2|^{\frac{5}{4}} + k_1^{\frac{5}{4}} \xi_1 \right]^{\frac{m-3}{5}} z_3 + \left(1 - \frac{3}{m} \right) k_2^{\frac{m}{3}} \left| |z_2|^{\frac{5}{4}} + k_1^{\frac{5}{4}} \xi_1 \right|^{\frac{m}{5}},$$

$$V_2(\xi_1, z_2) = \frac{5}{m} \gamma_1 |\xi_1|^{\frac{m}{5}} + \frac{4}{m} |z_2|^{\frac{m}{4}} + k_1^{\frac{m-4}{4}} |\xi_1|^{\frac{m-4}{5}} z_2 + \left(1 - \frac{4}{m} \right) k_1^{\frac{m}{4}} |\xi_1|^{\frac{m}{5}}.$$

It can be shown that $V(z)$ is positive definite for any positive constants $\gamma_1, \gamma_2, \gamma_3 > 0$. Note that it is required to have the degree $m \geq 9$ for the powers in $V(z)$ to be larger than one, for making $V(z)$ differentiable everywhere. Now we proceed to show that $V(z)$ is positive definite and radially unbounded for *any* $\gamma_1 > 0, \gamma_2 > 0$ and $\gamma_3 > 0$.

- Note that $\gamma_1 \frac{5}{m} |\xi_1|^{\frac{m}{5}}$, which is the first term in $V_2(\xi_1, z_2)$, is positive $\gamma_1 \frac{5}{m} |\xi_1|^{\frac{m}{5}} \geq 0$ and it is zero only when $\xi_1 = 0$. In this case we have that $V_2(0, z_2) = \frac{4}{m} |z_2|^{\frac{m}{4}} \geq 0$, which is positive, except when $z_2 = 0$. Since $V_2(\xi_1, z_2)$ is continuous and homogeneous, Lemma 1 implies that selecting $\gamma_1 > 0$ sufficiently large function $V_2(\xi_1, z_2)$ is positive definite (in its two variables). In fact, using Young's inequality it is possible to show that with $\gamma_1 = 0$ V_2 is positive semi-definite. This implies that V_2 is positive definite for any $\gamma_1 > 0$.
- The first term in $V_3(\xi_1, z_2, z_3)$ is $V_2(\xi_1, z_2)$, which is positive definite, and so it vanishes only when $(\xi_1, z_2) = 0$. When this happens $V_3(0, 0, z_3) = \frac{3}{m} |z_3|^{\frac{m}{3}} \geq 0$, which is positive, except for $z_3 = 0$. Again, Lemma 1 implies that selecting $\gamma_2 > 0$ sufficiently large function $V_3(\xi_1, z_2, z_3)$ becomes positive definite (in its three variables). Again, Young's inequality shows that $V_3 \geq 0$ when $\gamma_2 = 0$. Thus, V_3 is positive definite for any $\gamma_2 > 0$.
- Finally, the first term in $V_4(z)$ is $V_3(\xi_1, z_2, z_3)$, which is positive definite, and so it vanishes only when $(\xi_1, z_2, z_3) = 0$. When this happens $V_4|_{(\xi_1, z_2, z_3)=0} = \frac{2}{m} |z_4|^{\frac{m}{2}} +$

$\frac{1}{m} |z_5|^m \geq 0$, which is positive, except for $z_4 = z_5 = 0$. Again, Lemma 1 implies that selecting $\gamma_3 > 0$ sufficiently large function $V_4(z)$ becomes positive definite (in its five variables). Once more, Young's inequality shows that $V_4 \geq 0$ when $\gamma_3 = 0$. Thus, $V_4(z)$ is positive definite for any $\gamma_3 > 0$

Moreover, $V_4(z)$ being homogeneous and positive definite is also radially unbounded. And thus it is an appropriate LF candidate.

Its derivative along the trajectories of (3.22) is given by

$$\dot{V}_4 = \gamma_3 [\gamma_2 F_{k_{2,3}} + F_{k_{3,4}}] + \beta(t, z) k_4 G_{k_4} + F_{k_4} + [z_5]^{m-1} \dot{z}_5, \quad (\text{A.1})$$

where

$$\begin{aligned} G_{k_4} &= - \left[[z_4]^{\frac{m-2}{2}} + k_3^{\frac{m-2}{2}} \left[[z_3]^{\frac{5}{3}} + k_2^{\frac{5}{3}} [z_2]^{\frac{5}{4}} + k_2^{\frac{5}{3}} k_1^{\frac{5}{4}} \xi_1 \right]^{\frac{m-2}{5}} \right] \times \\ &\quad \left[-k_4^{-1} z_5 + \left[[z_4]^{\frac{5}{2}} + k_3^{\frac{5}{2}} [z_3]^{\frac{5}{3}} + k_3^{\frac{5}{2}} k_2^{\frac{5}{3}} [z_2]^{\frac{5}{4}} + k_3^{\frac{5}{2}} k_2^{\frac{5}{3}} k_1^{\frac{5}{4}} \xi_1 + k_4^{-5} [z_5]^5 \right]^{\frac{1}{5}} \right], \\ F_{k_4} &= \left(\frac{m-2}{5} \right) k_3^{\frac{m-2}{2}} \left| [z_3]^{\frac{5}{3}} + k_2^{\frac{5}{3}} [z_2]^{\frac{5}{4}} + k_2^{\frac{5}{3}} k_1^{\frac{5}{4}} \xi_1 \right|^{\frac{m-7}{5}} \times \\ &\quad \left[\frac{5}{3} |z_3|^{\frac{2}{3}} z_4 + \frac{5}{4} k_2^{\frac{5}{3}} \alpha_2 |z_2|^{\frac{1}{4}} z_3 + k_2^{\frac{5}{3}} k_1^{\frac{5}{4}} [\alpha_1 z_2 - 5k_\xi |z_5|^4 \dot{z}_5] \right] \times \\ &\quad \left[z_4 + k_3 \left[[z_3]^{\frac{5}{3}} + k_2^{\frac{5}{3}} [z_2]^{\frac{5}{4}} + k_2^{\frac{5}{3}} k_1^{\frac{5}{4}} \xi_1 \right]^{\frac{2}{5}} \right], \\ F_{k_{3,4}} &= \left[[z_3]^{\frac{m-3}{3}} + k_2^{\frac{m-3}{3}} \left[[z_2]^{\frac{5}{4}} + k_1^{\frac{5}{4}} \xi_1 \right]^{\frac{m-3}{5}} \right] z_4 + \left(\frac{m-3}{5} \right) k_2^{\frac{m-3}{3}} \left| [z_2]^{\frac{5}{4}} + k_1^{\frac{5}{4}} \xi_1 \right|^{\frac{m-8}{5}} \times \\ &\quad \left[z_3 + k_2 \left[[z_2]^{\frac{5}{4}} + k_1^{\frac{5}{4}} \xi_1 \right]^{\frac{3}{5}} \right] \left[\frac{5}{4} \alpha_2 |z_2|^{\frac{1}{4}} z_3 + k_1^{\frac{5}{4}} [\alpha_1 z_2 - 5k_\xi |z_5|^4 \dot{z}_5] \right], \\ F_{k_{2,3}} &= \gamma_1 [\xi_1]^{\frac{m-5}{5}} [\alpha_1 z_2 - 5k_\xi |z_5|^4 \dot{z}_5] + \alpha_2 \left[[z_2]^{\frac{m-4}{4}} + k_1^{\frac{m-4}{4}} [\xi_1]^{\frac{m-4}{5}} \right] z_3 \\ &\quad + \left(\frac{m-4}{5} \right) k_1^{\frac{m-4}{4}} |\xi_1|^{\frac{m-9}{5}} [z_2 + k_1 [\xi_1]^{\frac{4}{5}}] [\alpha_1 z_2 - 5k_\xi |z_5|^4 \dot{z}_5]. \end{aligned}$$

Using (2.3), the term G_{k_4} is negative semi-definite and it vanishes only on the set

$$S_1 = \left\{ z_4 = -k_3 \left[[z_3]^{\frac{5}{3}} + k_2^{\frac{5}{3}} [z_2]^{\frac{5}{4}} + k_2^{\frac{5}{3}} k_1^{\frac{5}{4}} \xi_1 \right]^{\frac{2}{5}} \right\}.$$

Evaluating \dot{V}_4 on this set, and noting that $F_{k_4}|_{S_1} = 0$ and $F_{k_{3,4}}|_{S_1} = k_3 G_{k_3} + F_{k_3}$, it is obtained

$$\dot{V}_4|_{S_1} = \gamma_3 [\gamma_2 F_{k_{2,3}} + k_3 G_{k_3} + F_{k_3}] + z_5^{m-1} \dot{z}_5|_{S_1},$$

where

$$G_{k_3} = - \left[[z_3]^{\frac{m-3}{3}} + k_2^{\frac{m-3}{3}} \left[[z_2]^{\frac{5}{4}} + k_1^{\frac{5}{4}} \xi_1 \right]^{\frac{m-3}{5}} \right] \left[[z_3]^{\frac{5}{3}} + k_2^{\frac{5}{3}} [z_2]^{\frac{5}{4}} + k_2^{\frac{5}{3}} k_1^{\frac{5}{4}} \xi_1 \right]^{\frac{2}{5}},$$

$$F_{k_3} = \left(\frac{m-3}{5} \right) k_2^{\frac{m-3}{3}} \left| [z_2]^{\frac{5}{4}} + k_1^{\frac{5}{4}} \xi_1 \right|^{\frac{m-8}{5}} \left[z_3 + k_2 \left[[z_2]^{\frac{5}{4}} + k_1^{\frac{5}{4}} \xi_1 \right]^{\frac{3}{5}} \right] \times$$

$$\left[\frac{5}{4} \alpha_2 |z_2|^{\frac{1}{4}} z_3 + k_1^{\frac{5}{4}} \left[\alpha_1 z_2 - 5k_\xi |z_5|^4 \dot{z}_5|_{S_1} \right] \right].$$

The term G_{k_3} is negative semi-definite and it is zero only on the set

$$S_2 = \left\{ z_3 = -k_2 \left[[z_2]^{\frac{5}{4}} + k_1^{\frac{5}{4}} \xi_1 \right]^{\frac{3}{5}} \right\}.$$

Evaluating $\dot{V}_4|_{S_1}$ on this set, and noting that $F_{k_3}|_{S_2} = 0$ and $F_{k_{2,3}}|_{S_2} = F_{k_2} + k_2 G_{k_2}$, we get

$$\dot{V}_4|_{S_1 \cap S_2} = \gamma_3 \gamma_2 [F_{k_2} + k_2 G_{k_2}] + [z_5]^{m-1} \dot{z}_5|_{S_1 \cap S_2},$$

where

$$G_{k_2} = - \alpha_2 \left[[z_2]^{\frac{m-4}{4}} + k_1^{\frac{m-4}{4}} [\xi_1]^{\frac{m-4}{5}} \right] \left[[z_2]^{\frac{5}{4}} + k_1^{\frac{5}{4}} \xi_1 \right]^{\frac{3}{5}},$$

$$F_{k_2} = \gamma_1 [\xi_1]^{\frac{m-5}{5}} \left[\alpha_1 z_2 - 5k_\xi |z_5|^4 \dot{z}_5|_{S_1 \cap S_2} \right] + \left(\frac{m-4}{5} \right) k_1^{\frac{m-4}{4}} |\xi_1|^{\frac{m-9}{5}} \times$$

$$\left[z_2 + k_1 [\xi_1]^{\frac{4}{5}} \right] \left[\alpha_1 z_2 - 5k_\xi |z_5|^4 \dot{z}_5|_{S_1 \cap S_2} \right].$$

Now, G_{k_2} is negative semi-definite and it vanishes only on the set

$$S_3 = \left\{ z_2 = -k_1 [\xi_1]^{\frac{4}{5}} \right\}.$$

Evaluating $\dot{V}_4|_{S_1 \cap S_2}$ on this set it is obtained

$$\dot{V}_4|_{S_1 \cap S_2 \cap S_3} = \gamma_2 \gamma_3 F_{k_2}|_{S_3} + [z_5]^{m-1} \dot{z}_5|_{S_1 \cap S_2 \cap S_3}$$

$$= - \alpha_1 k_1 \gamma_3 \gamma_2 \gamma_1 |\xi_1|^{\frac{m-1}{5}} - k_{I1} \left[[z_5]^{m-1} - 5k_\xi \gamma_3 \gamma_2 \gamma_1 [\xi_1]^{\frac{m-5}{5}} |z_5|^4 \right] \times$$

$$\left[\left[\left[1 - k_{I2} k_1^{\frac{m}{4}} \right] \xi_1 + k_\xi [z_5]^5 \right]^0 + [-\bar{L}, \bar{L}] \right].$$

Since $k_1 > 0$ the first term in the latter expression is non-positive and it is zero only on the set

$$S_4 = \{ \xi_1 = 0 \}.$$

Evaluating $\dot{V}_4|_{S_1 \cap S_2 \cap S_3}$ on this set it is obtained

$$\dot{V}_4|_{S_1 \cap S_2 \cap S_3 \cap S_4} \in -k_{I1} \lceil z_5 \rceil^{m-1} \left[\lceil z_5 \rceil^0 + [-\bar{L}, \bar{L}] \right].$$

The latter expression is negative if $\bar{L} = \frac{L}{k_{I1}} < 1$, that is, for

$$L < k_{I1}, \quad (\text{A.2})$$

since $\lceil z_5 \rceil^0$ is a multivalued function, defined as

$$\lceil z_5 \rceil^0 = \begin{cases} +1 & \text{if } z_5 > 0, \\ [-1, +1] & \text{if } z_5 = 0, \\ -1 & \text{if } z_5 < 0. \end{cases}$$

Lemma 2 implies that it is possible to render $\dot{V}_4|_{S_1 \cap S_2 \cap S_3} < 0$ selecting $k_{I1} > 0$ small. Applying Lemma 2 once more, it can be concluded that $\dot{V}_4|_{S_1 \cap S_2} < 0$ selecting $k_2 > 0$ sufficiently large. Again, Lemma 2 shows that one can get $\dot{V}_4|_{S_1} < 0$ selecting $k_3 > 0$ sufficiently large. Finally, Lemma 2 implies that $\dot{V}_4|_{S_1} < 0$ if $k_4 > 0$ is sufficiently large.

Since \dot{V}_4 is negative definite by appropriate selection of the gains (what is always feasible), then the origin of system (3.22) is asymptotically stable. Moreover, since the system is homogeneous of negative degree, the origin is finite-time stable (see e.g. [28]). Since (3.22) is a local homogeneous approximation of system (3.11), one conclude that it is locally finite-time stable. ■

.2 Appendix B: LFTS Gain Selection

From the previous proof conditions for the gains can be derived to render $\dot{V}_4 < 0$. The following inequalities are obtained for the gain selection:

$$k_1 > 0, \quad (\text{B.1})$$

$$k_{I1}^{-1} > \max_{z \in \Omega_1} \left\{ \frac{-k_1^{\frac{m}{4}} \gamma_3 \gamma_2 \gamma_1 |\xi_1|^{\frac{m-1}{5}}}{\left[\lceil z_5 \rceil^{m-1} - 5k_\xi \gamma_3 \gamma_2 \gamma_1 \lceil \xi_1 \rceil^{\frac{m-5}{5}} |z_5|^4 \right] \dot{z}_5|_{S_1 \cap S_2 \cap S_3}} \right\}, \quad (\text{B.2})$$

$$k_2 > \max_{z \in \Omega_2} \left\{ \frac{F_{k_2} + \gamma_3^{-1} \gamma_2^{-1} \lceil z_5 \rceil^{m-1} \dot{z}_5|_{S_1 \cap S_2}}{G_{k_2}} \right\}, \quad (\text{B.3})$$

$$k_3 > \max_{z \in \Omega_3} \left\{ \frac{\gamma_2 F_{k_{2,3}} + F_{k_3} + \gamma_3^{-1} \lceil z_5 \rceil^{m-1} \dot{z}_5|_{S_1}}{G_{k_3}} \right\}, \quad (\text{B.4})$$

$$k_4 > \frac{1}{b_m} \max_{z \in \Omega_4} \left\{ \frac{\gamma_3 [\gamma_2 F_{k_{2,3}} + F_{k_{3,4}}] + F_{k_4} + [z_5]^{m-1} \dot{z}_5}{G_{k_4}} \right\}, \quad (\text{B.5})$$

where the homogeneous unit spheres Ω_i are given by $\Omega_1 = \{|\xi_1|^{\frac{1}{5}} + |z_5| = 1\}$, $\Omega_2 = \{|\xi_1|^{\frac{1}{5}} + |z_2|^{\frac{1}{4}} + |z_5| = 1\}$, $\Omega_3 = \{|\xi_1|^{\frac{1}{5}} + |z_2|^{\frac{1}{4}} + |z_3|^{\frac{1}{3}} + |z_5| = 1\}$, and $\Omega_4 = \{|\xi_1|^{\frac{1}{5}} + |z_2|^{\frac{1}{4}} + |z_3|^{\frac{1}{3}} + |z_4|^{\frac{1}{2}} + |z_5| = 1\}$.

Functions (B.2)-(B.5) are shown to have a maximum value. Since they are homogeneous of degree $d = 0$ the maximum can be found on the homogeneous unit sphere Ω_i .

.3 Appendix C: Proof of Theorem 2

Considering the homogeneous candidate Lyapunov function (with $m \geq 7$ to make it differentiable) as

$$V_3(\xi_1, z_2, z_3) = \gamma_2 V_2 + \frac{2}{m} |z_3|^{\frac{m}{2}} + k_2^{\frac{m-2}{2}} \left[|z_2|^{\frac{4}{3}} + k_1^{\frac{4}{3}} \xi_1 \right]^{\frac{m-2}{4}} z_3 + \left(1 - \frac{2}{m}\right) k_2^{\frac{m}{2}} \left[|z_2|^{\frac{4}{3}} + k_1^{\frac{4}{3}} \xi_1 \right]^{\frac{m}{4}} + \frac{1}{m} \gamma_3 |z_4|^m,$$

where

$$\xi_1 = z_1 - k_\xi [z_4]^4, \quad \dot{\xi}_1 = W \sin(z_2) - 4k_\xi |z_4|^3 \dot{z}_4, \quad k_\xi = k_3^{-4} k_2^{-\frac{4}{2}} k_1^{-\frac{4}{3}},$$

$$V_2(\xi_1, z_2) = \frac{4}{m} \gamma_1 |\xi_1|^{\frac{m}{4}} + \frac{3}{m} |z_2|^{\frac{m}{3}} + k_1^{\frac{m-3}{3}} [\xi_1]^{\frac{m-3}{4}} z_2 + \left(1 - \frac{3}{m}\right) k_1^{\frac{m}{3}} |\xi_1|^{\frac{m}{4}},$$

it can be proved analytically with a similar procedure as .1, that $V_3(\xi_1, z_2, z_3)$ is positive definite and its derivative along the trajectories of the system (3.29) is negative definite close to the origin. In consequence, can be concluded that the origin of system (3.29) is locally asymptotically stable. Furthermore, for homogeneous properties [28] the origin is finite-time locally stable and by Eq. (3.24), the origin of system (3.11) is finite-time locally stable.

As a result of this, an analytic estimated of the domain of attraction of the origin is $V_3(z) \leq C$, with $C > 0$.

Numerical estimation of the domain of attraction

The main advantage of the coordinates transformation (3.24) is that a global representation of the (3.11) is obtained. As a result of this, a region of attraction can be estimated to show that the points of interest of the state space are contained in that region. This cannot be done, using the coordinates transformation presented in [57] because this transformation is only valid locally.

On the other hand, to conclude local finite-time stability of the (3.27) origin, a homogeneous approximation of the 3-RWP system has to be made. This approximation, in principle, restrict the analysis to be really close to the origin. But, as seen in the next estimation of the attraction domain, the term $W(z_2)$ can be dominated close the origin by the 3-DIA, making the approximation good enough to include the downward position of the pendulum in such domain of attraction.

The problem of designing the 3-DIA's gains ensuring the positive definiteness of the Lyapunov function and negative definiteness of its derivative, stabilizing the origin of the system (3.29) far from the origin, analytically, is a really difficult task. Therefore, the set of gains can be obtained, using a numerical method in Matlab. Firstly the points over the level surfaces of the Lyapunov function should be obtained, *i.e.*,

$$\begin{aligned} V_3 = & \gamma_2 V_2 + \frac{2}{m} |z_3|^{\frac{m}{2}} + k_2^{\frac{m-2}{2}} \left[|z_2|^{\frac{4}{3}} + k_1^{\frac{4}{3}} \xi_1 \right]^{\frac{m-2}{4}} z_3 + \\ & \left(1 - \frac{2}{m} \right) k_2^{\frac{m}{2}} \left[|z_2|^{\frac{4}{3}} + k_1^{\frac{4}{3}} \xi_1 \right]^{\frac{m}{4}} + \frac{1}{m} \gamma_3 |z_4|^m = C, \end{aligned} \quad (\text{C.1})$$

where $C \in \Re$.

This, in the practice, is not a simple task, but the fact that the Lyapunov function is homogeneous is used. Therefore, values of \bar{z} in a unit sphere are chosen, *i.e.*, $\|\bar{z}\| = 1$:

$$\bar{z} = \begin{bmatrix} \bar{z}_1 \\ \bar{z}_2 \\ \bar{z}_3 \\ \bar{z}_4 \end{bmatrix} = \begin{bmatrix} \cos(\theta) \cdot \sin(\phi) \cdot \sin(\psi) \\ \sin(\theta) \cdot \sin(\phi) \cdot \sin(\psi) \\ \cos(\phi) \cdot \sin(\psi) \\ \cos(\psi) \end{bmatrix}, \quad (\text{C.2})$$

where $\theta \in [0, 2\pi]$, $\phi \in [0, \pi]$, $\psi \in [0, 2\pi]$. Now, as the Lyapunov function satisfies the property of homogeneity, it holds

$$V_3(\Delta_\epsilon^r \bar{z}) = \epsilon^m V_3(\bar{z}) = C, \quad (\text{C.3})$$

so the points on the unit sphere can be translate to a level surface $V_3(z) = C$ as follows

$$\epsilon = \left(\frac{C}{V(\bar{z})} \right)^{\frac{1}{m}}, \quad (\text{C.4})$$

$$z = \begin{bmatrix} \epsilon^4 \bar{z}_1 \\ \epsilon^3 \bar{z}_2 \\ \epsilon^2 \bar{z}_3 \\ \epsilon \bar{z}_4 \end{bmatrix}. \quad (\text{C.5})$$

Note that the points z are already over the level surfaces of the Lyapunov function, and the sign of its derivative (A.1) has to be checked for a different kind of level surfaces.

In Figure 1, it is shown the level surfaces for gains $\gamma_1 = 0.6$, $\gamma_2 = 20$, $\gamma_3 = 0.0001$, $m = 7$, $k_1 = 0.55$, $k_2 = 2.3$, $k_3 = 13$, $k_{I1} = 0.15$, $k_{I2} = k_{I3} = 0$, $\beta(t, z) = 1$ and $L = 0$

(nominal case) in the plane $z_1 - z_2$. The blue level surfaces represent the ones whose Lyapunov function derivative is negative. This implies that the trajectories which start in these regions will be taken to the origin. Meanwhile, the red level surfaces represent points whose Lyapunov function derivative is non-negative. This means that the Lyapunov function can not ensure the stability if the trajectories start in this level surfaces. On the other hand, it is presented three equilibrium points which correspond to the origin, which is stable, and the nearest ones, which are unstable, and the points where the pendulum is in the downward position with zero velocities, as it is wanted to see them inside of the estimated region of attraction.

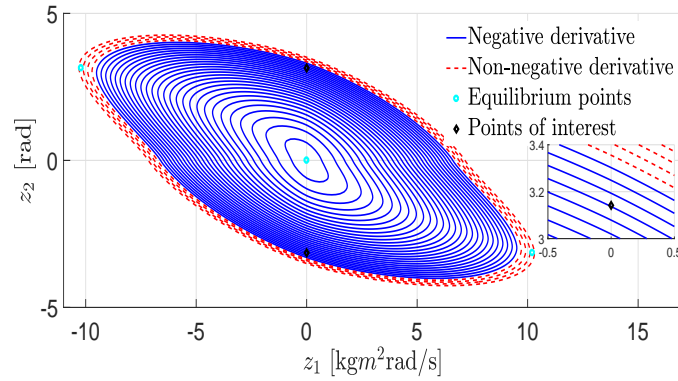


Figure 1: Level surfaces of the Lyapunov function.

Therefore, it is shown at which level surface of V_3 , its derivative \dot{V}_3 is negative definite, and the origin of system (3.29) is locally asymptotically stable. This results in an estimate of the region of attraction in which the points of interest are inside of it. Furthermore, due to homogeneous properties [28] close of the origin, the origin is finite-time locally stable. Finally, by Eq. (3.24), the origin of system (3.11) is finite-time locally stable.

Now, the case when the Lipschitz constant of the perturbation $\varphi(t)$ is $L \neq 0$ is considered. The calculated constant for which the derivative of the Lyapunov function becomes non-negative with the 3-DIA's gains founded was $L = 0.14$. This agrees to the condition $k_{I1} > L$ for the finite-time local stability of the origin obtained in [18].

This procedure can be summarized as follows:

1. Obtain points \bar{z} over the unit sphere from the Eq. (C.2).
2. Evaluate the Lyapunov function $V_3(\bar{z})$, choosing the gains $k_1, k_2, k_3, k_{I1}, k_{I2}, k_{I3}, m, \gamma_1, \gamma_2, \gamma_3, L = 0$.
3. Choose a value of C small for the level surface.
4. Obtain the value of ϵ from Eq. (C.4).
5. Obtain points z over the level surface of the Lyapunov function from Eq. (C.5).

-
6. Evaluate the Lyapunov function $V_3(z)$ and its derivative $\dot{V}_3(z)$, checking the sign of it.
 7. If all the points negative derivative, choose a bigger value of C and repeat the process from the step (4), until one point has non-negative derivative. If from the beginning one point has non-negative derivative, or the estimation of the region of attraction is not the one needed, repeat the process from the step (2).
 8. Repeat the process from the step (3), but now with $L \neq 0$ to see at which constant, the derivative of the Lyapunov functions becomes non-negative. That will give the Lipschitz constant of the perturbation that the algorithm can reject.
 9. $V_3(z) \leq C$ (with the greater C) is an estimation of the region of attraction.

■

.4 Appendix D: Proof of Theorem 3 and 5

Since the Slave system is ISS with respect to $\mu_1(t)$ [42, 40], it suffices to analyze the stability of the Master subsystem

$$\begin{aligned}\dot{\mu}_1 &= \mu_2, \\ \dot{\mu}_2 &= \beta(t, z)[\nu + \varphi(t)].\end{aligned}\tag{D.1}$$

The closed-loop of (D.1), with controller (3.37) and the new variable $\mu_3 = \zeta + \varphi(t)$, is

$$\begin{aligned}\dot{\mu}_1 &= \mu_2, \\ \dot{\mu}_2 &= \beta(t, z) \left[-k_1 [\mu_1]^{\frac{1}{3}} - k_2 [\mu_2]^{\frac{1}{2}} + \mu_3 \right] \\ \dot{\mu}_3 &= -k_3 [\mu_1]^0 - k_4 [\mu_2]^0 + \dot{\varphi}(t).\end{aligned}\tag{D.2}$$

For the case with known coefficient β , the origin is proven to be global and finite-time stable in [65], when the gains k_1, k_2, k_3, k_4 are properly designed, using the following homogeneous Lyapunov function

$$V(\mu) = \alpha_1 |\mu_1|^{\frac{5}{3}} + \alpha_2 \mu_1 \mu_2 + \alpha_3 |\mu_2|^{\frac{5}{2}} + \alpha_4 \mu_1 [\mu_3]^2 - \alpha_5 \mu_2 \mu_3^3 + \alpha_6 |\mu_3|^5.$$

For the case with uncertain coefficient a similar proof can be obtained.

On the other hand, the closed-loop system of (D.1), with the controller (3.38) and the new variable $\mu_3 = \zeta + \varphi(t)$, is given by

$$\begin{aligned}\dot{\mu}_1 &= \mu_2, \\ \dot{\mu}_2 &= -\beta(t, z) \left[k_2 \left[[\mu_2]^{\frac{3}{2}} + k_1^{\frac{3}{2}} \mu_1 \right]^{\frac{1}{3}} - \mu_3 \right] \\ \dot{\mu}_3 &= -k_{I1} \left[\mu_1 + k_{I2} [\mu_2]^{\frac{3}{2}} \right]^0 + \frac{d\varphi(t)}{dt}.\end{aligned}\tag{D.3}$$

Similar to the proof in [39], it can be proved that, designing properly the gains k_1, k_2, k_{I1}, k_{I2} , the origin is globally and finite-time stable by using the following homogeneous and smooth Lyapunov function

$$V(\mu) = \frac{3}{5}\gamma_1 |\xi_1|^{\frac{5}{3}} + \xi_1 \xi_2 + \frac{2}{5}k_1^{-\frac{3}{2}} |\xi_2|^{\frac{5}{2}} + \frac{1}{5} |\xi_3|^5,$$

where $\xi_1 = \mu_1 - [\xi_3]^3$, $\xi_2 = \mu_2$, $\xi_3 = k_1^{-\frac{1}{2}} k_2^{-1} \mu_3$.

The derivative of V is given by

$$\begin{aligned} \dot{V}(\mu) = & -\beta(t, z) k_2 k_1^{-\frac{3}{2}} \left(k_1^{\frac{3}{2}} \xi_1 + [\xi_2]^{\frac{3}{2}} \right) \left(\left[k_1^{\frac{3}{2}} \xi_1 + [\xi_2]^{\frac{3}{2}} + k_1^{\frac{3}{2}} [\xi_3]^3 \right]^{\frac{1}{3}} - k_1^{\frac{1}{2}} \xi_3 \right) + \\ & \left(\gamma_1 [\xi_1]^{\frac{2}{3}} + \xi_2 \right) \xi_2 - k_{I1} k_1^{-\frac{1}{2}} k_2^{-1} \left[-3 \left(\gamma_1 [\xi_1]^{\frac{2}{3}} + \xi_2 \right) |\xi_3|^2 + [\xi_3]^4 \right] \times \\ & \left[[\xi_1 + [\xi_3]^3 + k_{I2} [\xi_2]^{\frac{3}{2}}]^0 - [-\tilde{L}, \tilde{L}] \right], \end{aligned}$$

where $\tilde{L} = \frac{L}{k_{I1}}$. Using (2.3) one can conclude that the first term is negative semi-definite and it vanishes only on the set $S_1 = \left\{ k_1^{\frac{3}{2}} \xi_1 + [\xi_2]^{\frac{3}{2}} = 0 \right\}$. Evaluating \dot{V} on this set it is obtained

$$\begin{aligned} \dot{V}|_{S_1} = & - \left(\gamma_1 k_1^{-1} - 1 \right) \xi_2^2 - k_{I1} k_1^{-\frac{1}{2}} k_2^{-1} |\xi_3|^2 \left[3 \left(\gamma_1 k_1^{-1} - 1 \right) \xi_2 + [\xi_3]^2 \right] \times \\ & \left[\left[[\xi_3]^3 + \left(k_{I2} - k_1^{-\frac{3}{2}} \right) [\xi_2]^{\frac{3}{2}} \right]^0 - [-\tilde{L}, \tilde{L}] \right]. \end{aligned}$$

If $\gamma_1 > k_1$ the first term is negative semi-definite, and it is zero only on the set $S_2 = \{\xi_2 = 0\}$. Evaluating $\dot{V}|_{S_1}$ on this set one can get

$$\dot{V}|_{S_1 \cap S_2} = -k_{I1} k_1^{-\frac{1}{2}} k_2^{-1} [\xi_3]^4 \left[[\xi_3]^0 - [-\tilde{L}, \tilde{L}] \right].$$

This is negative if $\tilde{L} = \frac{L}{k_{I1}} < 1$. By Lemma 2 one can render $\dot{V}|_{S_1} < 0$ selecting $k_{I1} > 0$ small. Using Lemma 2 again it can be concluded that it is possible to make $\dot{V} < 0$ selecting $k_2 > 0$ sufficiently large.

Therefore, the controllers (3.37) or (3.38) globally stabilize in finite-time $\mu_1 = \mu_2 = 0$ for the μ -subsystem of (3.36). Then, the origin of the system (3.36) is globally asymptotically stable. Furthermore, by the change of coordinates (3.5) and (3.34), the original states of the system (3.2) will be driven to the origin asymptotically and globally. ■

Bibliography

- [1] J. A. Acosta, R. Ortega, A. Astolfi, and A. D. Mahindrakar. Interconnection and damping assignment passivity-based control of mechanical systems with underactuation degree one. *IEEE Transactions on Automatic Control*, 50(12):1936–1955, Dec 2005.
- [2] V. Andrieu, L. Praly, and A. Astolfi. Homogeneous approximation, recursive observer design and output feedback. *SIAM J. Control Optim.*, 47(4):1814–1850, 2008.
- [3] B.R. Andrievsky. Global stabilization of the unstable reaction-wheel pendulum. *Automation and Remote Control*, 72(9):1981–1993, 2011.
- [4] K.J. Aström and K. Furuta. Swinging up a pendulum by energy control. *Automatica*, 36:287–295, 2000.
- [5] A. Bacciotti and L. Rosier. *Lyapunov functions and stability in control theory*. Springer-Verlag, 2nd ed., New York, 2005.
- [6] Andrea Bacciotti and Lionel Rosier. *Liapunov functions and stability in control theory*. Communications and Control Engineering. Springer, Berlin, 2001.
- [7] A. Chalanga, S. Kamal, and B. Bandyopadhyay. Continuous integral sliding mode control: A chattering free approach. In *IEEE International Symposium on Industrial Electronics*, Taipei, Taiwan, 2013.
- [8] C.C. Chung and J. Hauser. Nonlinear control of a swinging pendulum. *Automatica*, 31(6):851–862, 1995.
- [9] E. Cruz-Zavala and J.A. Moreno. Homogeneous high order sliding mode design: a Lyapunov approach. *Automatica*, 80:232–238, 2017.
- [10] S. U. Din, Q. Khan, F. Rehman, and R. Akmeliawanti. A comparative experimental study of robust sliding mode control strategies for underactuated systems. *IEEE Access*, 5:10068–10080, 2017.
- [11] Sami Ud Din, Fazal Ur Rehman, and Qudrat Khan. Smooth super-twisting sliding mode control for the class of underactuated systems. *PloS one*, 13(10):e0203667–e0203667, 10 2018.

- [12] C. Edwards and Y.B. Shtessel. Adaptive continuous higher order sliding mode control. *Automatica*, 65:183–190, 2016.
- [13] S.V. Emelyanov, S.K. Korovin, and L.V. Levantovsky. Higher-order sliding regimes in the binary control systems. *Soviet Physics Doklady*, 31(4):291–293, 1986.
- [14] A.F. Filippov. *Differential Equations with Discontinuous Right-hand Sides*. Kluwer Academic Publishers, Dordrecht, The Netherlands, 1988.
- [15] L. Fridman, J.A. Moreno, B. Bandyopadhyay, S. Kamal, and A. Chalanga. *Recent Advances in Sliding Modes: From Control to Intelligent Mechatronics*. Studies in Systems, Decision and Control 24. Springer, Switzerland, 2015.
- [16] J. W. Grizzle, C. H. Moog, and C. Chevallereau. Nonlinear control of mechanical systems with an unactuated cyclic variable. *IEEE Transactions on Automatic Control*, 50(5):559–576, May 2005.
- [17] Y.-L. Gu. A direct adaptive control scheme for underactuated dynamic systems. In *IEEE Conference on Decision and Control*, Texas, USA, 1993.
- [18] D. Gutiérrez-Oribio, A. Mercado-Uribe, J.A. Moreno, and L. Fridman. Stabilization of the reaction wheel pendulum via a third order discontinuous integral sliding mode algorithm. In *15th International Workshop on Variable Structure Systems*, Graz, Austria, 2018.
- [19] INTECO. *Pendulum-Cart System*. User’s Manual. INTECO, U.S.A., 2012.
- [20] R. Iriarte, L.T. Aguilar, and L. Fridman. Second order sliding mode tracking controller for inertia wheel pendulum. *Journal of the Franklin Institute*, 350:92–106, 2013.
- [21] M. Jankovic, D. Fontaine, and P.V. Kokotovic. TORA example: Cascade and passivity-based control designs. *IEEE Transactions on Control Systems Technology*, 4(3):292–297, 1996.
- [22] H. Khalil. *Nonlinear Systems*. Prentice Hall, New Jersey, U.S.A., 2002.
- [23] Qudrat Khan, Rini Akmeliawati, Aamer Iqbal Bhatti, and Mahmood Ashraf Khan. Robust stabilization of underactuated nonlinear systems: A fast terminal sliding mode approach. *ISA Transactions*, 66:241 – 248, 2017.
- [24] S. Laghrouche, M. Harmouche, and Y. Chitour. Higher order super-twisting for perturbed chains of integrators. *IEEE Transactions on Automatic Control*, 62(7):3588–3593, 2017.
- [25] A. Levant. Sliding order and sliding accuracy in sliding mode control. *International Journal of Control* 58, pages 1247–1263, 1993.

-
- [26] A. Levant. Robust exact differentiation via sliding mode technique. *Automatica*, 34(3):379–384, 1998.
- [27] A. Levant. Universal single-input-single-output (SISO) sliding-mode controllers with finite-time convergence. *IEEE Trans. Automat. Contr.*, 46(9):1447–1451, 2001.
- [28] A. Levant. Homogeneity approach to high-order sliding mode design. *Automatica*, 41(5):823–830, 2005.
- [29] A. Levant. Higher-order sliding modes, differentiation and output-feedback control. *International Journal of Control*, 76(9/10):924–941, 2008.
- [30] S. Li, C.H. Moog, and W. Respondek. Maximal feedback linearization and its internal dynamics with applications to mechanical systems on \mathbb{R}^4 . *International Journal of Robust and Nonlinear Control*, 29:2639–2659, 2019.
- [31] Y. Liu and H. Yu. A survey of underactuated mechanical systems. *IET Control Theory Applications*, 7(7):921–935, May 2013.
- [32] B. Lu, Y. Fang, and N. Sun. Continuous sliding mode control strategy for a class of nonlinear underactuated systems. *IEEE Transactions on Automatic Control*, 63(10):3471–3478, Oct 2018.
- [33] Z. Man, A.P. Paplinski, and H.R. Wu. A robust MIMO terminal sliding-mode control scheme for rigid robotic manipulators. *IEEE Transaction on Automatic Control*, 39(12):2464–2469, 1994.
- [34] Riccardo Marino. On the largest feedback linearizable subsystem. *Systems & Control Letters*, 6(5):345 – 351, 1986.
- [35] J. Mendoza-Avila, J. A. Moreno, and L. Fridman. Continuous twisting algorithm for third order systems. *IEEE Transactions on Automatic Control*, pages 1–1, 2019.
- [36] J. Mendoza-Ávila, J.A. Moreno, and L. Fridman. An idea for lyapunov function design for arbitrary order continuous twisting algorithm. In *IEEE 56th Annual Conference on Decision and Control*, Melbourne, Australia, 2017.
- [37] A. Mercado-Uribe and J.A. Moreno. Full and partial state discontinuous integral control. *IFAC-PapersOnLine*, 51(13):573–578, 2018. 2nd IFAC Conference on Modelling, Identification and Control of Nonlinear Systems MICNON 2018.
- [38] J.A. Moreno. Discontinuous integral control for mechanical systems. In *International Workshop on Variable Structure Systems*, Nanjing, China, 2016.
- [39] J.A. Moreno. *Discontinuous Integral Control for Systems with relative degree two. Chapter 8 In: Julio Clempner, Wen Yu (Eds.)*, New Perspectives and Applications of Modern Control Theory; in Honor of Alexander S. Poznyak. Springer International Publishing, 2018.

- [40] R. Olfati-Saber. Control of underactuated mechanical systems with two degrees of freedom and symmetry. In *Proceedings of the 2000 American Control Conference. ACC (IEEE Cat. No.00CH36334)*, volume 6, pages 4092–4096 vol.6, June 2000.
- [41] R. Olfati-Saber. Global stabilization of a flat underactuated system: The inertia wheel pendulum. In *40th IEEE Conference on Decision and Control*, Florida, USA, 2001.
- [42] R. Olfati-Saber. *Nonlinear Control of Underactuated Mechanical Systems with Application to Robotics and Aerospace Vehicles*. PhD thesis, Massachusetts Institute of Technology, USA, 2001.
- [43] R. Olfati-Saber. Normal forms for underactuated mechanical systems with symmetry. *IEEE Transactions on Automatic Control*, 47(2):305–308, Feb 2002.
- [44] S.-E. Oltean. Swing-up and stabilization of the rotational inverted pendulum using PD and fuzzy-PD controllers. *Procedia Technology*, 12(7):57–64, 2014.
- [45] U. Perez-Ventura and L. Fridman. When it is reasonable to implement the discontinuous sliding-mode controllers instead of the continuous ones? frequency domain criteria. *International Journal of Robust and Nonlinear Control*, 29(3):810–828, 2019.
- [46] M. Reyhanoglu, S. Cho, N.H. McClamroch, and I. Kolmanovsky. Discontinuous feedback control of a planar rigid body with an unactuated internal degree of freedom. In *IEEE Conference on Decision and Control*, Florida, USA, 1998.
- [47] Samer Riachy, Yuri Orlov, Thierry Floquet, Raul Santiesteban, and Jean-Pierre Richard. Second-order sliding mode control of underactuated mechanical systems i: Local stabilization with application to an inverted pendulum. *International Journal of Robust and Nonlinear Control*, 18(4-5):529–543, 2008.
- [48] R. Seeber and M. Horn. Stability proof for a well-established super-twisting parameter setting. *Automatica*, 84:241–243, 2017.
- [49] R. Seeber and M. Horn. Necessary and sufficient stability criterion for the super-twisting algorithm. In *15th International Workshop on Variable Structure Systems (VSS)*, Graz, Austria, 2018.
- [50] A.S. Shiriaev, O. Egeland, H. Ludvigsen, and A.L. Fradkov. VSS-version of energy based control for swinging up a pendulum. *Syst. and Contr. Lett*, 44(1):41–56, 2001.
- [51] Y. Shtessel, C. Edwards, L. Fridman, and A. Levant. *Sliding Mode Control and Observation*. Intuitive theory of sliding mode control. Birkhauser, New York, USA, 2014.
- [52] M. W. Spong. Partial feedback linearization of underactuated mechanical systems. In *Proceedings of IEEE/RSJ International Conference on Intelligent Robots and Systems (IROS'94)*, volume 1, pages 314–321 vol.1, 1994.

-
- [53] M. W. Spong. Swing up control of the acrobot. In *Proceedings of the 1994 IEEE International Conference on Robotics and Automation*, pages 2356–2361 vol.3, 1994.
- [54] M.W. Spong. The swing up control problem for the acrobot. *IEEE Control Systems Magazine*, 15(1):49–55, 1995.
- [55] M.W. Spong. Energy based control of a class of underactuated mechanical systems. In *13th IFAC World Congress*, San Francisco, USA, 1996.
- [56] M.W. Spong and D.J. Block. The pendubot: a mechatronic system for control research and education. In *34th IEEE Conference on Decision and Control*, New Orleans, USA, 1995.
- [57] M.W. Spong, P. Corke, and R. Lozano. Nonlinear control of the reaction wheel pendulum. *Automatica*, 37:1845–1851, 2001.
- [58] M.W. Spong and M. Vidyasagar. *Robot dynamics and control*. Wiley, New York, USA, 1989.
- [59] B. Srinivasan, P. Huguenin, K. Guemghar, and D. Bonvin. A global stabilization strategy for an inverted pendulum. In *15th IFAC World Congress*, California, USA, 2002.
- [60] C.-Y. Su and Y. Stepanenko. Sliding mode control of nonholonomic systems: Underactuated manipulator case. In *IFAC Nonlinear Control Systems Design*, California, USA, 1995.
- [61] A.R. Teel. Using saturation to stabilize a class of single-input partially linear composite systems. *IFAC Proceedings Volume*, 25(13):379–384, 1992.
- [62] A.R. Teel and L. Praly. Tools for semiglobal stabilization by partial state and output feedback. *SIAM Journal of Control and Optimization*, 33(5):1443–1488, 1995.
- [63] Maria Thomas, Shyam Kamal, Bijnan Bandyopadhyay, and Leena Vachhani. Continuous higher order sliding mode control for a class of uncertain MIMO nonlinear systems: An ISS approach. *European Journal of Control*, 41:1 – 7, 2018.
- [64] V. Torres-González, L. Fridman, and J.A. Moreno. Continuous twisting algorithm. In *IEEE 54th Annual Conference on Decision and Control*, Osaka, Japan, 2015.
- [65] V. Torres-González, T. Sánchez, L. Fridman, and J.A. Moreno. Design of continuous twisting algorithm. *Automatica*, 80:119–126, 2017.
- [66] R. Urnezis and E. Geguzis. Hybrid fuzzy logic and adaptive LQR controller for swing-up, positioning and stabilization of inverted pendulum. *Elektronika ir Elektrotechnika*, 20(3):11–15, 2014.

- [67] V. Utkin. *Sliding modes in control and optimization*. Springer Verlag, Berlin, Germany, 1992.
- [68] V. Utkin, J. Guldner, and J. Shi. *Sliding Modes in Electromechanical Systems*. Taylor and Francis, London, 1999.
- [69] G. Viola, R. Ortega, R. Banavar, J. A. Acosta, and A. Astolfi. Total energy shaping control of mechanical systems: Simplifying the matching equations via coordinate changes. *IEEE Transactions on Automatic Control*, 52(6):1093–1099, June 2007.
- [70] Rong Xu and Ümit Özgüner. Sliding mode control of a class of underactuated systems. *Automatica*, 44(1):233 – 241, 2008.